Experimental and Analytical Evaluation of the Flexural and Axial Capacity of Rectangular

Steel Hollow Structural Section (HSS) End-Plate Connections

Edward J. Nelson

Civil and Architectural Engineering and Construction Management Department

Milwaukee School of Engineering

Author Note

Correspondence concerning this article should be addressed to Edward J. Nelson, 1025 N. Broadway, Milwaukee, WI 53202. E-mail: nelsonedwa@msoe.edu

Abstract

There are many challenges involved in the design of hollow structural sections (HSS) steel end-plate connections. To solve these challenges, structural designers use design guides which have been developed based on several simplifying assumptions to streamline the design procedure, such as *Steel Design Guide 24* (Packer et al., 2010). The purpose of this research is to investigate if the current design procedures in *Steel Design Guide 24* for rectangular HSS steel end-plate connections are comprehensive and accurate. Twelve axial physical HSS end-plate connection specimens using square HSS designed with varying bolt patterns (side and corner) and weld patterns (all-around and workable-flats) were tested under axial tensile loading. Another twelve flexural specimens using rectangular HSS were designed with the varying bending axes (strong and weak) and weld pattern configurations (all-around and workable-flats) were tested under lateral eccentric loading. Linear strain gages, and strain rosettes were used to measure strains in the end-plates and HSS. Linear variable differential transformers (LVDTs) were used to measure end-plate and HSS displacement. The results for the axial specimens indicate that side bolt configurations provide more capacity than corner bolt configurations and the all-around weld provides more capacity than the workable-flats weld. The side bolts connections reached the 100-kip capacity of the test load cell without yielding, so the results were inconclusive. However, because of the stiff behavior of the end-plate, it is reasonable to suggest that the calculated connection capacity using the design procedure in Section 5.6 of *AISC Design Guide 24* (2010), governed by bolt strength, would have been reached. The corner bolt specimens underwent significant yielding at loads less than the calculated capacity, suggesting that the design procedures in *AISC Design Guide 24* are not applicable to the corner bolt configuration and would require a separate design procedure with adjusted equations. Results from the flexural tests indicate that the strong axis configurations provide more capacity than the weak axis configurations and the all-around weld provides more capacity than the workable-flats weld. Results were compared to calculated capacities using the design procedure from Example 4.1 in *AISC Design Guide 24* (2010) and the design procedure developed by Wheeler et al. (1998). The capacities from weld strength based on the *AISC Design Guide 24* (2010) procedure for the all-around weld specimens were conservative and showed good correlation; however, for the workable-flat welds specimens some capacities were unconservative. The calculated strength and serviceability capacities, based on plate and bolt strength from the Wheeler et al. (1998) design procedure, were conservative and showed good correlation with results for the all-around weld specimens. Therefore, it is recommended that the design procedure be considered for implementation into *AISC Design Guide 24*.

Keywords: hollow structural section (HSS), steel, end-plate, rectangular HSS, square HSS, flexural capcity, axial capacity, axial loading, lateral loading, fillet welds, American Institute of Steel Construction (AISC), shear, tension, moment, prying action

Table of Contents

List of Figures

List of Tables

Nomenclature

Symbols:

a – distance from the bolt hole centerline to edge of connecting element flange or angle leg, but not more than $1.25b$, in. (see Figures 4, 10, and 11)

a' – equal to $a + \dfrac{d}{2}$, in.

A_b – nominal unthreaded body area of bolt or threaded part, in.^{2}, (mm^2)

A_w – effective throat area of weld

A_{we} – effective area of the weld, in.^{2} (mm^2)

b – for a tee type connecting element, the distance from the bolt centerline to the face of the tee stem; for an angle-type connecting element, the distance from the bolt centerline to centerline of the angle; for HSS, the distance from the bolt centerline to the face of the HSS wall, in. (see Figures 4, 10, and 11)

b' – equal to $b + \dfrac{d}{2}$, in.

b_e - effective plate width

d – diameter of bolt, in

d' – nominal width of the hole along the length of the connecting element from AISC *Specification* Table J3.3, in

f_{rv} – required shear stress using LFRD or ASD load combinations, ksi (MPa)

F_n – nominal tensile stress, F_{nt}, or shear stress, F_{nv}, ksi (MPa)

F_{nt} – nominal tensile stress from Table J3.2, ksi (MPa)

$F_{nt'}$ – nominal tensile stress modified to include the effects of shear stress, ksi (MPa)

F_{nv} – nominal shear stress from Table J3.2, ksi (MPa)

F_{nw} – nominal stress of the weld material, ksi (MPa)

F_u – specified minimum tensile strength, ksi

F_w – 60% weld electrode strength, ksi

F_{wc} – design weld strength, ksi

F_{yp} – yield strength of plate, ksi

h_i - dimension of HSS, in. (see Figure 10)

k_{ds} – directional strength increase factor

L - distance from anchor rod to HSS corner

L_w – total weld length, in.

n – number of bolts

M_1 – moment at the stem line, kip-in

M_2 – moment at the bolt line, kip-in

q_r – prying force per bolt at required design load, kips

p – tributary length per bolt

p_a – tributary bolt length for pattern A, in. (see Figure 10)

p_b – tributary bolt length for pattern B, in. (see Figure 10)

p_c – tributary bolt length for pattern C, in. (see Figure 10)

p_i – tributary length of end-plate per bolt for the ith pattern, A, B or C, in.

$p_{i,max}$ – maximum bolt spacing for the ith pattern, in.

P_a – ASD factored load, kips

P_n – design/allowable strength

P_u – LRFD factored load, kips

P_y – yield load, kips

Q – bolt factor

R_{hss} - HSS thickness ratio

R_n – design/allowable strength

s – bolt hole spacing, in.

t – thickness of tee flange or angle leg, in.

t_b – wall thickness of HSS branch member

t_c – connecting element thickness required to develop T_c in bolts with no prying action

t_{min} – minimum connecting element thickness, in.

t_{hss} – wall thickness of HSS

t_{np} – minimum connecting element thickness that eliminates prying action

t_p – plate thickness, in.

t_w – weld effective throat thickness

T_a – ASD factored tensile load, kips

T_c – available tensile strength per bolt based on limit state of tension only as determined by

    AISC *Specification* Section J3.7 or the combined lint states of tension and shear rupture as

    determined by AISC *Specification* Section J3.8, kips

$T_{c,adj}$ – adjusted bolt available tensile strength

T_r – required tensile strength per bolt (exclusive of initial tightening and prying force), kips

T_u – LFRD factored tensile load, kips

w – weld size, in.

w_i – dimension of HSS, in. (see Figure 10)

W_t – throat width of the weld $= w \times (0.707)$

X_u – ultimate strength of weld metal

δ – ratio of the net tributary length at bolt line to gross tributary length at the face of the stem or

angle per leg $= 1 - \dfrac{d'}{p}$

α – ratio of the moment at the stem line, kip-in. $= \frac{M_1}{\delta M_2}$

Θ – angle between the line of action of the required force and the weld longitudinal axis, degrees

Ω_b – 1.67, ASD bending resistance factor

Ω – ASD resistance factor

ϕ_b – 0.90, LRFD bending resistance factor

ϕ – LRFD resistance factor

ρ – equal to $\frac{a'}{b'}$

Abbreviations:

AACB – All-Around Corner Bolt

AASB – All-Around Side Bolt

AAST– All-Around Strong Axis

AAWK – All-Around Weak Axis

AISC – American Institute of Steel Construction

ASD – Allowable Stress Design

FE – Finite Element

FEA – Finite Element Analysis

HSS – Hollow Structural Sections

ksi – kips per square inch

LVDT – Linear Variable Differential Transformer

LFRD – Load and Resistance Factor Design

MSOE – Milwaukee School of Engineering

SG – Strain Gage

WFCB – Workable-Flat Corner Bolt

WFSB – Workable-Flat Side Bolt

WFST– Workable-Flat Strong Axis

WFWK– Workable-Flat Weak Axis

Experimental and Analytical Evaluation of the Flexural and Axial Capacity of Steel HSS End-Plate Connections

Hollow Structural Sections (HSS) are widely used in the steel industry for steel construction because of their aesthetics and reduced weight compared to equivalent open steel sections; however, one of the drawbacks of using HSS members is that the design and fabrication of HSS connections is more challenging than open steel sections (Packer et al., 2010). Because of their closed shape, accessing the inside of the members is limited, which can reduce the strength of welded connections or introduce stress concentrations at the interface of HSS members and other steel members. Furthermore, determining the stress distribution around closed HSS sections and determining limit states in HSS connections is more complex compared to open steel sections. Because of the complexity of the analysis of HSS connections, it is very difficult to directly determine modes of failure and limit states and eventually the nominal capacity of HSS connections. To solve this problem, structural designers have been using design guides which have been developed based on several simplifying assumptions to streamline the design procedure, such as *Steel Design Guide 24* (Packer et al., 2010). It is important to verify the level of safety, reliability, and efficiency associated with these design guides and their applicability during different stages of construction through further experimental and analytical studies.

Steel Design Guide 24, published by the American Institute of Steel Construction (AISC), includes design examples for various HSS connections, including welded HSS to bolted end-plate connections (Packer et al., 2010). Figure 1 illustrates one configuration of this common connection, which consists of an HSS member, fillet welded at its end to a perpendicular steel plate that is then connected to another structural element via bolts or anchor rods. It is used for

various framing connections such as column end, beam-to-column, and splice connections. In

these various configurations and loading, the connection can be subjected to shear, flexural

(moment), and axial (tension and compression) forces; the connection may see only one force or

a combination of the forces (Kanvinde et al., 2024). These forces should be carefully determined

through structural analysis of all possible loading as they can cause the connection to have

several limit states that must be checked during design. These limit states include the yielding

and rupture limits of the different elements of the connection, which can be affected by complex

phenomenon such as prying action, yield lines of the plate, and fillet weld behavior (Packer et

al., 2010).

Figure 1

HSS End-Plate Connection

The purpose of this Milwaukee School of Engineering Master of Science in Architectural

Engineering (MSAE) capstone project was to investigate if the current design procedures in *Steel*

Design Guide 24 for rectangular HSS steel end-plate connections are comprehensive and

accurate. This investigation was aided by literature research followed by physical testing and

analysis of results. For the physical testing, the capacities of HSS end-plate connections were tested under two types of loading, in two major phases. Phase 1 involved the testing of the connections under pure axial loading, subjecting the connections to only tension; this phase involved square HSS and investigated two-bolt patterns: corner bolts and side bolts. Phase 2 involved testing of the connection with lateral loading, subjecting the connection to bending moment and shear; this phase involved rectangular HSS and investigated bending about the weak and strong axes. Both phases investigated two weld patterns: all-around welds and workable-flat welds. Load cells, strain gages, and linear variable differential transformers (LVDTs) were used to collect load, strain, and displacement data, respectively.

This paper is organized in several sections to define the purpose and methods of this research and support any conclusions and recommendations made. First, background information is provided to introduce the key subtopics behind the research. Second, a literature review is presented consisting of several studies involving the key subtopics of this research to further define relevant knowledge and equations behind them. Third, the methods of the experimental testing conducted in this research are presented. Fourth, the results of the experimental tests are presented, analyzed, and discussed. Fifth, conclusions are made based on the results. Finally, recommendations are made based on the conclusions.

Background

Structural steel connections often have various limit states, or ways an element can fail, that need to be checked. Different loading configurations can apply shears, moments, and axial forces on the connection that cause various limit states to occur. Tamboli (2017) describes significant challenges associated with the design of structural connections.

> Connection design is an interesting subject because it requires a great deal of rational analysis in arriving at a solution. There are literally an infinite number of possible connection configurations, and only a very small number of these have been subjected to physical testing. Even within the small group that has been tested, changes in load directions, geometry, material types, fastener type, and arrangement very quickly result in configurations that have not been tested and therefore require judgment and rational analysis on the part of the designer… Connection design is both an art and a science. The science involves equilibrium, limit states, load paths, and the lower bound theorem of limit analysis. The art involves the determination of the most efficient load paths for the connection, and this is necessary because most connections are statically indeterminate.

> (Chapter 2, 2.1 Introduction, 2.1.1 Philosophy)

Connections are an intricate part of structures that require in depth analysis and experimental testing to develop models and procedures for design.

Axial tension loading is one configuration of loading that an HSS end-plate could be subjected to; for example, it is common in splice connections (Willibald et al., 2002) and can occur in column base plate connections when wind causes net uplift on a structure (Kanvinde et al., 2024). Figure 2 shows the two configurations of axially loaded end-plates in this project. The

configuration on the left includes four bolts, one centered on each side of the HSS member.

Various studies have investigated this configuration; for example, Thornton (2017) developed a

design method based of testing conducted by Willibald et al., Kato and Mukai (1985),

Caravaggio (1988), and Willibald et al. (2003). The configuration on the right also includes four

bolts, but they are instead located at the corners of the HSS member. This case was investigated

by Christensen (2010). Only the side bolted configuration is considered in *AISC Steel Design*

Guide 24.

Figure 2

Configurations of Axially Loaded HSS End-Plate Connections

Side Bolts   **Corner Bolts**
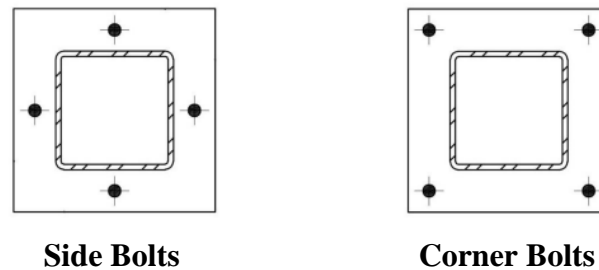
Lateral loading is another loading configuration that an HSS end-plate connection could

be subjected to; for example, it can be caused by wind and earthquake loading. Lateral loading

causes bending (moment) and shear on the connection. Literature on HSS moment connections is

limited (Packer et al., 2010). Wheeler et al. (1998) developed an analytical model to determine

the moment capacity of rectangular HSS end-plate connections. Heinisuo et al. (2012)

investigated yield mechanisms of rectangular HSS end-plate connections. *AISC Steel Design*

Guide 24 provides limited design for HSS end-plate moment and shear connections.

One limit state for both axial tension and lateral loading is the bolt tensile capacity, or

how much tension the bolts can undergo before yielding or rupturing; all four bolts in axial

loading and two bolts in lateral loading will be in tension. Both axial tension loading, and lateral

loading can cause prying action to occur in the connection, which increases the bolt tension

force. The *AISC Steel Construction Manual* defines prying action as "…a phenomenon that

occurs in bolted joints with tensile bolt forces. The tensile force in the bolt is increased due to the

deformation of the connecting element" (American Institute of Steel Construction, 2022a). In

other words, the deformation of the end-plate causes it to lever against the connected element to

increase the tensile force on the bolts. See Figure 3(b) for a diagram of prying action where the

deformation of the plate results in the prying forces, Q, which increase the bolt force, B_u.

Figure 3

Forces Diagrams for (a) Rigid Plates with No Prying Action and (b) Flexible Plates with

Prying Action
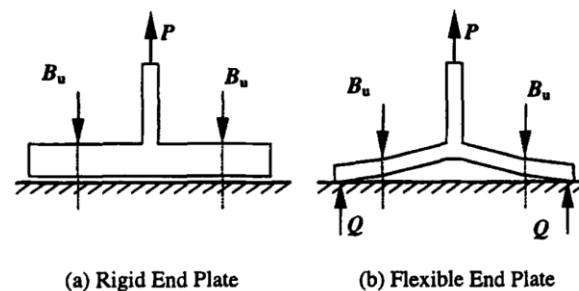
(a) Rigid End Plate   (b) Flexible End Plate

Note. Adapted from "Design Model For Bolted Moment End-Plate Connections Using Rectangular Hollow

Sections" by A. T. Wheeler et al., 1998, *Journal of Structural Engineering, 124*(2), p. 165

(https://doi.org/10.1061/(ASCE)0733-9445(1998)124:2(164)).

The deformation of the end-plate, which affects the prying force in the bolt, depends on

how the plate yields about yield lines. The tributary length (p in Figure 4) is based on yield line

theory (American Institute of Steel Construction, 2022a). Prying action and yield lines

complicate the design of HSS steel end-plate connections; *AISC Steel Design Guide 24* states

"due to the complexity of the analysis accounting for prying action and the position of yield lines in the plate, it is difficult to directly determine nominal capacities according to the AISC *Specification* provisions" (Packer et al., 2010, p. 51).

The thickness, configuration, and loading of the end-plate can affect its behavior and whether yield lines and prying action occur before failure. Wheeler et al. (1998) observe that

As outlined by Nair et al. (1974), the ultimate strength of the connection may be reached either before or after yielding has occurred in the end-plate. In the former case, the end-plate is said to be "rigid," but in the latter case, the end-plate is said to be "flexible." The design of rigid end-plate connections may be less difficult than design of flexible end-plate connections due to the need to consider prying effects in the latter, but the flexible end-plate provides a substantially more economical and ductile connection. (p. 164)

The difficulty in design due to prying effects in flexible plate connections is mentioned but is justified because of better economics and ductility. Ductility is important in connections for several reasons. For example, it increases strength, leads to more robust structures, provides warning of failure, and helps structures survive earthquake loading (Engelhardt, 2007).

Wheeler et al. (1998) note that the behavior of the end-plate can be classified further into three categories depending on plate thickness.

As suggested by Kennedy et al. (1981), the behavior of the end-plate can be divided into three distinct categories based on the plate thickness and magnitude of loading. The first mode is termed thick plate behavior and is characterized by the absence of prying effects and yield lines, resulting in a direct relationship between the bolt loads and the applied moment. At the other extreme, the third mode is termed thin plate behavior and is

characterized by yield lines through the bolt positions and a maximum value of the prying

force. The resulting bolt loads are the superposition of the bolt pretension, the prying

forces, and the forces induced in the bolts from the applied moment. The second mode,

termed intermediate plate behavior, falls between the thick and thin plate behavior and is

characterized by the prying force ranging from zero to the maximum attainable value. (p.

164)

For thin and intermediate plates, the resultant bolt force has three components: the bolt

pretension, the prying forces, and the tension forces resulting from an applied moment or axial

load.

Another limit state for both loading configurations is the fillet weld capacity; the capacity

of HSS fillet weld connections have been investigated recently by Wilsmann (2012), Packer et

al. (2016), and Tousignant and Packer (2017). Depending on the end-plate configuration and

loading, the entire length of weld length may not be effective and only the effective portions

should be considered for design (Kanvinde et al., 2024). The applicability of the directionality

factor, which can allow for a strength increase of up to one and a half times depending on the

direction of the loading relative to the direction of the weld, must also be considered for HSS

end-plate connections (Packer et al., 2016).

Packer et al. (2016) subsequently performed a large number of laboratory tests on HSS-

to-rigid end-plate connections to investigate the applicability of the sin θ factor to single-

sided fillet welds to HSS, joined to a rigid end-plate. These experiments removed the

influence of a flexible landing surface for the fillet weld, and hence removed the weld

effective length phenomenon. It was shown that HSS-to-plate fillet welds still did not

provide the adequate structural reliability if the sin θ factor was implemented.

(Tousignant & Packer, 2017)

Literature Review

The purpose of this literature review was to find relevant sources of information and guidance on the design of HSS end-plate connections. To find relevant literature beyond theses from past research conducted at MSOE and AISC design guides and specifications, keywords were used in online search engines and databases. The literature review is organized in four main categories: design guides, axial, flexural, and fillet welds. Relevant knowledge and equations from the sources in each category pertaining to the design of the components of HSS end-plate connections are highlighted.

Design Guides and Specifications

AISC *Steel Construction Manual* and *AISC 360 Specification for Structural Steel Buildings*

AISC publishes the AISC *Steel Construction Manual,* or *Manual,* along with the AISC *Specification for Structural Steel Buildings,* or *Specification*. The most recent versions at the time of writing are the 16th edition of the *Manual* and AISC 360-22 for the *Specification*. For purposes of this literature review, the most recent versions will be referenced.

Part 9 of the *Manual* provides design guidance and equations to account for prying action, based on Thornton (1992) and Swanson (2002). Figure 4 illustrates the variables, forces, and dimensions, associated with prying action on tee and angle connections.

Figure 4

Illustration of Variables in Prying Action Calculations

(a) Typical bolt location *(b) Edge bolt*

(c) Prying forces in tee *(d) Prying forces in angle*
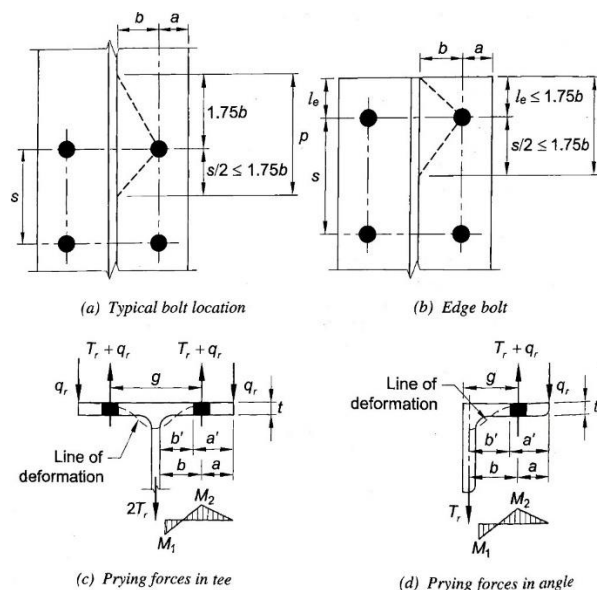
Note. Adapted from *Steel Construction Manual (16th ed.)* by American Institute of Steel Construction, 2022a, p. 9-12.

There are two inequalities that govern the prying action design and analysis methods

presented in the *Manual*, for the connecting element:

$$\frac{T_r}{T_c} \le (1 + \delta\alpha)\left(\frac{t}{t_c}\right)^2 , \tag{1}$$

and for the bolts:

$$\frac{T_r}{T_c} \le \frac{1+\delta\alpha}{1+\delta\alpha(1+\rho)} . \tag{2}$$

There are three solution methods given. The first method is to "design assuming no

prying forces, which results in the smallest bolt diameter" (American Institute of Steel

Construction, 2022a); this method will result in a thicker plate, with a thickness, t_{np}, that

effectively eliminates prying action. Equations (3) and (4) calculate the required plate thickness

for no prying action to occur for load and resistance factor design (LFRD) and allowable stress

design (ASD), respectively:

$$t_{np} \ge \sqrt{\frac{4T_c b'}{\phi_b p F_u}}\sqrt{\frac{T_r}{T_c}} = \sqrt{\frac{4T_r b'}{\phi_b p F_u}} , \tag{3}$$

$$t_{np} \ge \sqrt{\frac{4\Omega_b T_c b'}{p F_u}}\sqrt{\frac{T_r}{T_c}} = \sqrt{\frac{4\Omega_b T_r b'}{p F_u}} . \tag{4}$$

The second method is the method that "results in the smallest required connecting element

thickness" (American Institute of Steel Construction, 2022a). This method accounts for the

effects of prying action and gives equations for the minimum required plate thickness, t_{min}, given

by Equations (5) and Equation (6) for LFRD and ASD, respectively. Thus,

$$t_{min} = \sqrt{\frac{4T_r b'}{\phi_b p F_u (1 + \delta \alpha')}} \, , \tag{5}$$

$$t_{min} = \sqrt{\frac{4\Omega_b T_r b'}{p F_u (1 + \delta \alpha')}} \, . \tag{6}$$

The α' factor for this method is determined by first calculating β using:

$$\beta = \frac{1}{\rho}\left(\frac{T_c}{T_r} - 1\right). \tag{7}$$

If β is greater than or equal to one ($\beta \geq 1$) then:

$$\alpha' = 1. \tag{8}$$

Otherwise, if β is less than 1 ($\beta < 1$) then:

$$\alpha' = \frac{1}{\delta}\left(\frac{\beta}{1-\beta}\right) \leq 1. \tag{9}$$

The third and final method involves an "analysis to find the tensile strength of the connecting element" (American Institute of Steel Construction, 2022a). A bolt factor, Q, is determined to adjust the bolt available strength. There are three steps to this method. The first step is to calculate the α' factor for this method using the following equation:

$$\alpha' = \frac{1}{\delta(1+\rho)}\left[\left(\frac{t_c}{t}\right)^2 - 1\right]. \tag{10}$$

Depending on the value of α', there are three possible values for the bolt factor, Q. The first value for Q applies when α' is less than or equal to zero ($\alpha' \leq 0$), which occurs when the connecting element of thickness t has sufficient strength to develop the tensile strength of the bolt, and is given as

$$Q = 1 \, . \tag{11}$$

The second value for Q applies when α' falls between zero and one or is equal to one ($0 < \alpha' \leq$ 1), which occurs when the connecting element and bolt both control the design, and is given as

$$Q = \left(\frac{t_c}{t}\right)^2 - (1 + \delta\alpha'). \tag{12}$$

The third value for Q applies when α' is greater than one ($\alpha' > 1$), which occurs when the connecting element controls the design and is given as

$$Q = \left(\frac{t_c}{t}\right)^2 - (1 + \delta). \tag{13}$$

Finally, the adjusted bolt available tensile strength can be calculated using the calculated bolt force from Equation (11), (12), or (13) as

$$T_{c,adj} = QT_c. \tag{14}$$

Chapter J of the *Specification* contains information and equations on connecting elements, connectors, and the affected elements of connected members (American Institute of Steel Construction, 2022b). Section J2 addresses welds; the question provided to calculate the strength of fillet welds is

$$R_n = F_{nw}A_{we}k_{ds}, \tag{15}$$

where k_{ds} is the directional strength increase factor. If strain compatibility of the various weld elements is considered it can be calculated by:

$$k_{ds} = (1.0 + 0.50sin^{1.5}\theta), \tag{16}$$

where if an increase of strength of up to one and a half times can be taken if the line of action of the force is perpendicular to the weld longitudinal axis. However, for fillet weld to the ends of rectangular HSS loaded in tension k_{ds} must be limited to 1.0:

$$k_{ds} = 1.0.$$

Section J3 addresses bolts; Section J3.7 addresses the tensile and shear strength of bolts and threaded parts and provides an equation based on the limit states of tension rupture and shear rupture:

$$R_n = F_n A_b. \tag{17}$$

It is mentioned that the required tensile strength should include tension resulting from prying action. A user note addresses the consideration of whether the bolt in shear is sheared through its shank or threads, as it will affect its available strength; if a bolt is loaded through the threads there will be less effective area, A_b, and thus lower strength. Another user note mentions the limit states of bolt bearing and bolt tearout in strength that are present in a snug-tightened or pre-tensioned high-strength bolt or threaded part; these additional limit states are addressed in Section J3.11, and the effective strength of an individual fastener may be taken as the lesser of the strength per Section J3.7 or J3.11. Section J3.7 addresses tension and shear acting alone, but special consideration must be taken when both tension and shear act together, this is address in Section J3.8, with the following equation:

$$R_n = F_{nt}{}' A_b, \tag{18}$$

where the combined effects are addressed by the modified tensile stress, $F_{nt}{}'$, given by Equation (19) and Equation (20) for LFRD and ASD, respectively:

$$F_{nt}{}' = 1.3 F_{nt} - \frac{F_{nt}}{\phi F_{nv}} f_{rv} \le F_{nt}, \tag{19}$$

$$F_{nt}{}' = 1.3 F_{nt} - \frac{\Omega F_{nt}}{F_{nv}} f_{rv} \le F_{nt}. \tag{20}$$

Section J3 provides a table for the minimum edge distance from center of a standard hole to the

edge of the connected part, see Table 1.

Table 1

Bolt Hole Edge Distance

Bolt Diameter, in.	Minimum Edge Distance
$1/2$	$3/4$
$5/8$	$7/8$
$3/4$	1
$7/8$	$1^1/8$
1	$1^1/4$
$1^1/8$	$1^1/2$
$1^1/4$	$1^5/8$
Over $1^1/4$	$1^1/4 \times d$

Note. Adapted from *ANSI/AISC 360-22: Specification for Structural Steel Buildings* by American Institute

of Steel Construction, (2022b), p.16.1-139.

Chapter K of the *Specification* addresses additional requirements for connections to HSS

members. A user note states that that "connection strength is often governed by the size of HSS

members…, and this must be considered in the initial design" (American Institute of Steel

Construction, 2022b).

AISC Steel Design Guide 1: Base Connection Design, Fabrication, and Erection

for Steel Structures

A significant amount of research was conducted and changes to related codes and standards were made following the publication by AISC of the second edition of *Steel Design Guide 1* (Fisher & Kloiber, 2006), leading to the third edition. Kanvinde, Maamouri, and Buckholt (2024) authored the third edition of *Steel Design Guide 1*; it offers guidance in the design, fabrication, and erection of steel base connections (Kanvinde et al., 2024). Chapter 4 covers the design of exposed column base connections for axial, bending, and shear forces, alone and in combination, considering the various components of the connection, i.e., the anchor rods, steel base plate, and welds.

Steel Design Guide 1 breaks out the design of base connections into six steps. The first step is to select the length and width of the base plate ("base plate footprint"). The second step is to determine how internal forces are distributed. The third step is to select the base plate thickness. The fourth step is anchoring design. The fifth step is footing design considerations. The sixth, and final, step is the design and detailing of the welds. The research of this paper will involve all steps, except the portion of the fifth step involving concrete design. These are the general steps involved with designing base connections; there are special considerations for the different loadings on the connection within the various steps that need to be accounted for.

Steel Design Guide 1 Section 4.3.2 offers guidance for design for axial tension. Section 4.3.3 covers design for shear and Section 4.3.6 covers design for bending. There is no section in *Steel Design Guide 1* that addresses only the combination of bending and shear forces, but Sections 4.3.9 and 4.3.10 cover design for combined axial forces, bending, and shear. These

sections reference prior sections and offer additional commentary on any additional stresses that could arise from the combination of forces.

Steel Design Guide 1 also covers material and type specification for the plates, anchors, and welds. The design guide provides tables for recommended base plate materials and anchor rod materials, see Tables 2 and 3. It is stated that "base plates should be designed using ASTM A572/A572M Grade 50 material unless the availability of an alternative grade is confirmed prior to specification". It is also mentioned that a typical minimum thickness of ½ in for posts and light HSS columns, and ¾ in for other structural columns (Kanvinde et al., 2024).

Table 2

Recommended Base Plate Materials

Thickness (t_p)	Plate Availability
$t_p \le 4$ in.	ASTM A36/A36M ASTM A572/A572M Gr 42 or 50[a] ASTM A588/A588M Gr 50
4 in. < $t_p \le 5$ in.	ASTM A36/A36M[a] ASTM A572/A572M Gr 42 ASTM A588/A588M Gr 46
5 in. < $t_p \le 6$ in.	ASTM A36/A36M[a] ASTM A572/A572M Gr 42 ASTM A588/A588M Gr 42
6 in. < $t_p \le 8$ in.	ASTM A36/A36M[a] ASTM A588/A588M Gr 42
$t_p > 8$ in.	ASTM A36/A36M[a]
[a] Preferred Material Specification	

Note. Adapted from *Steel Design Guide 1: Base Connection Design, Fabrication, and Erection for Steel Structures* (Third ed.) by A. M. Kanvinde et al., 2024, American Institute of Steel Construction, p. 8.

Table 3

Recommended Anchor Rod Materials

Material ASTM		Tensile Strength F_u, ksi	Nominal Tensile Stress[a] $F_{nt} = 0.75F_u$, ksi	Nominal Shear Stress (N type)[a, c] $F_{nv} = 0.450F_u$, ksi	Nominal Shear Stress (X type)[a, b] $F_{nv} = 0.563F_u$, ksi	Maximum Diameter, in.
F1554	Gr 36[d]	58	43.5	26.1	32.7	4
	Gr 55[d]	75	56.3	33.8	42.2	4
	Gr 105	125	93.8	56.3	70.4	3
A449		120	90.0	54.0	67.6	1
		105	78.8	47.3	59.1	1-1/2
		90	67.5	40.5	50.7	3
A36/A36M		58	43.5	26.1	32.7	15
A354 Gr BD		150	113	67.5	84.5	4

[a] Nominal stress on unthreaded body area of threaded part (gross area)
[b] Threads excluded from shear plane
[c] Threads included in the shear plane
[d] Preferred material specification

Note. Adapted from *Steel Design Guide 1: Base Connection Design, Fabrication, and Erection for Steel Structures* (Third ed.) by A. M. Kanvinde et al., 2024, American Institute of Steel Construction, p. 8.

The design guide mentions that load path from the column to the anchor rod should be considered when designing the weld between the column and the base plate. If the base plate is rigid, then the entirety of the weld could be considered effective. However, this is not often the case and, in most cases, only a portion of the weld could be considered effective in transferring the forces. An example that is given of such a case is when anchor rods are located at the corners of HSS columns; to account for the stress concentrations in this case, the design guide points to methods in *AISC Design Guide 10: Erection Bracing of Low-Rise Structural Steel Buildings* (West & Fisher, 2020) and the *AISC Hollow Structural Connections Manual* (American Institute of Steel Construction, 1997). It also mentions testing done by Christensen (Christensen, 2010) and Wilsmann (Wilsmann, 2012) which evaluated the methods and found them to be "generally conservative for the tested cases" (Kanvinde et al., 2024, p.36). Example 4.3 illustrates a second case in which "only welding adjacent to the anchor rod is considered effective" (Kanvinde et al., 2024). Ultimately it is noted that "a consistent model of load path from the column, through the

effective portions of the welding, through the effective portions of the base plate in bending,

through the anchor rods, and into the concrete should be used" (Kanvinde et al., 2024, p. 36).

AISC Steel Design Guide 24: Hollow Structural Steel Connections

Packer, Sherman, and Lecce (2010) authored *AISC Steel Design Guide 24* (Packer et al., 2010). It offers design methods and examples for various HSS connections. Chapter 5 covers HSS tension and compression connections, and Section 5.6 covers the design of an end-plate on rectangular HSS with bolts on four sides under axial tension. Chapter 4 covers HSS moment connections, with Section 4.1 covering W-beams to HSS columns and mentions "contemporary information concerning moment connections to HSS columns is limited in literature" (Packer et al., 2010, p. 29).

The design method for end-plate on rectangular HSS with bolts on four sides under axial tension, illustrated in Figure 4, in Section 5.6 outlines three limit states: yielding of the end-plate, tensile strength of the bolts (including prying action), and strength of the weld between the HSS and the end-plate.

Figure 5

AISC Steel Design Guide 24 - Rectangular End-Plate with Bolts on Four Sides
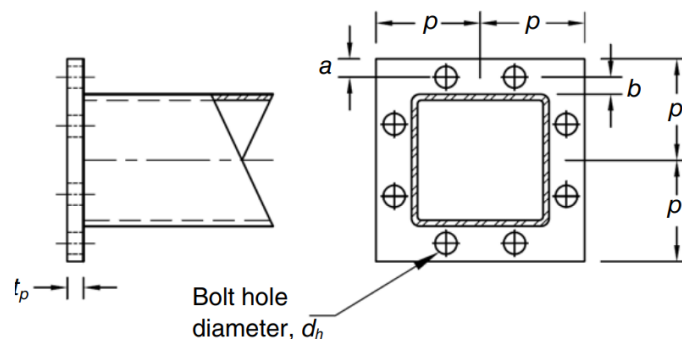
Note. Adapted from *Steel Design Guide 24: Hollow Structural Section Connections*, by J.A. Packer et al., 2010, American Institute of Steel Construction, p.53.

The design guide notes the difficulty in directly determining the capacity of this connection and

load configuration based on AISC Specification due to the complexities of prying action and

position of yield lines in the plate. The design guide does however present equations to assist in

designing the thickness of the plate, t_p, the number of bolts, n, and the weld size, w in Section

5.6. Equation (21) and Equation (22) are presented in the design guide to calculate the minimum

thickness required for no prying action to occur for LFRD and ASD, respectively. These

equations are simplified from AISC *Manual* Part 9 (Packer et al., 2010). Thus,

$$t_p \geq t_{min} = \sqrt{\frac{4.44(P_u/n)b'}{pF_{yp}}}, \tag{21}$$

$$t_p \geq t_{min} = \sqrt{\frac{6.66(P_a/n)b'}{pF_{yp}}}. \tag{22}$$

The design guide also provides equations for determining a lesser thickness that accounts for the

effects of prying action, Equations (23) and Equation (24) for LFRD and ASD, respectively.

Thus,

$$t_p \geq t_{min} = \sqrt{\frac{4.44(P_u/n)b'}{pF_{yp}(1+\delta\alpha')}}, \tag{23}$$

$$t_p \geq t_{min} = \sqrt{\frac{6.66(P_a/n)b'}{pF_{yp}(1+\delta\alpha')}}. \tag{24}$$

These equations are also adapted from AISC *Manual* Part 9. The prying action equations in this

section uses F_{yp} for the plate material strength, as experimentally validated by Willibald et al.

(2003), upon which the procedure is based, rather than higher capacity of F_{up} as in the AISC

Manual. Section 5.6 also provides equations for designing the weld based on the limit state of

shear rupture from AISC *Specification* J2.4, Equations (25) and (26) for LFRD and ASD,

respectively. Thus,

$$w \geq \frac{P_u\sqrt{2}}{F_{wc}L_w} , \tag{25}$$

$$w \geq \frac{P_a\sqrt{2}}{F_{wc}L_w} . \tag{26}$$

Limit states for HSS moment connections are covered in the examples section of chapter 4, Section 4.5. Example 4.1 involves a W-beam running over a HSS column connected by and end-plate moment connection, shown in Figure 5, and outlines the limit states that must be considered. These limit states include the effects of prying action on the W-shape flange and cap plate, tensile strength of the bolts, beam web local yielding, beam web local crippling, HSS wall strength, HSS wall local yielding, HSS wall crippling, and strength of the weld between the HSS and the end-plate.

Figure 6

AISC Steel Design Guide 24 - W-Beam Over HSS Column Connection (Moment Connection)
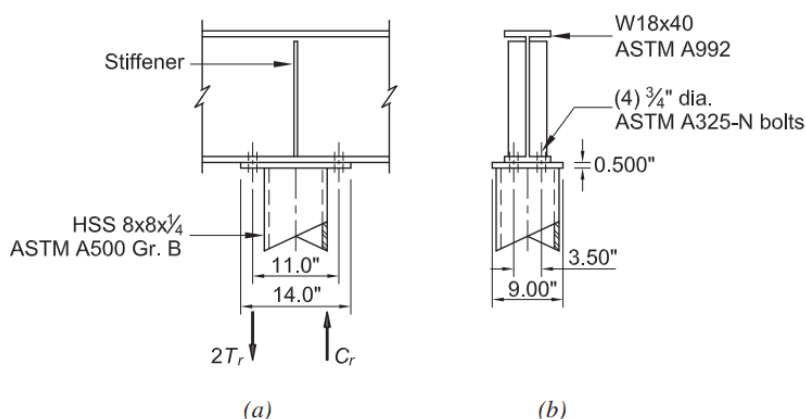
Note. Adapted from *Steel Design Guide 24: Hollow Structural Section Connections*, by J.A. Packer et al., 2010, American Institute of Steel Construction, p. 31.

A simplified check for prying action based on "no prying action" equation in Part 9 of the AISC

Manual is performed in Example 4.1 using Equations (27) and (28) for LFRD and ASD,

respectively. Prying action equations in this section use F_u, based on the prying action equation

in Part 9 of the *Manual*. Thus,

$$t_p \geq t_{min} = \sqrt{\frac{4.44 T_u b'}{p F_u}}, \tag{27}$$

$$t_p \geq t_{min} = \sqrt{\frac{6.66 T_a b'}{p F_u}}. \tag{28}$$

Example 4.1 also includes a method for designing the weld in which the effective length is

determined assuming a 45° maximum load dispersion angle. Because a moment force will put

one side of the HSS into compression, the HSS wall strength, wall local yielding, and wall local

crippling are also checked in this example.

Axial

Evaluation of the Axial Capacity of Steel HSS End-Plate Connections using

Nonlinear Finite Element Simulations and Analytical Methods

Zietlow (2022) used analytical methods and non-linear Finite Element Analysis (FEA) through ANSYS® Workbench R2 (2020) software to investigate the axial tensile capacity of HSS end-plate connections with all-around weld patterns and both side and corner bolt configurations. Figures 7 and 8 show the two FEA models investigated. Symmetry was used to simplify the model to one quarter of the specimen.

Figure 7

Axial Corner Bolt FEA Model - von Mises Stress Distribution
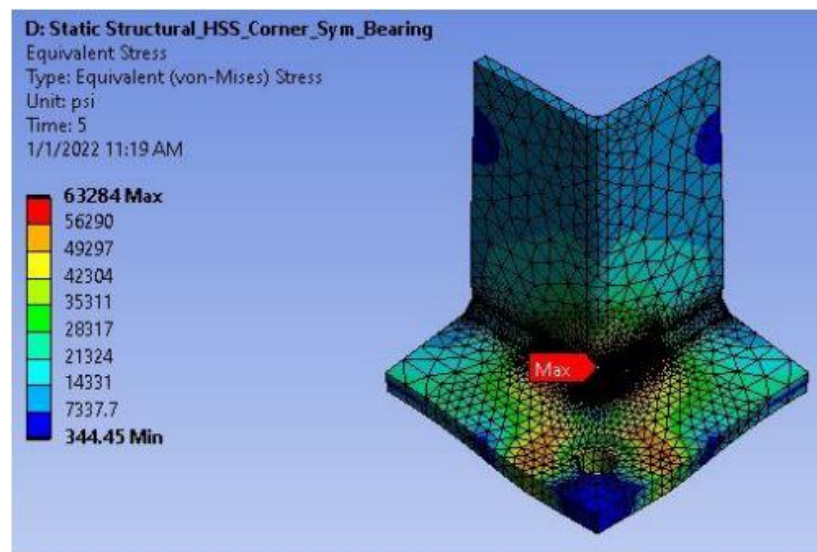
Note. Adapted from *Evaluation Of The Axial Capacity of Steel HSS End-Plate Connections Using Nonlinear Finite Element Simulations And Analytical Methods* [Unpublished master's thesis], by J. A. Zietlow, 2022, Milwaukee School of Engineering, p. 59.

Figure 8

Axial Side Bolt FEA Model - von Mises Stress Distribution
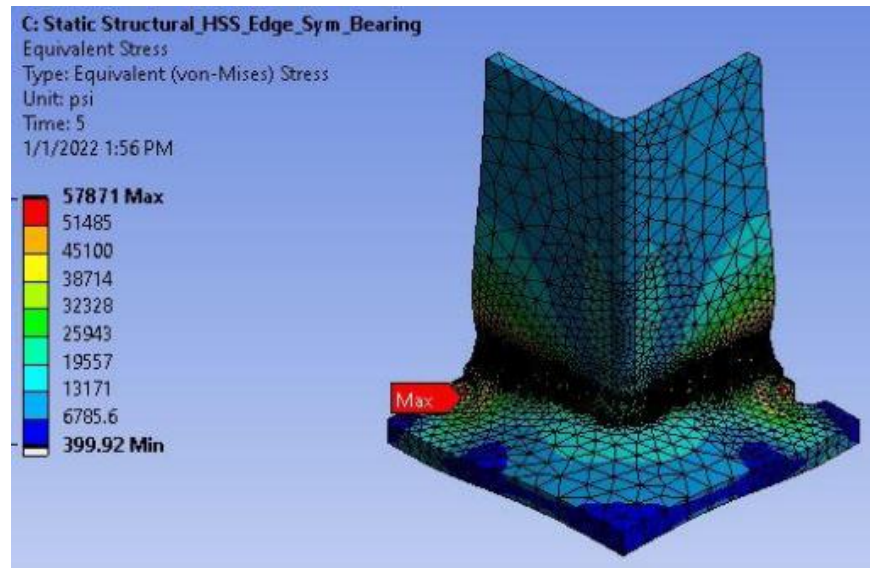
Note. Adapted from *Evaluation Of The Axial Capacity of Steel HSS End-Plate Connections Using Nonlinear Finite Element Simulations And Analytical Methods* [Unpublished master's thesis], by J. A. Zietlow, 2022, Milwaukee School of Engineering, p. 60.

For the corner bolt specimen, the maximum stress occurred in the weld at the corner of the HSS (see Figure 7). For the side bolt specimen, the maximum stress occurred at the bolt hole (see Figure 8). There was noticeable difference in the total deflection between the models, with the maximum deflection of the corner bolt specimen at an applied load of 20 kips being more than twice the maximum deflection of the side bolt specimen at an applied load of 25 kips. There was also a larger prying force in corner bolt specimen, with a maximum bolt force increase of 192% for the corner bolt specimen, while the maximum increase of 152% is seen in the side bolt specimen. The expected design strength of the connection calculated using *AISC Design Guide 24* was 119 kips, from the limit state of bolt strength (see Appendix A for calculations). However, it was found that significant plate and HSS yielding occurred at an applied load of 90

kips that would suggest a non-conservative solution from *AISC Steel Design Guide 24,* but it was

also mentioned that "these results cannot be appropriately confirmed without additional data

from experimental testing" (Zietlow, 2022, p. 73).

Determining the Validity of Design Provisions for HSS to Base Plate Connections with Corner Anchor Rods Subjected to Axial Tension

Christensen (2010) performed several tests on HSS end-plate connections with varying plate and HSS thicknesses and sizes that were subjected to axial tension to verify the procedures in the *HSS Connections Manual* (1997). The manual suggested a design procedure with an equation that considered effective plate width, yield strength, base plate thickness, and the distance from anchor rod to HSS corner to determine the strength of the connection; however, there was no physical testing to validate it at the time. In the design process, base plate behavior was described as thick, intermediate, or thin (see Figure 9). The research focused on the "plate stress-based equation" from the manual, but also investigated weld strengths and strains. Linear strain gages and strain rosettes were used to measure strain in the base plates, HSS tubes, and welds; the strain rosettes were used to determine principal stress. Plate deflection was also measured using LVDTs (Christensen, 2010).

Figure 9

Thick, Intermediate, and Thin Plate Behavior
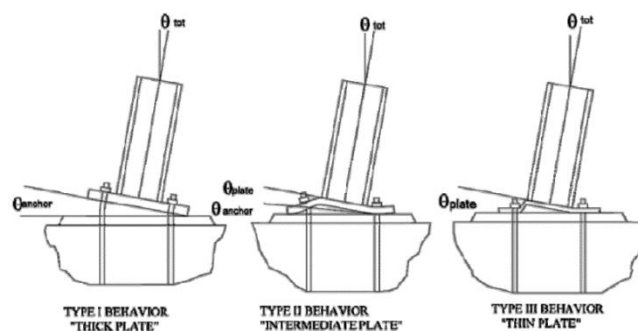
Note. Adapted from *Determining the Validity of Design Provisions for HSS to Base Plate Connections With Corner Anchor Rods Subjected to Axial Tension* [Unpublished master's thesis], H. Christensen, 2010, Milwaukee School of Engineering, p. 34.

It was found that the procedures based on plate thickness produced conservative results. The most important factor in determining plate behavior was found to be plate thickness, but HSS thickness was also found to impact stress results and was not considered in the manual (Christensen, 2010). Through the elimination of a factor from an error in the derivation of the equation and an additional factor for the HSS thickness, R_{hss}, calculations were comparable to experimental results (Christensen, 2010). The adjusted equation given for one corner of the connection was:

$$\phi P_n = \phi \frac{R_{hss} b_e t_p F_y}{L} = \phi 2 R_{hss} t_p{}^2 F_y \leq \phi \frac{4.75 R_{hss} t_p{}^2 F_y}{L}. \tag{29}$$

The results from weld data were found to be inconclusive as they did not match calculated design strength produced by the procedures in the manual; further investigation on weld strength was recommended.

Yield Line Approaches for Design of End-Plate Tension Connections for Square and Rectangular HSS Members Using End-Plate Tensile Strength

Thornton (2017) used experimental data for HSS end-plate connection subjected to axial tension produced by Willibald, Packer, and Puthli (2002, 2003); Kato and Mukai (1985); and Caravaggio (1988) to validate a design method based on the tensile strength F_u. The three bolt patterns considered in this paper, A, B, and C, are shown in Figure 10. The yield lines considered for each pattern are also shown in Figure 10.

> There are many possible yield line families are available for each of the three bolt patterns. For instance, circular yield lines at the HSS corners with radial fans are a possible family, as are straight line yield families. The author has reviewed a number of possibilities and determined by "trial and error" that the families chosen for this paper give the best correlation to the test data. (Thornton W. A., 2017, p. 142)

There were 55 physical tests available: 26 for pattern A, 2 for pattern B, and 27 for pattern C (Thornton W. A., 2017).

Figure 10

Bolt Patterns A, B, and C and associated Yield Lines
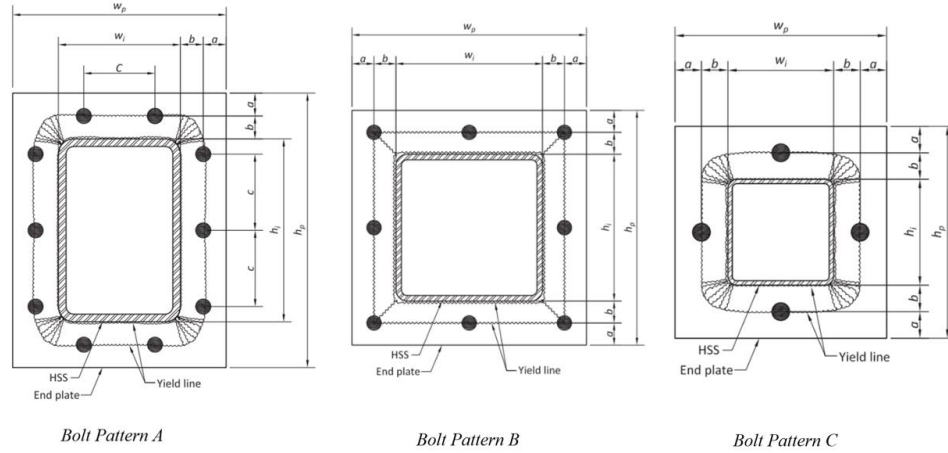
Bolt Pattern A   Bolt Pattern B   Bolt Pattern C

Note. Adapted From "Yield Line Approaches for Design of End-Plate Tension Connections for Square and Rectangular HSS Members Using End-Plate Tensile Strengths", W. A. Thornton, 2017, *Engineering Journal, 54*, p. 142-143.

An equation for the tributary bolt length, *p*, is given for each bolt pattern: Equation (30) for pattern A, Equation (31) for pattern B, and Equation (32) for pattern C (Thornton W. A., 2017):

$$p_a = \frac{2(w_i + h_i + \pi b)}{n}, \tag{30}$$

$$p_b = \frac{2(w_i + h_i + 4b)}{n}, \tag{31}$$

$$p_c = \frac{2(w_i + h_i + \pi b)}{n}. \tag{32}$$

It is assumed that the yield patterns shown in Figure 10 will develop as shown, but if the bolt spacing is too large, yield lines with less capacity than calculated by the above equations can develop (Thornton W. A., 2017). Dowswell (2011) showed that if the tributary length greater

than that shown in Figure 11, independent yield line with less capacity can develop at each bolt

(Thornton W. A., 2017).

Figure 11

Local Yield Line Pattern
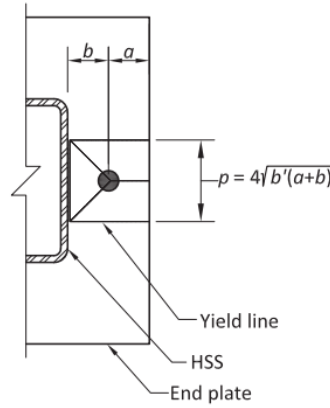
Note. Adapted From "Yield Line Approaches for Design of End-Plate Tension Connections for Square

and Rectangular HSS Members Using End-Plate Tensile Strengths", W. A. Thornton, 2017, *Engineering*

Journal, 54, p. 144.

Therefore, the tributary lengths p_a, p_b, and p_c are limited to:

$$p_{i,max} = 4\sqrt{b'(a + b)}. \tag{33}$$

This prevents the localized pattern from developing and maintains the validity of the patterns

assumed in Figure 10 (Thornton W. A., 2017).

Flexural

Design Model for Bolted Moment End-Plate Connections using Rectangular

Hollow Sections

Wheeler, Clarke, Hancock, and Murray (1998) developed an analytical design model for

HSS moment end-plate connections, of the type shown in Figure 12, subject to "pure flexural

bending" based on the modified stub tee (split tee) analogy and yield line analysis; comparisons

were made with the predictions from the design model to results from experimental testing

conducted on physical connections (Wheeler et al., 1995, 1997).

Figure 12

End-Plate Layout and Variables

Note. Adapted from "Design Model for Bolted Moment End-Plate Connections Using Rectangular Hollow

Sections", by A. T. Wheeler et al., 1998, *Journal of Structural Engineering, 124*(2), p. 165,

(doi:https://doi.org/10.1061/(ASCE)0733-9445(1998)124:2(164)).

Three yield line mechanisms were observed experimentally and are shown in Figure 13.

Figure 13

Three Yield Line Modes of Failure
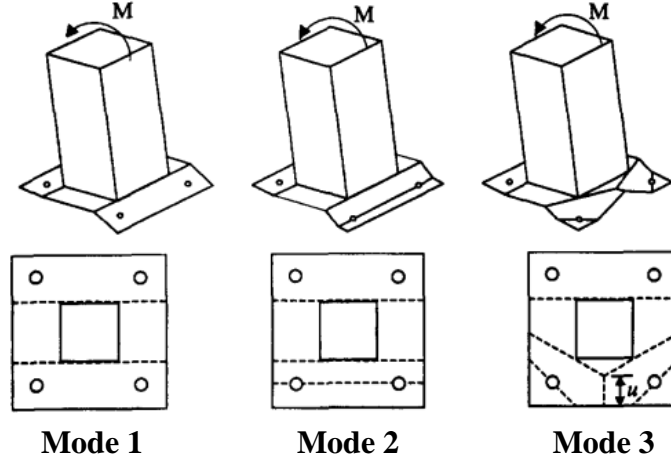
| Mode 1 | Mode 2 | Mode 3 |

Note. Adapted from "Design Model for Bolted Moment End-Plate Connections Using Rectangular Hollow Sections", by A. T. Wheeler et al., 1998, *Journal of Structural Engineering, 124*(2), p. 167, (doi:https://doi.org/10.1061/(ASCE)0733-9445(1998)124:2(164)).

Virtual work principles were used to obtain the analytical expressions for the yield moment for each mechanism, or mode. The three plate behaviors of thin, intermediate, and thick are considered and equations for the bolt force, including prying forces when applicable, and the moment capacity are derived. Ultimately equations are adapted for the capacity of the connection when limited by bolt failure and when limited by end-plate failure, Equations (34) and (35), respectively:

$$\phi_b M_{cb} = \phi_b \left(\frac{4n\left(B_{u1}a_p + \frac{\pi d_b{}^3 f_{yb}}{32}\right)d' + w_{eq}\left(d' + 2\left(s_0' + a_p\right)\right)t_p{}^2 f_p}{4\left(a_p + s_0'\right)d'} \right)(d - t_s), \qquad (34)$$

$$\phi_p M_{cp} = \phi_p \left(\frac{t_p{}^2 f_p\left(w_{eq}(d' + 2s_0')\right) + \left(w_{eq} - nd_f\right) + n\frac{\pi d_b{}^3 f_{yb}}{8}d'}{4d's_0'} \right)(d - t_s). \qquad (35)$$

The model presented is "simple and accurate" and is limited to square and rectangular HSS with

two bolt rows, one above the top flange and one below the bottom flange (Wheeler, Clarke,

Hancock, & Murray, 1998). The model was verified by experimentally tested connections with

only two bolts per row; however, it is stated:

> …the addition of extra bolts in the tensile (and compressive) bolt rows does not
>
> invalidate the model. The reason for this is that the use of additional bolts in the tensile
>
> row tends to enforce a mode 2 end-plate failure to which the model presented in this
>
> paper is well suited. (Wheeler et al., 1998, p.173)

It is recommended that connections be designed to act with intermediate behavior with the

connection strength being limited by bolt failure. Equations are also presented for serviceability

based on bolt and end-plate yielding, respectively:

$$\phi_b M_{cbs} = \phi_b \left(\frac{\left(d' + 2(s_0' + a_e)\right) w_{eq} t_p^2 f_y}{4(s_0' + a_e) d'} + \frac{n B_{yl} a_e}{s_0' + a_e} \right)(d - t_s), \tag{36}$$

$$\phi_p M_{cps} = \phi_p \left(\frac{\left((d' + s_0') w_{eq} - n d_f d'\right) t_p^2 f_y}{2 s_0' d'} \right)(d - t_s). \tag{37}$$

Welds

Weld Behavior in a Rectangular HSS Base Plate Connection with Corner Anchor Rods Subjected to an Axial Tensile Force

Following the research conducted by Christensen (2010) on axially loaded HSS end-plate connections, further research was conducted by Wilsmann (2012) with a focus on weld strength and validating the procedures for designing weld strength in the *HSS Connections Manual* (1997). Physical testing was done on specimens with varying base plate geometry and HSS size. Linear and rosette strain gages were placed on the weld to measure strain along its length, and LVDTs were used to measure displacements of the base plate and HSS column.

The experimental results were compared to two equations:

$$\phi R_n = \phi_w F_w W_t (4), \tag{38}$$

$$\phi R_n = \phi_p (50) W_t t_p^{1.5}, \tag{39}$$

where (4) and (50) are values for the effective length and grade of steel. The design capacity from Equation (38) is based on electrode strength and weld size. The design capacity from Equation (39) is based on weld size and plate thickness. Equation (38) was found to over calculate the weld strength because the four-inch effective length was not achieved in any of the tests. It was recommended that Equation (38) be modified to account for the effects from connection geometry on effective weld length, including plate size, anchor location, and HSS size. Equation (39) was determined to be overly conservative in determining weld strength and the origin could not be determined through literature review; because of these issues, it was recommended that Equation (39) be disregarded.

Numerical Investigation of Fillet Welds in HSS-to-Rigid End-Plate Connections

Tousignant and Packer (2017) perfomed a finite-element (FE) investigation on the behavior of fillet-welded HSS rigid end-plate connections. The validity of the FE models were confirmed by comparison to 33 experimental tests and then a parametric study was performed on 73 FE models. The FE models consisted of both rectangular hollow sections (RHS) and circular hollow sections (CHS) rigid end-plate connections that were tested to failure under axial tension loading. The study investigated "…the effect of the ratio of the weld throat dimension to the branch wall thickness (t_w/t_b), the branch wall slenderness (D_b/t_b and B_b/t_b), and the branch inclination angle (θ_i) on the weld strength" (Tousignant & Packer, 2017, p. 14). See Figures 14 and 15.

Figure 14

HSS-To-Rigid Welded End-Plate Connection
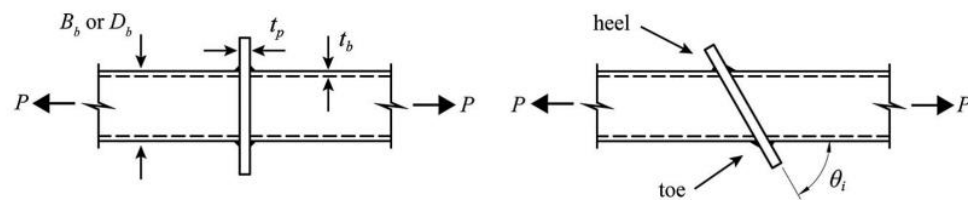
Note. Adapted from "Numerical Investigation of Fillet Welds in HSS-to-Rigid End-Plate Connections", K. Tousignant and J. Packer, 2017, *Journal of Structural Engineering, 143*(12), p. 2 (doi:10.1061/(ASCE)ST.1943-541X.0001889).

Figure 15

Effective Fillet Weld Dimensions
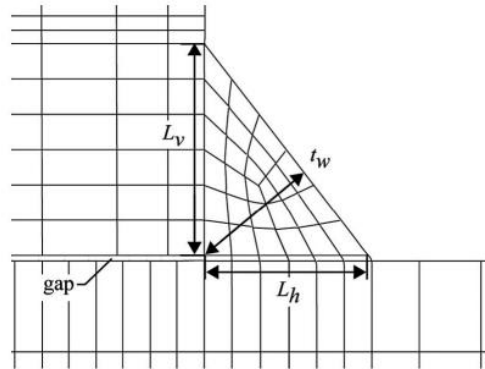
Note. Adapted from "Numerical Investigation of Fillet Welds in HSS-to-Rigid End-Plate Connections", K.

Tousignant and J. Packer, 2017, *Journal of Structural Engineering, 143*(12), p. 3

(doi:10.1061/(ASCE)ST.1943-541X.0001889).

It was found that:

> As t_w/t_b increases, the average stress on the weld throat area at failure significantly
>
> decreases. As D_b/t_b and B_b/t_b increase, the average stress on the weld throat area at failure
>
> slightly decreases. The branch inclination angle θ_i has a negligible effect on the weld
>
> strength per unit throat area; however, the longer weld length that results from a
>
> reduction in branch angle increases the absolute strength of the weld. (Tousignant &
>
> Packer, 2017, p. 14)

Simplified equations for the required weld strength for both RHS and CHS connections were

developed, Equations (40) and (41), respectively. Thus,

$$R_n = \left[0.90 - 0.25\left(\frac{P_r}{P_y}\right)\right] A_w X_u, \tag{40}$$

$$R_n = \left[1.00 - 0.25\left(\frac{P_r}{P_y}\right)\right] A_w X_u. \tag{41}$$

Based on Equations (40) and (41), the required weld size, t_w, can be determined as a function of

the branch wall thickness, t_b. Equations to calculate t_w for both RHS and CHS are given as

Equations (42) and (43), respectively:

$$t_w = \frac{1}{0.65}\left(\frac{F_y}{X_u}\right) t_b, \tag{42}$$

$$t_w = \frac{1}{0.75}\left(\frac{F_y}{X_u}\right) t_b. \tag{43}$$

It was ultimately recommended that "for all HSS connections, including HSS-to-HSS

connections where the effective length concept is used, and even HSS connections in which the

welds are "fully effective", the current AISC and Canadian Standards Association (CSA)

provisions (ANSI/AISC 360-16 and CSA S16-14, respectively) for the design of fillet welds be

used without the directional strength increase factor, or the presented alternative method be used

with North American resistance factors (Tousignant & Packer, 2017).

Methods

To test the validity of *AISC Design Guide 24* design procedures and the variables affecting the capacity of HSS end-plate connections, the initial test matrix in Table 4 was developed, with Phase 1 consisting of twelve HSS specimens subjected to axial loading (axial tests) and Phase 2 consisting of twelve HSS specimens subjected to lateral loading (flexural tests). The steel for this testing was donated by Zalk Josephs fabricators, and due to their availability of steel, HSS7x7x5/16 was the selected shape for axial tests and HSS7x4x5/16 was selected for flexural tests.

Table 4

Test Matrix

Weld Type		Experimental Tests and Phases				Instrumentation		
		PHASE 1 Axial Test		PHASE 2 Flexural Test		Number of Linear Strain Gauges	Number of Rosette Strain Gauges	Number of LVDT or String Pots.
		HSS 7x7x5/16		HSS 7x4x5/16		4 per specimen	1 per axial specimen 2 per flex Specimen	for all specimens
All-around		Bolts at Corners	3	Strong Axis Bending Bolts at Corners	3	48	18	
		Bolts at Sides	3	Weak Axis Bending Bolts at Corners	3			
Workable Flat Edges		Bolts at Corners	3	Strong Axis Bending Bolts at Corners	3	48	18	4
		Bolts at Sides	3	Weak Axis Bending Bolts at Corners	3			

Phase 1: Axial

For the axial tests, two variable bolt patterns, side and corner located bolts, were used.

Two variable weld patterns, all-around and workable-flat edges, were also used. Initially, as

Table 4 suggests, the twelve specimens were divided into four categories of three specimens

based on the differing bolt and weld patterns: three all-around weld corner bolted (AACB), three

all-around weld side bolted (AASB), three workable-flat welds corner bolted (WFCB), and three

workable-flat welds side bolted (WFSB). However, there were only two WFSB specimens and

four AASB specimens tested. Figure 16 shows the different bolt and weld patterns of the

specimens and the comparisons to be made between them. Figure 17 provides a closer look at the

different weld patterns.

Figure 16

Axial Specimens Variables and Comparisons

All-around Weld/Bolts at Corners

All-around Weld/Bolts at Sides

Workable Flat Edges Weld/Bolts at Corners

Workable Flat Edges Weld/Bolts at Sides
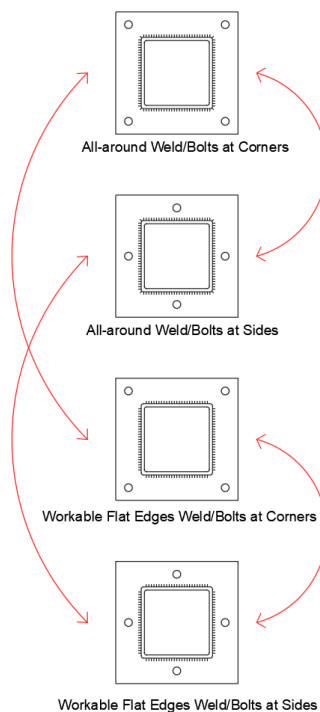
Figure 17

Weld Patterns

Initial calculations to size the axially loaded HSS end-plate connections were done by

Zietlow (2022). See Appendix A for all calculations. Figure 18 shows the configurations and

dimensions for the axial specimens. As previously mentioned HSS7x7x5/16 was used for all

axial specimens. The HSS was centered on the base plate. The base plate was twelve inches by

twelve inches (12 in. x 12 in.). A distance of one and one quarter inch (1 ¼ in.) was used for both

edge distances for the corner bolts and the one edge for the side bolts. The side bolts were

centered on the plate, or six inches (6 in.) from either edge. Rearranging Equation (25) and using

a one-quarter inch (¼ in.) fillet weld and an effective length of twenty-eight inches (28 in.), the

weld strength, from the limit state of weld rupture, was calculated to be 155.9 kips. The available

strength from the limit states of HSS yield, HSS rupture, and bolt strength were 341.5 kips, 352.9

kips, and 119.2 kips, respectively. Therefore, the limiting available strength was 119.2 kips, from

the available bolt strength; this strength was used in Equations (21) and (23), resulting in a

minimum base plate thickness based on prying action to be calculated as 0.439 inch; therefore,

base plates with thicknesses of one-half inch (0.500 in.) were used. Because the base plate was

the focus of this research, the cap plate thickness was increased by one and a half times the base

plate thickness. See Appendix D for full structural drawings and Appendix E for shop drawings

of the specimens.

Figure 18

Axial Specimen Structural Drawings
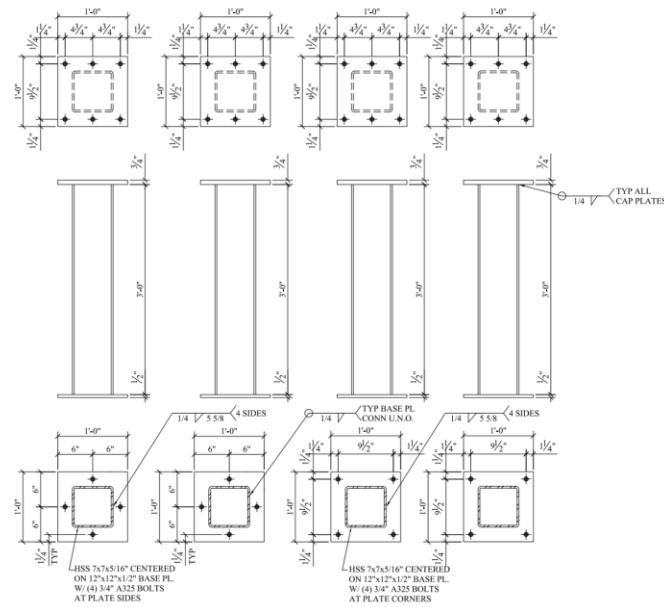
An existing test frame was used to anchor the specimens for loading. Figure 19 shows a diagram of the test setup.

Figure 19

Axial Specimen Test Frame and Setup
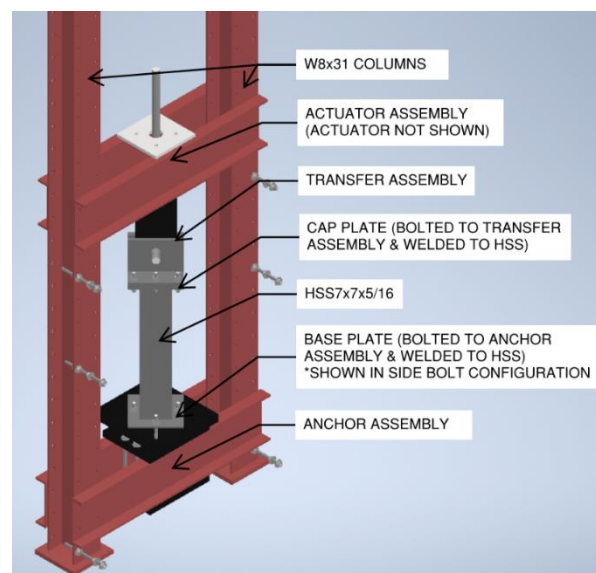
The test frame consists of two W8x31 columns with C12x20.7 cross beams for the actuator and

anchor assemblies. The actuator assembly is located above test specimen and consists of an

actuator anchored between two plates to the two C12 cross beams. The load is transferred

through the transfer assembly, consisting of a threaded rods and built-up plate connections, to the

cap plate of the HSS. See Figure 20 for a photo of the upper portion of the test setup.

Figure 20

Axial Test Setup Actuator and Transfer Assemblies

The force is transferred through the cap plate into the HSS, then through the HSS and into the

base plate. The base plate is held in place by the anchor assembly. The base plate was the focus

of this research; thus, every other part of the test setup was sized to have greater capacity.

The actuator used to apply the axial tensile load to the specimen was an Enerpac Model

RRH-606; the load was measured with a Sensotec Model 41-A530-01-03 load cell. The

maximum load limit was 100,000 lbs (100 kips). Instrumentation, strain gages and LVDTs, were

used to measure the strains and displacements, respectively. Figures 21, 22, and 23 show the

positioning of instrumentation. For full instrumentation plans see Appendix F.

Figure 21

Axial Tests Instrumentation Plans
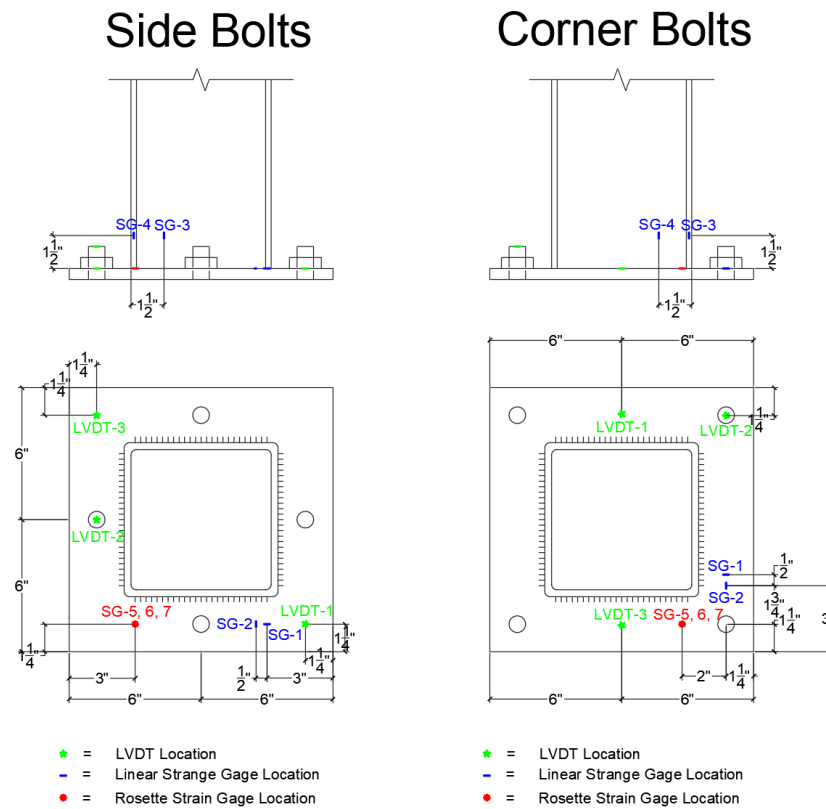
Figure 22

Axial Corner Bolt Specimen Strain Gages

Figure 23

Axial Side Bolt Specimen Strain Gages

Four linear strain gages (SG-1, SG-2, SG-3, SG-4) and one rosette strain gage (SG-5, SG-6, SG-7) were applied to each specimen. See Figure 24 for the rosette strain gage layout. Two LVDTs (LVDT-1 and LVDT-3) were used for all tests; for the first two tests an additional LVDT (LVDT-2) was placed on top of a bolt, but after bolt rupture on the second test (WFCB01) it was not used.

Figure 24

Rosette Strain Gage Layout
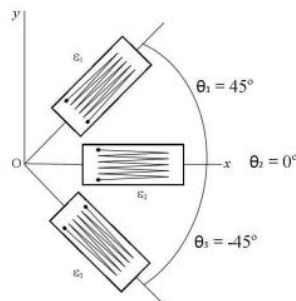
Phase 2: Flexural

For the flexural tests, two variable HSS orientations, strong axis and weak axis bending, were used. The two variable weld patterns, all-around and workable-flat, were also used. As Table 4 suggests, the twelve specimens were divided into four categories of three specimens each based on the differing bolt and weld patterns: three all-around weld strong axis bending (AAST), three all-around weld strong axis bending (AAST), three workable-flat welds weak axis bending (WFWK), and three workable-flat welds strong axis bending (WFST). Figure 25 shows the different bolt and weld patterns of the specimens and the comparisons to be made between them.

Figure 25

Axial Specimens Variables and Comparisons

All-around Weld/Strong Axis Bending

All-around Weld/Weak Axis Bending

Workable Flat Edges Weld/Strong Axis Bending

Workable Flat Edges Weld/Weak Axis Bending
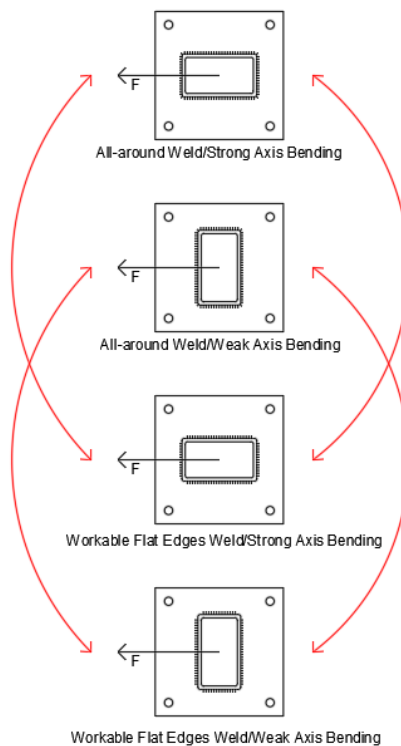
Initial calculations to size the laterally loaded HSS end-plate connections were also done by Zietlow (2022). See Appendix A for all calculations. Figure 26 shows the configurations and dimensions for the axial specimens. As previously mentioned HSS7x4x5/16 was used for all flexural specimens. The HSS was centered on the base plate. The base plate was twelve inches by twelve inches (12 in. x 12 in.). A distance of one and one quarter inch (1 ¼ in.) was used for edge distances for the bolts. Rearranging Equation (25) and using a one-quarter inch (¼ in.) fillet weld and an effective length of twenty-two inches (22 in.), the weld strength, from the limit state of weld rupture, was calculated to be 122.5 kips. The available strength from the limit states of HSS yield, HSS rupture, and bolt strength were 263.2 kips, 272.0 kips, and 119.2 kips, respectively. Therefore, the limiting available strength was 119.2 kips, from the available bolt strength; this strength was used in Equations (21) and (23), resulting in a minimum base plate thickness based on prying action to be calculated as 0.599 inch; therefore, base plates with thicknesses of five-eighths inch (0.625 in.) were used. Because the base plate was the focus of this research, the cap plate thickness was increased by one and a half times the base plate thickness. See Appendix D for full structural drawings and Appendix E for shop drawings of the specimens.

Figure 26

Axial Specimen Structural Drawings

An existing test frame was used to anchor the specimens for loading. Figure 27 shows a diagram of the test setup.
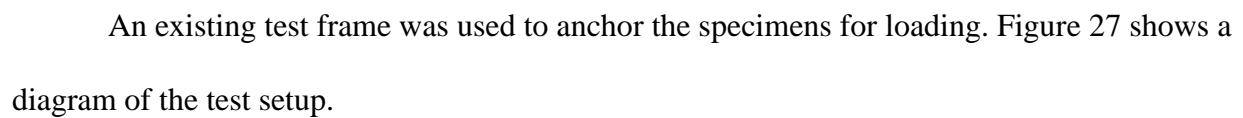
Figure 27

Flexural Specimen Test Frame and Setup
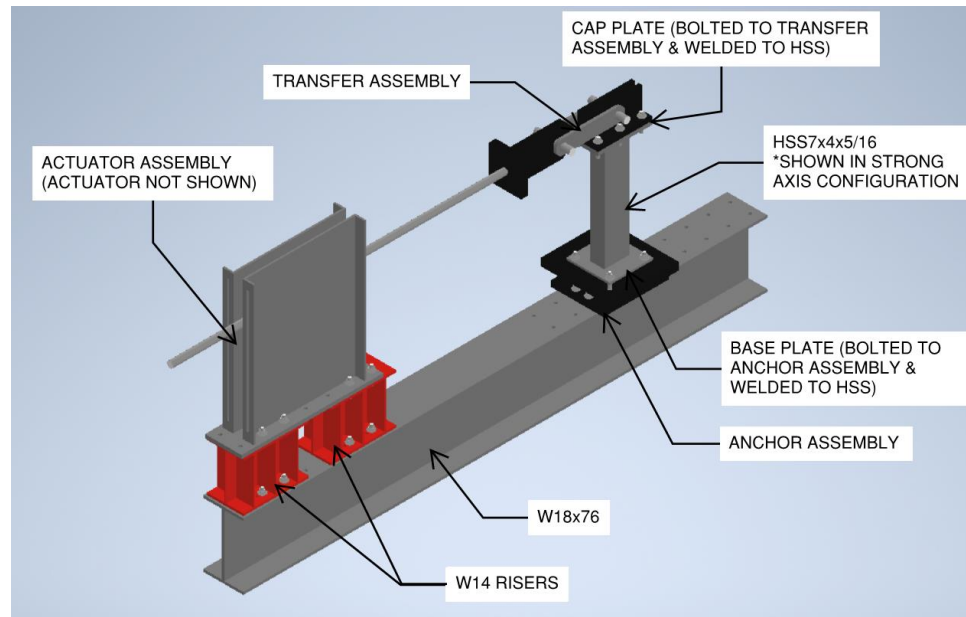
The test frame consists of a W18x76 beam base. The actuator assembly consists of an actuator

connected to a plate assembly that is then connected through two W14 risers to the base. The

force from the actuator is transferred through the transfer assembly, consisting of threaded rods

and built-up plate connections, to the HSS cap plate, then through the cap plate into the HSS, and

finally through the HSS and into the base plate. The base plate is held in place by the anchor

assembly, which is attached to the base. The base plate was the focus of this research; thus, every

other part of the test setup was sized to have greater capacity.

The actuator used to apply the lateral load to the specimen was an Enerpac Model RRH-

606; the load was measured with a Sensotec Model 41-A530-01-03 load cell. The maximum load

limit was 100,000 lbs (100 kips). Instrumentation, strain gages and LVDTs, were used to

measure the strains and displacements, respectively. Figures 28 to 31 show the positioning of

instrumentation. For instrumentation plans see Appendix F.

Figure 28

Axial Tests Instrumentation Plans
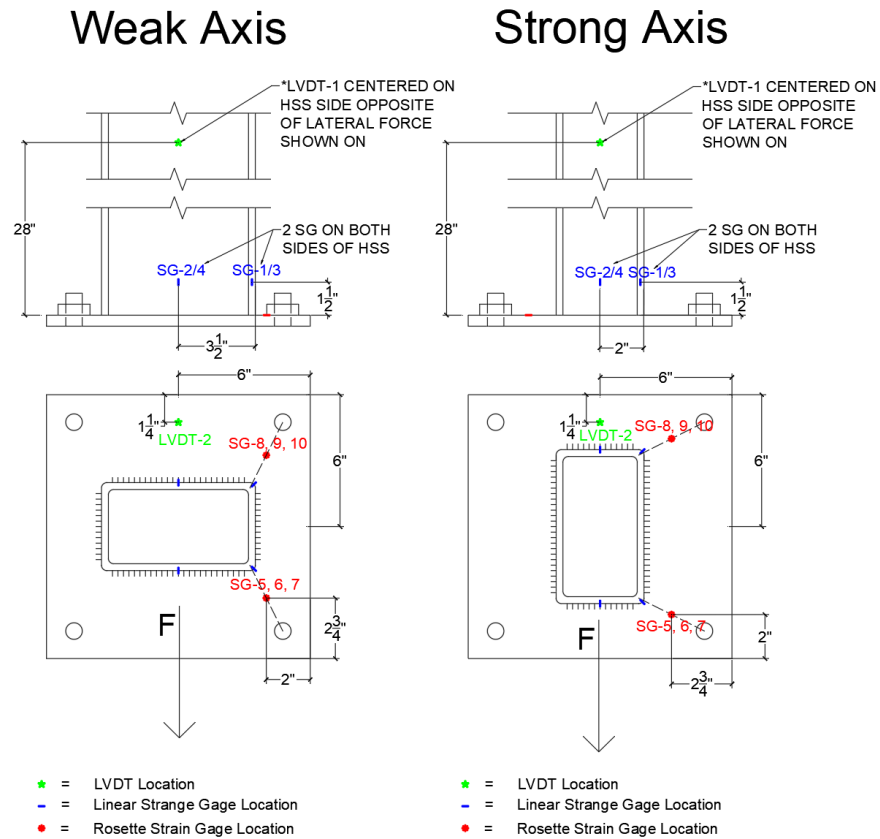
Figure 29

Flexural Specimen Compression Side Strain Gages
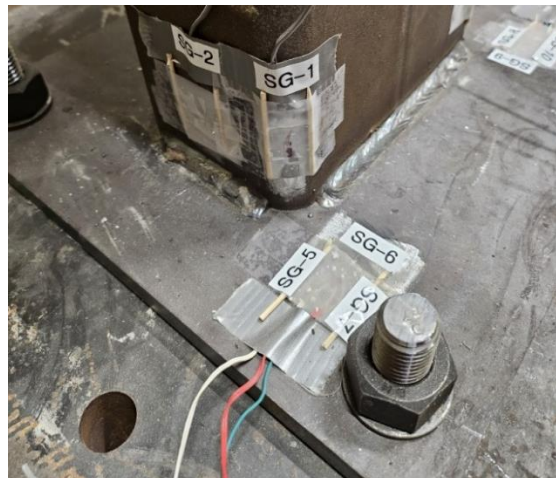
Figure 30

Flexural Specimen Tension Side Strain Gages

Figure 31

Flexural Specimen LVDT 1

Four linear strain gages (SG-1, SG-2, SG-3, SG-4) and two rosette strain gage (one consisting of

SG-5, SG-6, SG-7 and the other consisting of SG-8, SG-9, SG-10) were applied to each

specimen. See Figure 24 for the rosette strain gage layout. Two LVDTs (LVDT-1 and LVDT-2)

were used for all tests. LVDT-1 was placed twenty-eight inches up from the end-plate on the

side of the HSS to measure lateral displacement. LVDT-2 was placed on the end-plate between

the bolts on the tension side to measure end-plate deformation.

Material Strengths

Threaded rods were used in various parts of the test setup. Four three-quarter inch (¾ in.) diameter ASTM A193, Grade B7, were used to anchor the base plate to the anchor assembly for all axial and flexural tests. ASTM A193, Grade B7, rods were selected because of availability and having similar material properties to ASTM A325 bolts and ASTM F1852 threaded rods, which were used in the initial calculations performed by Zietlow (2022). See Tables 5 and 6 for ASTM A193 and ASTM A325/ASTM F1852 material properties, respectively. Because the base plate was the focus of the research, all threaded rods elsewhere, used for the transfer, anchor, and cap plate assemblies, were high strength ASTM A354, Grade B, threaded rods.

Table 5

ASTM A193 Mechanical Properties

A193 Mechanical Properties

Grade	Size	Tensile ksi, min	Yield, ksi, min	Elong, %, min	RA % min
	Up to 2-1/2	125	105	16	50
B7	2-5/8 - 4	115	95	16	50
	4-1/8 - 7	100	75	18	50

Note. Adapted from *ASTM A193*, by Portland Bolt, retrieved November, 2023,

https://www.portlandbolt.com/technical/specifications/astm-a193/

Table 6

ASTM A325/F1852 Mechanical Properties

F3125 Mechanical Properties

Grade	Tensile, ksi	Yield, ksi min	Elongation, % min	RA, % min
120ksi (A325/F1852)	120 min	92	14	35
150ksi (A490/F2280)	150-173	130	14	40

Note. Adapted from *ASTM F3125*, by Portland Bolt, retrieved November, 2023,

https://www.portlandbolt.com/technical/specifications/astm-f3125/

The plate used for the specimens was certified to be in conformace with both ASTM

A36, "Standard Specification for Carbon Structural Steel," and ASTM A572, Grade 50,

"Standard Specification for High-Strength Low-Alloy Columbium-Vanadium Structural Steels."

The HSS used for the specimens was certified to be in conformance with ASTM A500, Grade B,

"Standard Specification for Cold-Formed Welded and Seamless Carbon Steel Structural Tubing

in Rounds and Shapes," and ASTM A1085, "Standard Specification for Cold-Formed Welded

Carbon Steel Hollow Structural Sections (HSS)." See Table 7 for results of a tensile test report

from Metallurgical Associates, Inc. See Appendix G for the full report. For the plate, the average

tensile strength was 82.9 ksi, and the average yield strength was 57.1 ksi. For the HSS, the

average tensile strength was 66.8 ksi, and the average yield strength was 53.2 ksi. The HSS

likely also conforms to ASTM A500 Grade C, but it was not formally confirmed by

Metallurgical Associates.

Table 7

Tensile Testing Report

Property	Plate 1	Plate 2	Plate 3	ASTM A36	ASTM A572, Grade 50
Test Bar Dimensions, Diameter, inch	0.496	0.495	0.496	D	D
Gage Length, inches	2.0	2.0	2.0	4D	4D
Tensile Strength, psi	82,900	82,900	82,900	58,000 - 80,000	65,000 min.
Yield Strength, psi (1)	57,300	56,900	57,200	36,000 min.	50,000 min.
Elongation, %	30	30	29	23 min.	21 min.
Elongation, %	67	66	67	Not Specified	Not Specified

Property	Tube 1	Tube 2	Tube 3	ASTM A500, Grade B	ASTM A1085
Test Bar Dimensions Width, inch	0.493	0.489	0.493	0.50	0.50
Thickness, inch	0.295	0.293	0.293	Material Thickness	Material Thickness
Gage Length, inches	2.0	2.0	2.0	2.0	2.0
Tensile Strength, psi	65,500	67,200	67,700	58,000 min.	65,000 min.
Yield Strength, psi (1)	53,100	53,300	53,300	46,000 min.	50,000 - 70,000
Elongation, %	35	32	32	23 min.	21 min.

(1): at 0.2% offset

Results and Discussion

Phase 1: Axial

Twelve physical axial specimens were tested. Load versus strain plots were made with strain readings from all strain gages for each specimen. Load versus displacement plots with displacement from all LVDTs were made for each specimen and the average displacement for each specimen was calculated. All plots with locations of strain gages and LVDTs can be found in Appendix B. Table 8 provides a summary of the tests and the maximum measured tension forces and displacements. Figure 32 shows a plot of the average maximum tension loads versus the average maximum displacement for the different end-plate configurations.

Table 8

Axial Tests Maximum Tension Forces and Displacements

Weld Pattern	Bolt Pattern	Specimen	Max Tension Force (lb)*	Max Displacement (in)	Average Max Tension Force (lb)	Average Max Displacement (in)
All-Around Weld	Corner Bolts	AACB01	100002	0.554	99974	0.673
		AACB02	99962	0.741		
		AACB03	99958	0.723		
	Side Bolts	AASB01	99959	0.076	99844	0.089
		AASB02	99573	0.084		
		AASB03	100000	0.107		
		AASB04	99968	0.075		
Workable-Flat Welds	Corner Bolts	WFCB01	90771	1.321	89494	1.308
		WFCB02	89564	1.441		
		WFCB03	88147	1.162		
	Side Bolts	WFSB01	100001	0.140	99957	0.096
		WFSB02	99912	0.053		
*The load cell upper limit is 100 kips. Tests conducted often exceeded the load cell's maximum capacity.						

Figure 32

Axial Tests Average Tension Loads versus Average Displacements
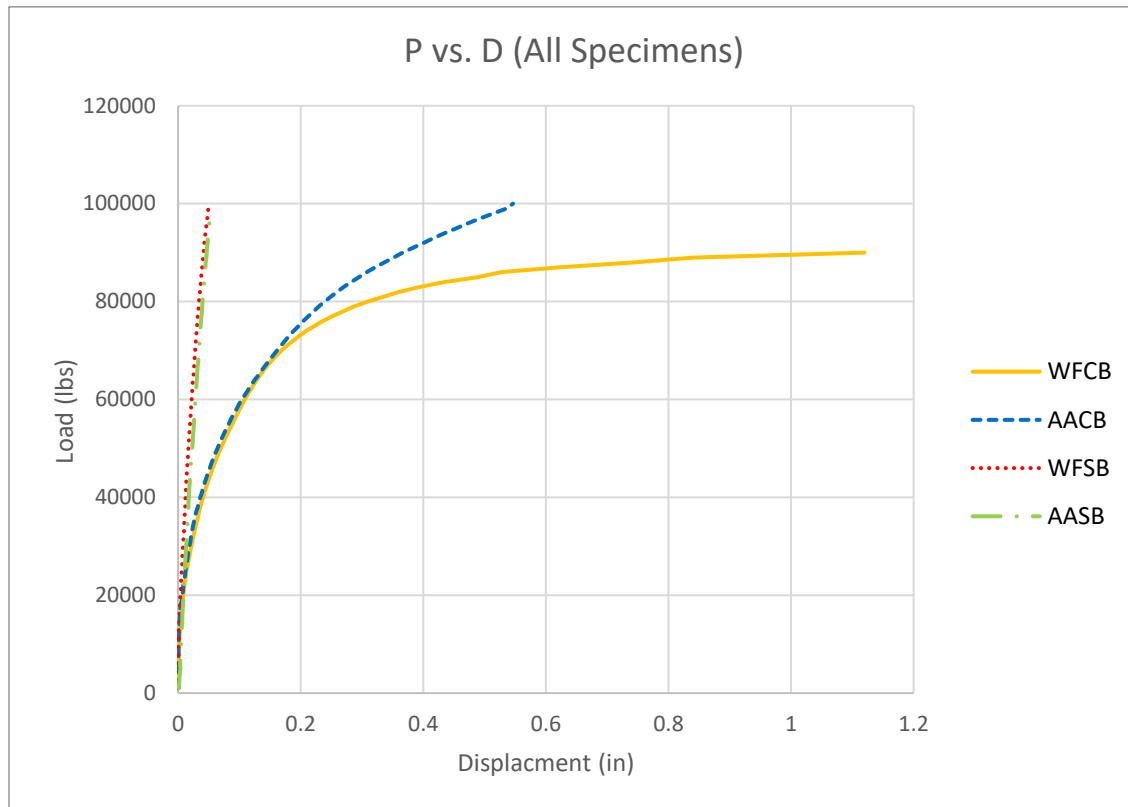
The specimens with corner bolt patterns had significant yielding and high displacements compared to the specimens with side bolt patterns with almost no yielding and very small displacements, as seen in Figures 33 and 34. The strain for the specimens with corner bolts showed higher and more concentrated stress closer to the hole, perpendicular to the HSS, and up into the corner of the HSS whereas the strain for the specimens with side bolts show lower and better distributed stress with higher strain parallel to the HSS and in the HSS side wall.

Figure 33

Axial First Trial Specimen Comparison
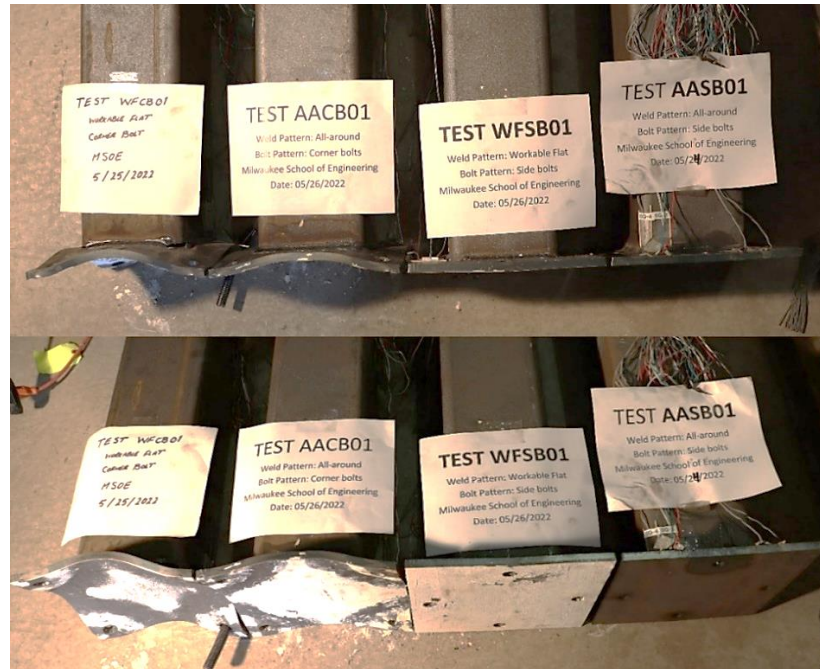
Figure 34

Axial Second Trial Specimen Comparison

All-Around Weld with Corner Bolts (AACB)

This configuration was tested to the 100-kip capacity of the load cell. The base plate

exhibited significant yielding with an average maximum displacement of 0.673 in. The highest

strain values of 6000 to 10000 µin/in occur at the strain gages closest to the holes (SG-2 and SG-

5). SG-2 was perpendicular to the HSS, and SG-5 was at a 135-degree angle in line with the

corner of the HSS (for all strain gage locations and orientations see Appendices B and F). SG-3,

located on the corner of the HSS, had higher strain than SG-4 which was located one- and one-

half inches away from the corner. There was slight bending and permanent deformation visible

in the rods indicating they have yielded, but very little to no rupture visually apparent in the

welds.

Workable-Flat Welds with Corner Bolts (WFCB)

This configuration was tested to its ultimate capacity, with two of the three specimens

being loaded to rupture of the rods with an average maximum load of just under 90 kips. The

specimens had significant deformation and yielding with an average maximum plate

displacement of 1.308 in. The strain values were similar to that of the all-around weld specimens

with the highest strain of 6000 to 8000 µin/in occurring at the strain gages closest to the holes

(SG-2 and SG-5). SG-3 again had higher strains than SG-4. Rupture was observable at the ends

of the welds and significant bending and permanent deformation was observable in the rods.

Some of these specimens also exhibited rupture in the rods, after the specimens were loaded past

their ultimate strength, as shown in Figures 35 and 36.

Figure 35

WFCB01 Bolt Rupture

Figure 36

WFCB02 Bolt Rupture

This rupture was likely caused by prying action as the plate exhibited significant yielding. In the initial calculations the thickness of the plate was determined by using the controlling limit state of the bolt tensile strength for A325 bolts to be under one-half inch and it was verified for the change to A193 rods to still be under one-half inch; see calculations in Appendix A. However, the equations used from *AISC Design Guide 24* are for a side bolt configuration and may not be directly applicable to the corner bolt configuration.

All-Around Weld with Side Bolts (AASB)

This configuration was tested to the 100-kip capacity of the load cell used in this testing, and the specimen did not undergo any significant yielding with a small max displacement of 0.089 in. The highest strains of 1000 to 2000 µin/in occurred at SG-1 and SG-5. SG-1 was parallel to the HSS, and SG-5 was at a 135-degree angle. SG-3, located on the HSS one- and one-half inch from the corner, had higher strain than SG-4, located on the HSS corner, for all specimens. There was no observable bending or permanent deformation in the rods and no observable rupture in the welds.

Workable-Flat Welds with Side Bolts (WFSB)

This configuration was tested to the 100-kip capacity of the load cell used in this testing, and the specimen did not undergo any significant yielding with a small max displacement of 0.096 in. Similar to the all-around weld with side bolts specimens, the highest strains of 1000 to 2000 µin/in occurred at SG-1 and SG-5. SG-3 also had higher strain than SG-4 in all specimens. There was minor bending/yielding in the rods and no rupture in the welds.

Discussion

For the corner bolt configuration, using Equation (29), the capacity of the connection was calculated to be 114.2 kips using no R_{hss} factor, 68.52 kips using a R_{hss} factor of 0.6 for a t_{hss} of one-quarter inch, and 79.94 kips using a R_{hss} factor of 0.7 for a t_{hss} of three-eighths inch . The bolt tributary width, p, used in Equations (21) and (23) for the initial calculations performed by Zietlow (2022) was taken as the greater of the plate width and length, or twelve inches; using this, and a load of 119.2 kips from the limiting state of bolt strength (using A325N bolts), a minimum plate thickness of 0.439 inch was calculated. Recalculating the minimum plate thickness using Equation (23) with the same bolt tributary width, p, of twelve inches but considering the higher capacity of the A193 rods used, 139.2 kips, and the average plate yield strength from MAI material testing, 57.1 ksi, resulted in a thickness of 0.444 inch. This thickness is still under the end-plate thickness used of one-half inch; however, these design procedures and equations apply directly to the side bolt configuration.

Plate thicknesses using more recent procedures from Thornton (2017) and the *Manual* (AISC, 2022) were calculated; the bolt tributary width, p, was calculated as 5.916 inches from the minimum of Equations (32) and (33). Equations from the *Manual* were then used to calculate the required plate thicknesses. From Equation (3), for no prying action the required thickness of the plate was 0.533 inch. This is over the one-half inch plate thickness of the end-plates used; the actual thickness of one-half inch was used and Equation (3) was rearranged to calculate a tension force of 113.6 kips. However, the end-plates of the corner bolt specimens underwent significant deformation well before 113.6 kips, and this procedure still applies to the side bolt configuration. One way the procedure could be modified to possibly account for the corner bolt confiugration is to set the tributary width equal to the effective width, b_e (see Figure 37); another way may be to

increase the a and b dimensions. Calculations considering these adjustments can be found in

Appendix A.

Figure 37

Axial Corner Bolt Effective Width, b_e
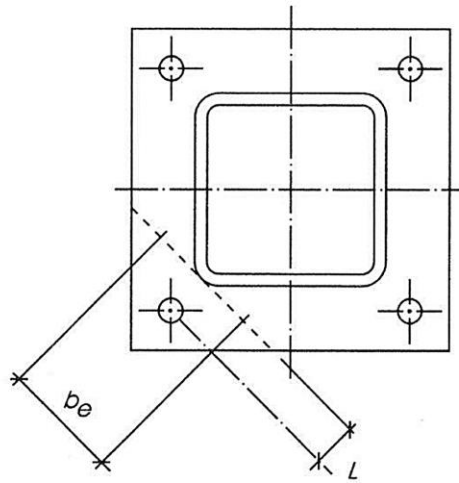
Note. Adapted from *Hollow Structural Sections Connections Manual* by American Institute of Steel

Construction, 1997.

The specimens with all-around welds showed to have greater capacity over the specimens

with workable-flat welds for the corner bolt configuration; the all-around specimens reached the

100-kip capacity of the load cell without ultimate failure, whereas the workable-flat welds

reached ultimate failure at an average load of just under 90 kips. Although both weld patterns for

the side bolt configurations reached the 100-kip capacity of the load cell, the specimens with

welds on the workable flats exhibited slightly higher displacement and more visible permanent

deformation compared to the all-around weld specimens.

Phase 2: Flexural

Twelve physical flexural specimens were tested. Table 9 provides a summary of the tests and the maximum measured lateral forces and displacements. The moments were also calculated using a distance of 35.5 inches from the base of the end-plate to the middle of the transfer rod.

Table 9

Flexural Tests Maximum Forces and Displacements

Weld Pattern	Bending Axis	Specimen	Max Lateral Force (lbs)	Max Moment at Base (lb-ft)	HSS Displacement at Max Load (in)	Plate Displacement at Max Load (in)
All-Around Welds	Weak	AAWK01	13621	40296	5.362	0.639
		AAWK02	13175	38977	4.668	0.552
		AAWK03	12692	37548	4.391	0.520
	Strong	AAST01	16161	47809	4.566	1.275
		AAST02	17573	51986	4.965	1.357
		AAST03	16393	48496	5.056	1.355
Workable-Flat Welds	Weak	WFWK01	11772	34827	5.157	0.560
		WFWK02	10986	32501	2.914	0.477
		WFWK03	10516	31109	2.348	0.459
	Strong	WFST01	12834	37968	2.854	0.764
		WFST02	11827	34989	3.227	-
		WFST03	12686	37530	2.257	0.661

Weld Pattern	Bending Axis	Average Max Lateral Force (lb)	Average Max Moment at Base (lb-ft)	Average Max HSS Displacement (in)	Average Max Plate Displacement (in)
All-Around Welds	Weak	13163	38940	4.807	0.571
	Strong	16709	49431	4.862	1.329
Workable-Flat Welds	Weak	11092	32813	3.473	0.499
	Strong	12449	36829	2.780	0.713

The specimens with welds at the workable flats had relatively less capacity than the specimens with welds all-around when considering the same bending axis, due to weld rupture occurring in most of the workable-flat weld specimens. In all specimens when weld rupture did not occur, the ultimate load was not reached before the actuator reached maximum stroke. However, there was significant deformation and yielding of the end-plate; the all-around weld specimens exhibited more deformation and higher displacements in both the HSS (LVDT-1) and the end-plate (LVDT-2). Specimen comparison photos can be seen in Figures 38 through 44; the plate failure for all end-plate was observed to be Mode 3 failure as shown in Wheeler et al. (1998), see Figure 13. Load versus displacement plots for all specimens and LVDTs and load versus strain plots for all specimens and gages can be found in Appendix C.

Figure 38

Comparison Photo of AAWK Specimens

Figure 39

Comparison Photo of AAST Specimens

Figure 40

Comparison Photo of WFWK Specimens

Figure 41

Comparison Photo of WFST Specimens

Figure 42

Comparison Photo of First Trial Specimens

Figure 43

Comparison Photo of Second Trial Specimens

Figure 44

Comparison Photo of Third Trial Specimens

All-Around Weld Strong Axis

This configuration reached an average maximum lateral load of 16.7 kips, resulting in an average maximum moment at the base of 49.4 kip-ft, before the actuator reached its maximum stroke at an average displacement of 4.807 inches at LVDT 1; the actuator reached full stroke before the ultimate load was reached for all three specimens. There was a small fracture in the weld on the corners of the tension side of the HSS, see Figure 45. There was significant deformation in the base plate with an average maximum displacement of 1.329 inches at LVDT 2, see Figure 46.

Figure 45

Corner Weld Cracking in All-Around Weld Strong Axis Specimen (AAST03)

Figure 46

End-Plate Deformation in All-Around Weld Strong Axis Specimen (AAST03)

Figure 47

AAST Specimens Load versus Displacement for LVDT 1 (End-plate)
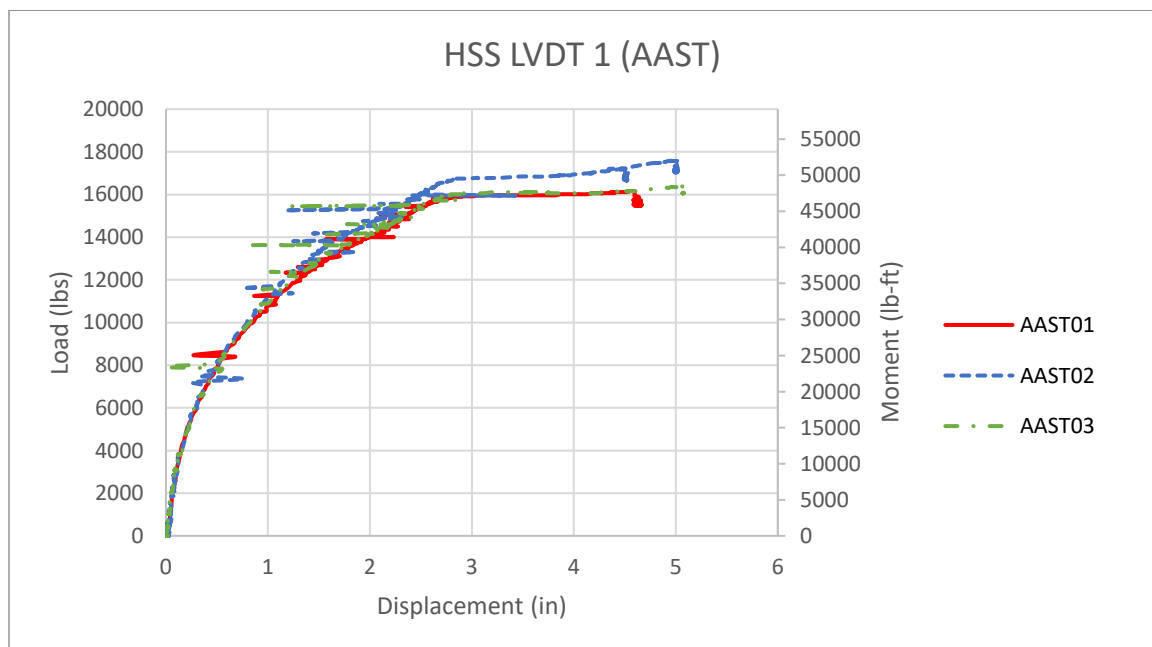
Figure 48

AAST Specimens Load versus Displacement for LVDT 2 (HSS)
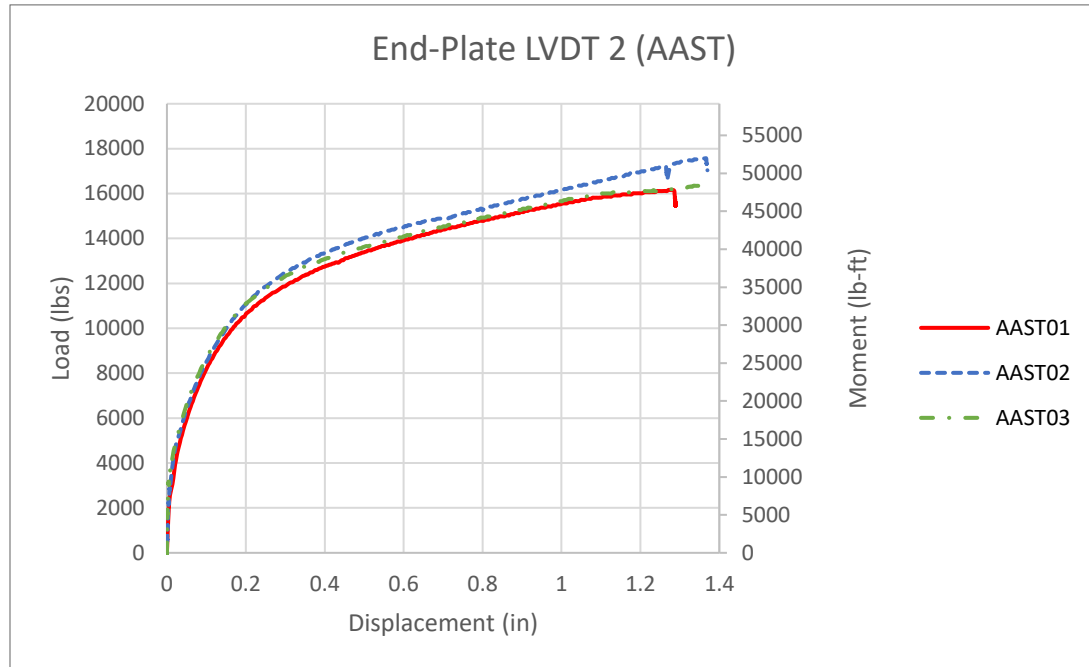
Figure 47 shows a load versus displacement plot for LVDT 1, located at the top of the HSS, and Figure 48 shows a load versus displacement plot for LVDT 2, located on the tension side of the plate between bolts.

Workable-Flat Welds Strong Axis

This configuration reached an average maximum lateral load of 12.4 kips, resulting in a maximum moment at the base of 36.8 kip-ft, before weld rupture. Complete weld rupture occurred in all three specimens; therefore, all loads were ultimate loads. The HSS reached an average maximum displacement of 2.780 inches before weld rupture, see Figure 49. There was also significant deformation in the base plate before the weld rupture, with an average maximum displacement of 0.527 inches at LVDT 2, see Figure 50.

Figure 49

Weld Rupture in Workable-Flat Welds Strong Axis Specimen (WFST01)

Figure 50

End-Plate Deformation in Workable-Flat Welds Strong Axis Specimen (WFST01)
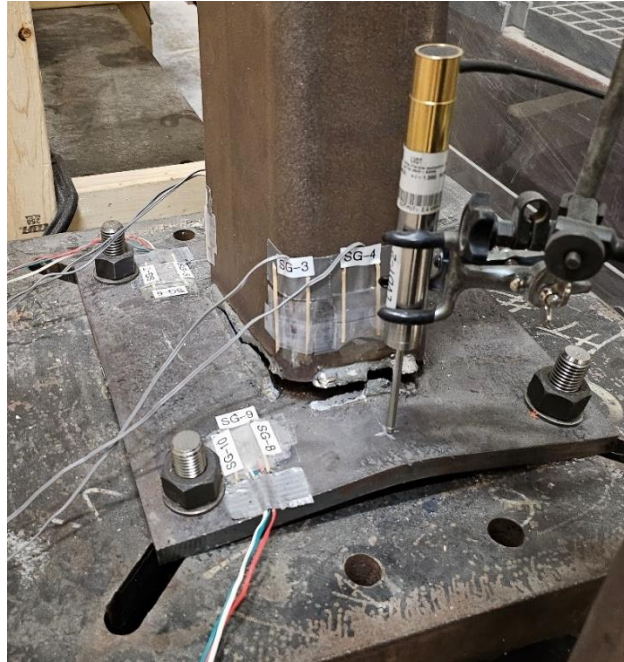
Figure 51

WFST Specimens Load versus Displacement for LVDT 1 (End-plate)
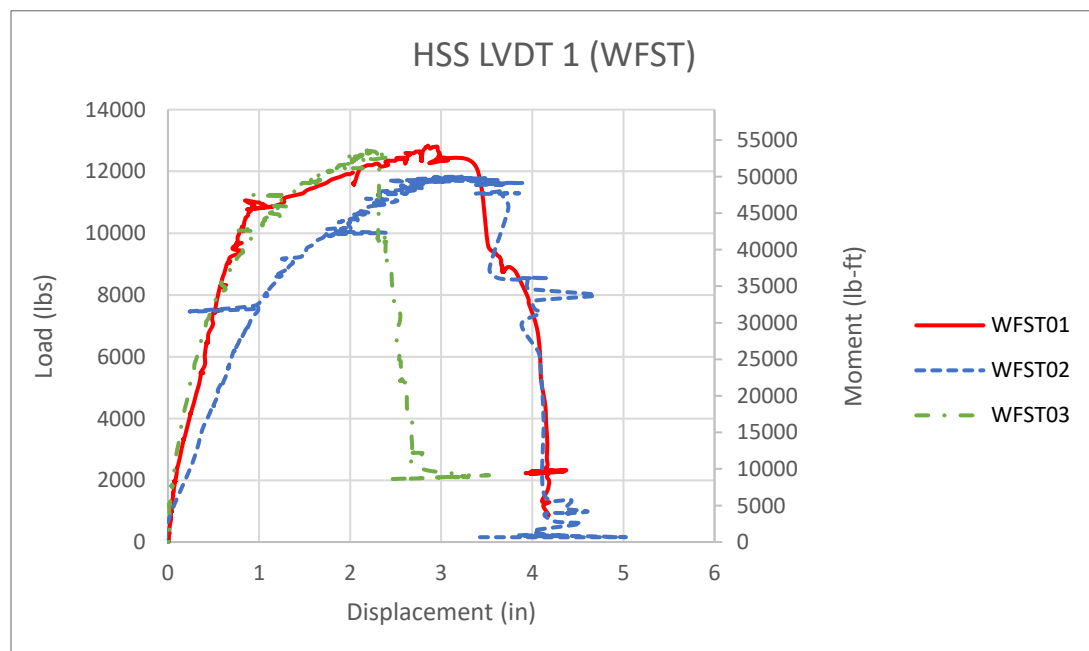
Figure 52

WFST Specimens Load versus Displacement for LVDT 2 (HSS)
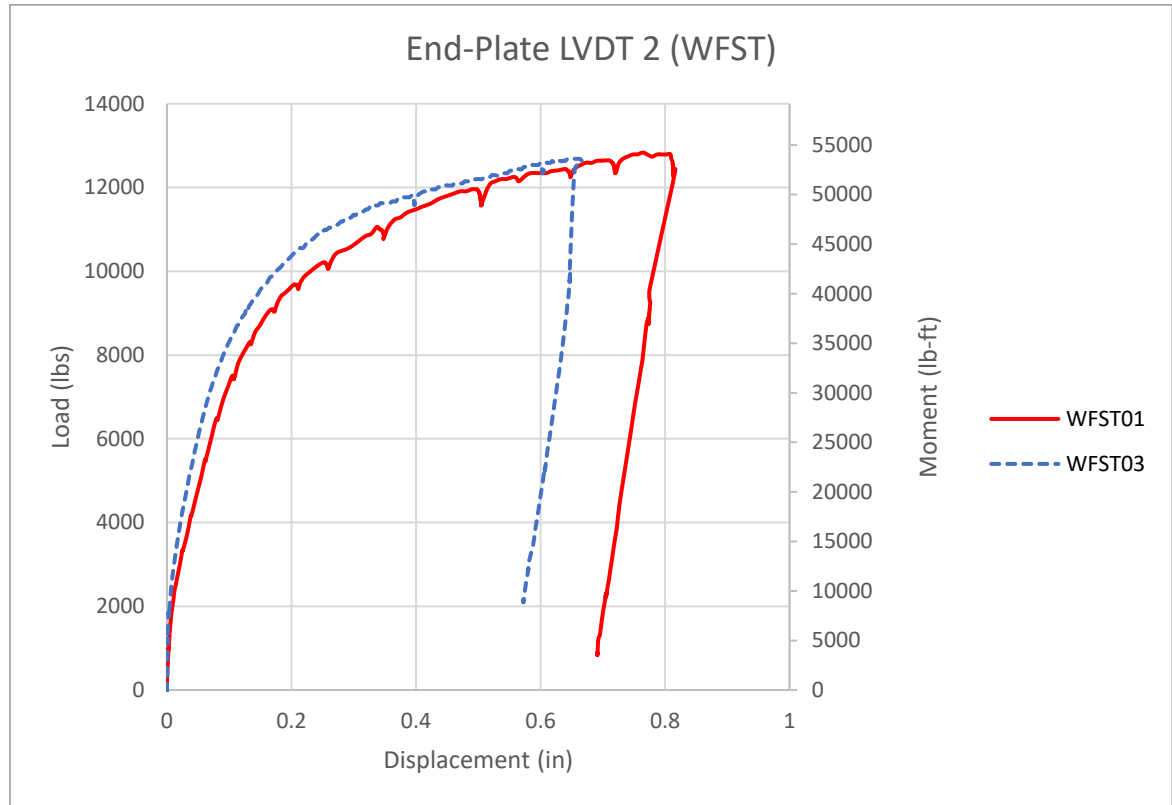
Figure 51 shows a load versus displacement plot for LVDT 1, located at the top of the HSS, and

Figure 52 shows a load versus displacement plot for LVDT 2, located on the tension side of the

plate between the bolts.

All-Around Weld Weak Axis

This configuration reached an average maximum lateral load of 13.2 kips resulting in an

average maximum moment at the base of 38.9 kip-ft, before the actuator reached its maximum

stroke at an average displacement of 4.862 inches at LVDT 1; the actuator reached full stroke

before the ultimate load was reached for all three specimens. There was no observable cracking

in the weld on the corners of the tension side of the HSS, see Figure 53. There was significant

deformation in the base plate with an average maximum displacement of 0.713 inches at LVDT

2, see Figure 54.

Figure 53

Corner Weld in All-Around Weld Weak Axis Specimen (AAWK03)

Figure 54

End-Plate Deformation in All-Around Weld Strong Axis Specimen (AAWK02)
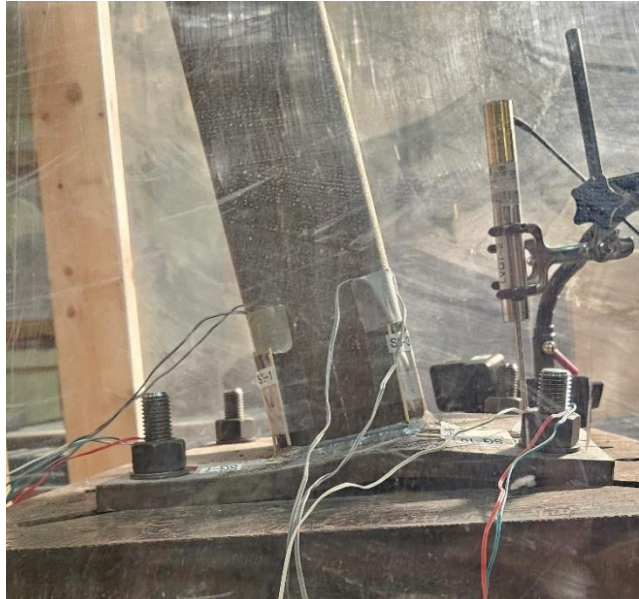
Figure 55

AAWK Specimens Load versus Displacement for LVDT 1 (End-plate)
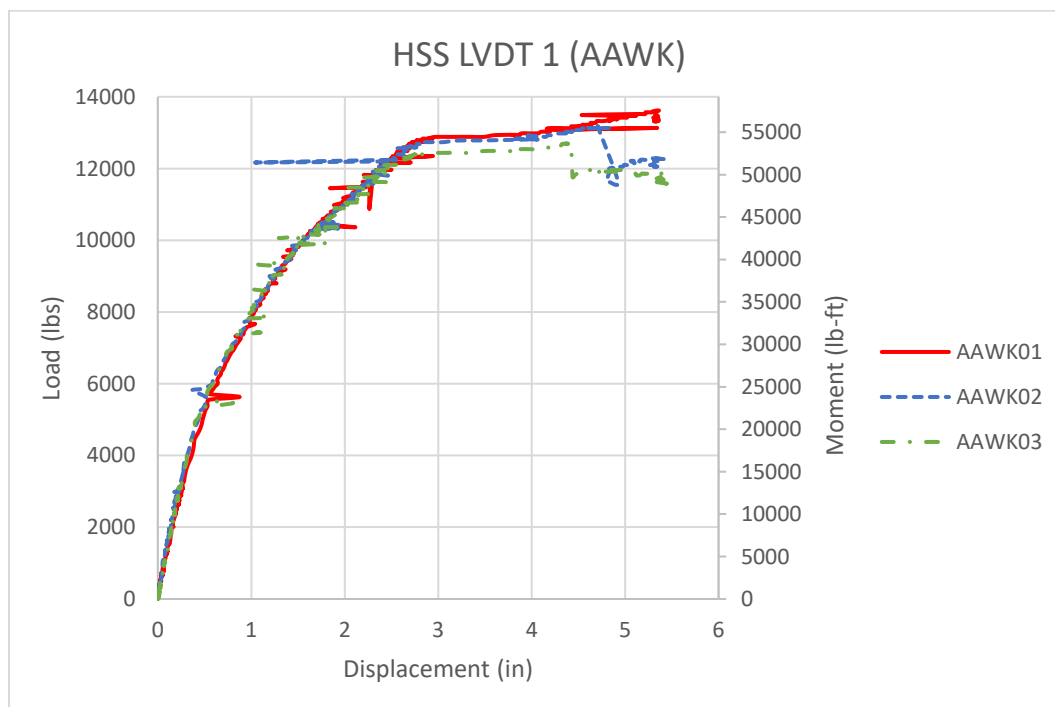
Figure 56

AAWK Specimens Load versus Displacement for LVDT 2 (HSS)
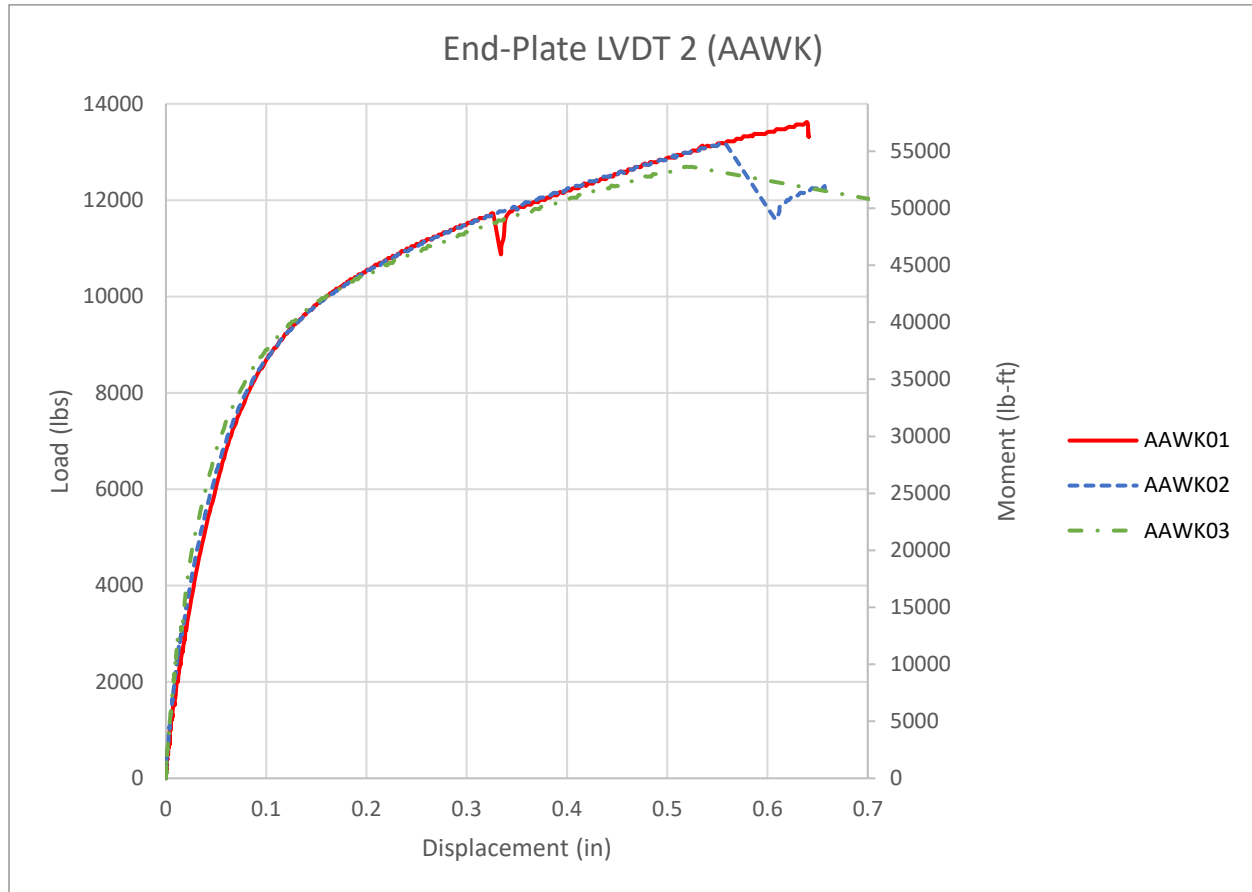
Figure 55 shows a load versus displacement plot for LVDT 1, located at the top of the HSS, and

Figure 56 shows a load versus displacement plot for LVDT 2, located on the tension side of the

plate between the bolts.

Workable-Flat Welds Weak Axis

This configuration reached an average maximum lateral load of 11.1 kips resulting in an

average maximum moment at the base of 32.8 kip-ft. For the first specimen, WFK01, the

actuator reached full stroke before the ultimate load was reached; there was observable cracking

in the welds, see Figure 57. The second specimen, WFWK02, reached an ultimate load at a HSS

displacement of 2.914 inches, measured by LVDT 1; there was observable rupture in the welds,

see Figure 58. The third specimen, WFWK03, reached an ultimate load at a HSS displacement of

2.348 inches, measured by LVDT 1; there was complete rupture in the welds, see Figure 59. The

average maximum HSS displacement at LVDT 1 for these specimens was 3.473 inches; the

average maximum end-plate displacement at LVDT 2 was 0.499 inches.

Figure 57

Corner Weld Cracking in All-Around Weld Weak Axis Specimen (WFWK01)
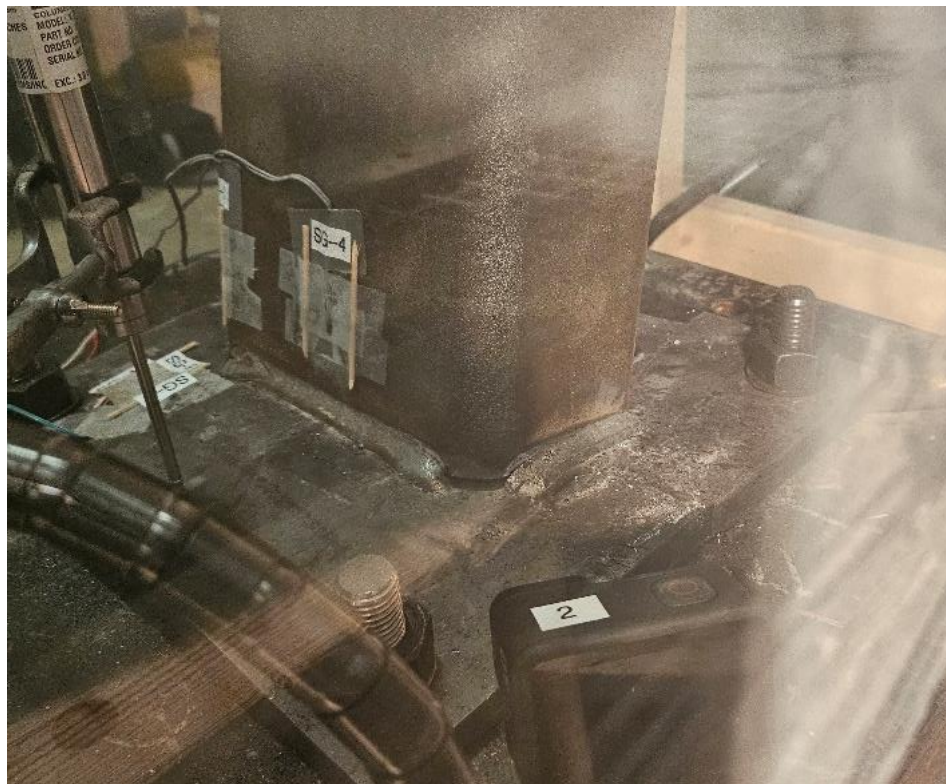
Figure 58

Weld Rupture in All-Around Weld Weak Axis Specimen (WFWK02)
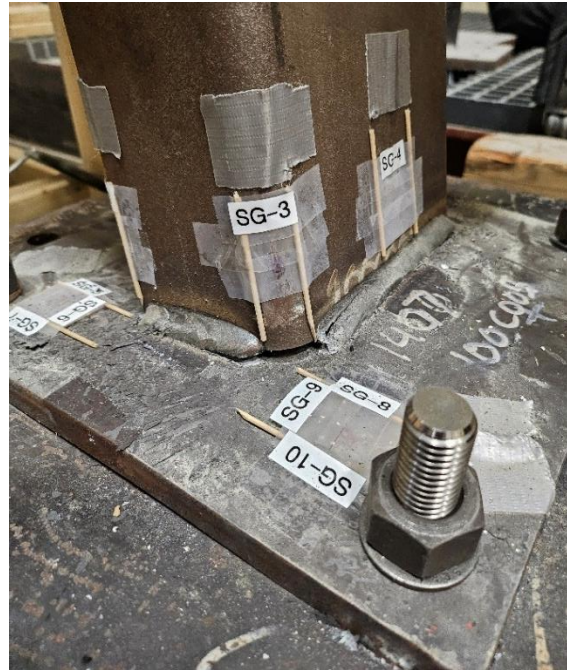
Figure 59

Weld Rupture in All-Around Weld Weak Axis Specimen (WFWK03)

Figure 60

AAWK Specimens Load versus Displacement for LVDT 1 (End-plate)
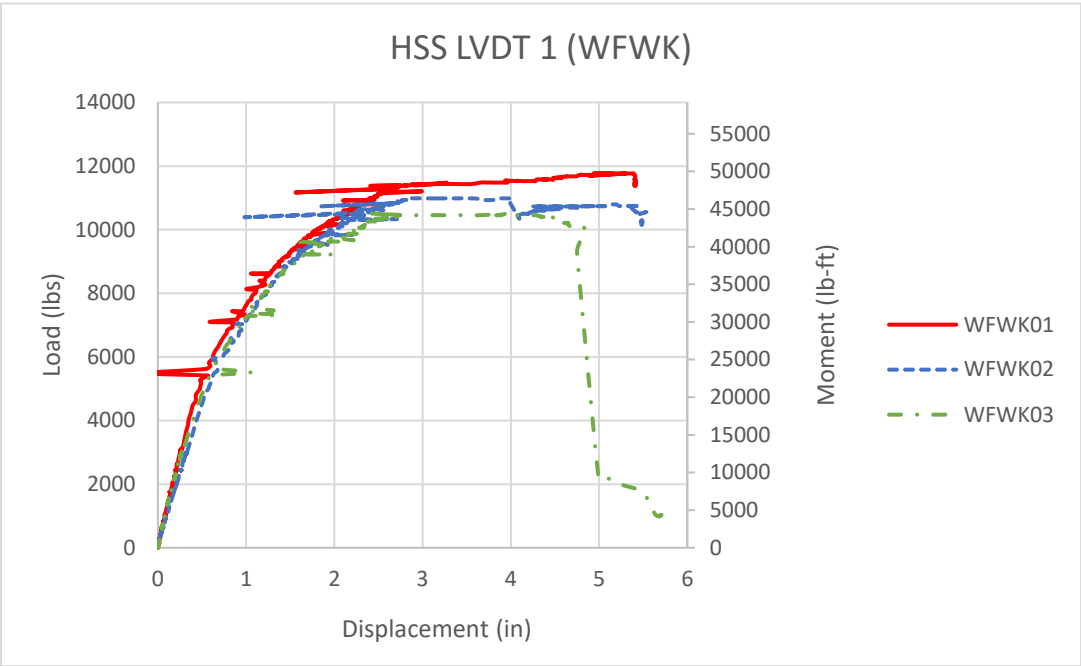
Figure 61

AAWK Specimens Load versus Displacement for LVDT 2 (HSS)
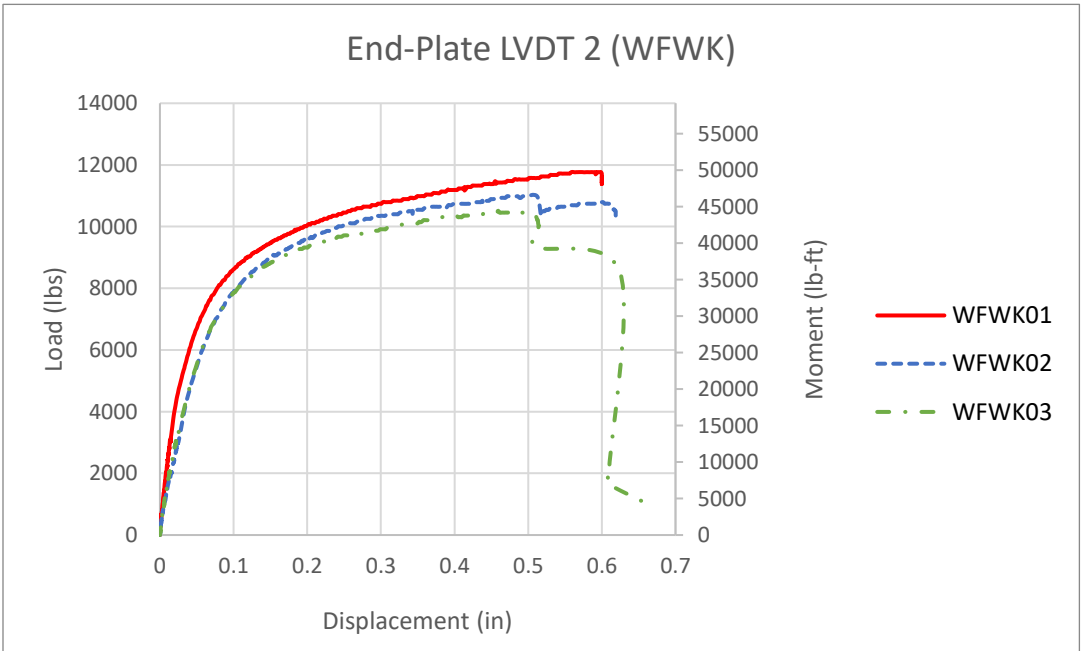
Figure 60 shows a load versus displacement plot for LVDT 1, located at the top of the HSS, and

Figure 61 shows a load versus displacement plot for LVDT 2, located on the tension side of the

plate between the bolts.

Discussion

As expected, the strong axis specimens were stronger than the weak axis specimens and the all-around weld specimens were stronger than the workable-flat welds specimens. The difference in stiffnesses can also be seen from the load versus displacement graphs for both LVDTs for all specimens, see Figures 62 and 63.

Figure 62

All Specimens Load versus Displacement for LVDT 1 (End-plate)
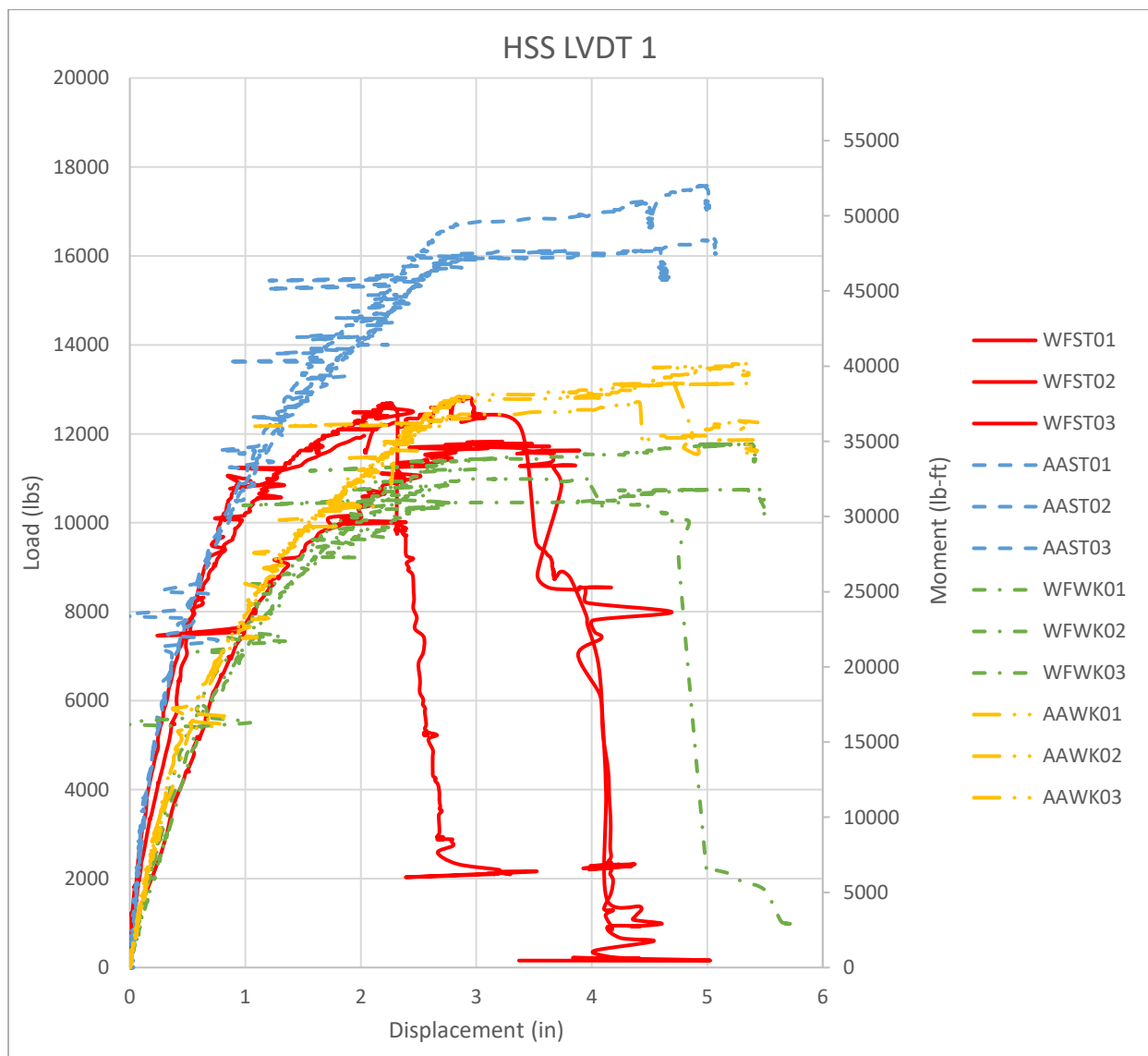
Figure 63

All Specimens Load versus Displacement for LVDT 2 (HSS)
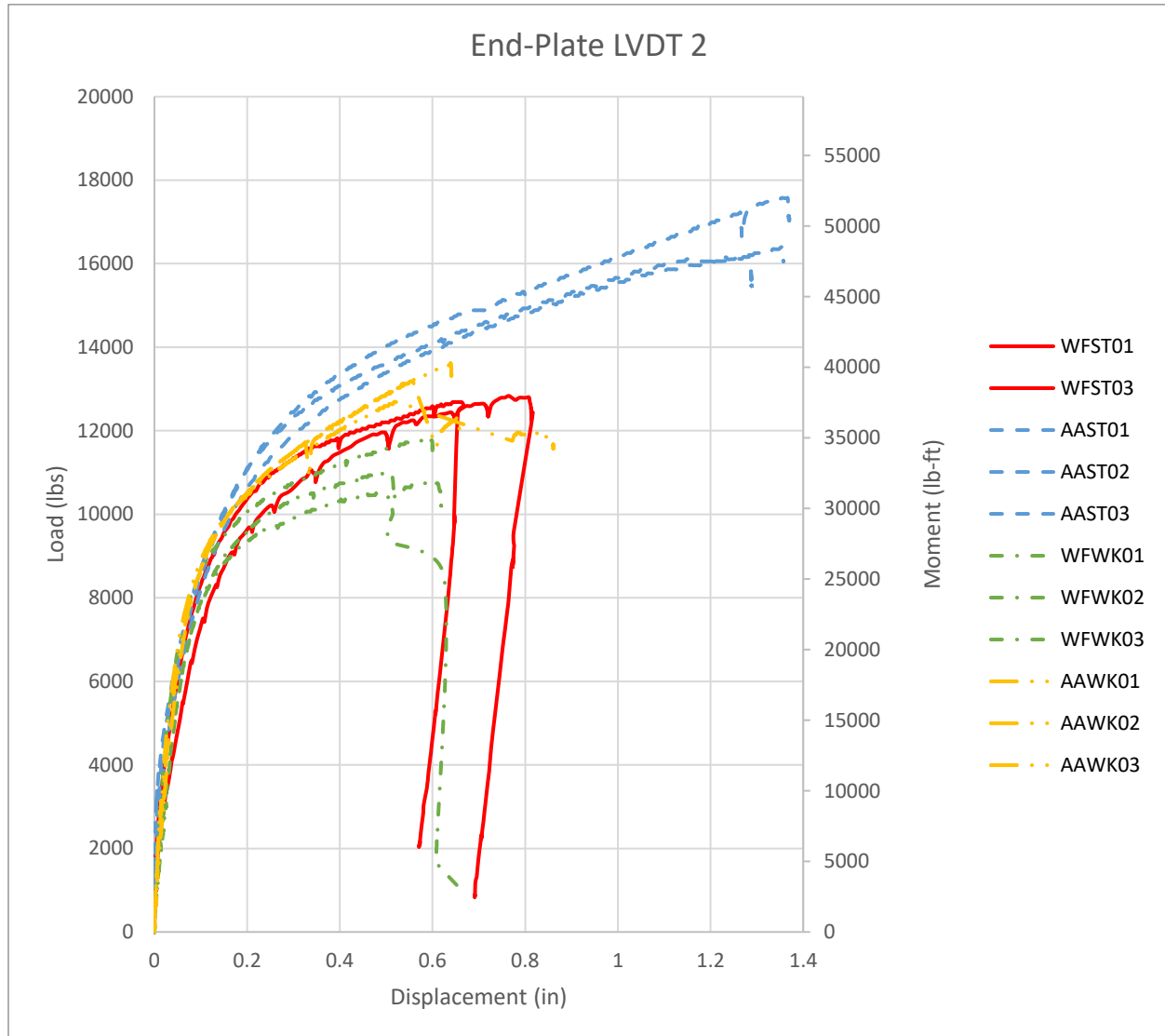
Figure 62 shows that the all-around weld specimens had higher overall stiffnesses over the workable-flat welds specimens for both the weak and strong orientations. Figure 63 shows that after yield the plate stiffnesses of the all-around weld specimens are higher than the workable-flat welds specimens. The stiffnesses are also similar between the same weld patterns and different HSS orientations.

Strength capacities were calculated using the design procedure presented in Wheeler et al. (1998) and AISC Design Guide 24 (2010). Serviceability loads were also calculated using the design procedure from Wheeler et al. (1998). All capacities are tabulated in Table 10; the tabulated strength loads do not include any safety factors. See Appendix A for all calculations. The maximum and estimated yield loads from experimental testing are tabulated in Table 11.

Table 10

Flexural Calculated Capacities

Axis	Force	Strength				Serviceability	
		Wheeler et al.		AISC 24		Wheeler et al.	
		Bolt	Plate	Weld	Prying	Bolt	Plate
Weak	Moment (k-ft)	28.4	**27.8**	35.3	**14.6**	22.1	**19.5**
	Lateral (k)	9.60	**9.39**	11.9	**4.93**	7.46	**6.58**
Strong	Moment (k-ft)	48.1	**37.3**	61.7	**39.6**	37.7	**20.5**
	Lateral (k)	16.3	**12.6**	20.9	**13.4**	12.8	**6.93**

	φ	0.8	0.9	0.75	0.9
Weak	Moment (k-ft)	22.7	**25.0**	26.4	**13.1**
	Lateral (k)	7.68	**8.45**	8.94	**4.44**
Strong	Moment (k-ft)	38.5	**33.6**	46.3	**35.6**
	Lateral (k)	13.0	**11.4**	15.6	**12.0**

Table 11

Flexural Experimental Capacities

		Average Max Lateral Force (k)	Average Max Moment at Base (k-ft)
Weak	AAWK	13.2	38.9
	WFWK	11.1	32.8
Strong	AAST	16.7	49.4
	WFST	12.4	36.8

The strengths calculated from the Wheeler et al. (1998) design procedures were controlled by plate failure and were conservative when compared to the average maximum forces for all specimen configurations except for the WFST specimens. The average maximum lateral force for the WFST was 12.4 kips, which was 0.2 kips less than the calculated 12.6 kips. However, if a safety factor (Φ=0.9) is applied this capacity would become conservative (11.4 kips). The serviceability loads calculated from the Wheeler et al. (1998) design procedures were controlled by plate yielding and were close to the experimental yield loads seen in the plate from LVDT 1, see Figure 63.

The strengths calculated from the design procedure from Example 4.1 in *AISC Design Guide 24* were governed by prying action and were conservative when compared to the average maximum forces for all specimen configurations except for the WFST specimens. The average maximum lateral force for the WFST was 12.4 kips, which was 1.0 kips less than the calculated 13.4 kips. However, if a safety factor (Φ=0.9) was applied this capacity would become conservative (12.0 kips). The strengths from weld capacity calculated from the design procedure from Example 4.1 in *AISC Design Guide 24* were conservative for the AAWK specimens (with and without safety factor), conservative for the AAST specimens (with safety factor), conservative for the WFWK specimens (with safety factor), and unconservative for the WFST specimens. It should also be noted that the all-around weld specimens did not exhibit failure in the welds, rather the maximum load was reached through yielding of the system and maximum stroke of the actuator being reached. Therefore, the all-around welds had some additional capacity, making the weld calculations more conservative.

Conclusions

Results from the axial tests indicate that the side bolt configurations provide more

capacity than the corner bolt configurations and the all-around weld provides more capacity than

the workable-flats weld. The *AISC Design Guide 24* procedure for designing HSS end-plate

connections under axial tension with the side bolt configuration cannot be fully validated

because the specimens reached the 100-kip capacity of the actuator. However, the strength of the

side bolt connections based on the design procedures exceeded 100 kips and the small

displacement and yielding seen in the connection suggest that the higher capacity could be

reached. The results for the corner bolt specimens suggest that the design procedure is not

directly applicable to this different configuration. Ultimate failure occurred in the WFCB

specimens at a load of just under 90 kips, well under the calculated capacity from the design

procedures. Although the AACB specimens reached the 100-kip capacity of the load cell, they

all exhibited significant displacement and yielding starting well before the capacity was reached.

Although an ultimate capacity was not reached, this significant deformation in the plate and rods

could be considered failure and suggest that the higher strength based on rod strength would not

have been reached before prying action would have caused rupture in the rods. The significant

deformation in the corner bolt specimens also correlates with the results of the finite element

analysis conducted by Zietlow (2022).

Results from the flexural tests indicate that the strong axis configurations provide more

capacity than the weak axis configurations and the all-around weld provides more capacity than

the workable-flats weld. *AISC Design Guide 24* does not have any apparent design procedure

that is directly applicable to the lateral loading applied to this configuration of an HSS end-plate

connection, and the design procedures for an axially loaded connection that were applied in the

initial design calculations appear to have overestimated the capacity of the laterally loaded

connection. Capacities of the connections for strength calculated using equations from the design

procedures presented in Wheeler et al. (1998) and Example 4.1 in *AISC Design Guide 24* were

more comparable to the experimental capacities of the HSS end-plate connection subjected to

lateral/flexural loading.

Recommendations

Results from the axial tests suggest that the procedure in *AISC Design Guide 24* is not

directly applicable to HSS end-plate connection with corner bolt configurations, and that the

corner bolt configuration offers less capacity than the side bolt configuration. Therefore, a

recommendation is to clearly state that the design procedure should not be applied to the design

of corner bolt HSS end-plate configurations in axial tension and the side bolt configuration

should be used, or that a separate design procedure be developed, potentially involving a reduced

bolt tributary length, *p,* increased *a* and *b* dimensions; the latter option would require more

testing and research for development and validation. All prying action calculations for the axial

specimens conducted in this research used the yield strength (F_y), as it is used in the axial prying

action equations in *AISC Design Guide 24*. However, the most current *AISC Steel Construction*

Manual uses the tensile strength (F_u). Thornton (2017) notes this discrepancy and explains the

reasons for F_u being initially adopted in 13th Edition *Manual* (2005). Thornton developed design

procedures using F_u and showed "excellent correlation" between experimental and predicted

capacities. Therefore, it recommended that the design procedure be considered for

implementation in *AISC Design Guide 24* for the side bolt configuration. The results also suggest

that the all-around weld pattern offers more capacity than the workable-flat welds pattern. Thus,

another recommendation is to use all-around welds for HSS end-plates in axial tension.

Results from the flexural tests suggest the weld design procedures of Example 4.1 in *AISC Design Guide 24* are conservative for the all-around weld but not necessarily for the workable-flat welds. The results also suggest that the all-around weld pattern offers significantly more capacity than the workable-flat welds pattern. Therefore, it is also recommended to use all-around welds for HSS end-plates in flexure. The results showed good correlation with the design procedure presented by Wheeler et al. (1998) and calculated capacities were conservative for all-around weld specimens. Therefore, it recommended that the design procedure be considered for implementation in *AISC Design Guide 24*. The results from the testing conducted by Wheeler et al. (1998) show that specimens with bolts in line with the HSS walls (c=0) had higher capacities compared to otherwise similar specimens with bolts located beyond the HSS walls (c>0). Therefore, if the bending is uniaxial, it may be best to locate the bolts in line with the HSS walls or inside as in Example 4.1 from *AISC Design Guide 24*. If bending is biaxial, it may be best to place bolts all around the HSS, that is to place additional bolts at the sides of the HSS walls.

For future research and testing it is recommended to focus on one variable of the connection. For example, it may be worth focusing on the welds with gages focused on them or the effects of prying action with instrumentation to measure bolt force. Instrumentation could have been better implemented; strain gages could have been focused better on anticipated yield lines and a LVDT should have been located off the HSS to measure overall displacement in the axial tests. It is also recommended that future research and testing be focused on one type of loading and to design specimens with a capacity that does not exceed the capacity of the actuators and load cells; another alternative would be to use actuators and load cells with higher capacities.

References

American Institute of Steel Construction. (1997). *Hollow structural sections connections manual.* Chicago: American Institute of Steel Construction.

American Institute of Steel Construction. (2022a). *Steel construction manual* (16th ed.). Chicago: American Institute of Steel Construction.

American Institute of Steel Construction. (2022b). *ANSI/AISC 360-22: Specification for structural steel buildings.* Chicago: American Institute of Steel Construction.

Carravaggio, A. (1988). *Test on steel roof joints for toronto sky dome* [Unpublished master's thesis]. University of Toronto.

Christensen, H. (2010). *Determining the validity of design provisions for HSS to base plate connections with corner anchor rods subjected to axial tension* [Unpublished master's thesis]. Milwaukee School of Engineering (MSOE).

Dowswell, B. (2011). A yield line component method for bolted flange connections. *Engineering Journal, 48*, 93-116.

Engelhardt, M. D. (2007). *Basic concepts in ductile detailing of steel structures* [Powerpoint Presentation]. University of Texas at Austin. AISC. Retrieved from https://www.aisc.org/globalassets/continuing-education/quiz-handouts/basic-concepts-in-ductile-detailing.pdf

Fisher, J. M., & Kloiber, L. A. (2006). *Steel design guide 1: Base plate and anchor rod design* (Second Edition ed.). American Institute of Steel Construction .

Heinisuo, M., Ronni, H., Perttola, H., Aalto, A., & Tiainen, T. (2012). End and base plate joints with corner bolts for rectangular tubular member. *Journal of Constructional Steel Research*, 85-92. doi:10.1016/j.jcsr.2012.03.013

Kanvinde, A. M., Maamouri, M., & Buckholt, J. R. (2024). *Steel design guide 1: Base connection design, fabrication, and erection for steel structures* (Third ed.). American Institute of Steel Construction.

Kato, B., & Mukai, A. (1985). Bolted tension flanges joining square hollow section members. *Journal of Constructional Steel Research, 5*, 163-177.

Kennedy, N. A., Vinnakota, S., & Sherbourne, A. N. (1981). The split-tee analogy in bolted splices and beam-column connections. *Joints in Structural Steelwork* (pp. 2.138-2.157). New York: John Wiley & Sons, Inc. .

Nair, R. S., Birkemoe, P. C., & Munse, W. H. (1974). High strength bolts subject to tension and prying. *Journal of the Structural Division, 100*(2). doi:https://doi.org/10.1061/JSDEAG.0003712

Packer, J. A., Sherman, D., & Lecce, M. (2010). *Steel design guide 24: Hollow structural section connections.* American Institute of Steel Construction.

Packer, J. A., Sun, M., & Tousignant, K. (2016). Experimental evaluation of design procedures for fillet welds to hollow structural sections. *Journal of Structural Engineering, 142*(5). doi:https://doi.org/10.1061/(ASCE)ST.1943-541X.0001467

Portland Bolt. (2024). *ASTM A193*. Retrieved from Portland Bolt: https://www.portlandbolt.com/technical/specifications/astm-a193/

Portland Bolt. (2024). *ASTM F3125*. Retrieved from Portland Bolt:

    https://www.portlandbolt.com/technical/specifications/astm-f3125/

Swanson, J. A. (2002). Ultimate strength prying models for bolted T-stub connections.

    Engineering Journal, 39, 136-147.

Tamboli, A. R. (2017). *Handbook of structural steel connection design and details* (Third ed.).

    New York: McGraw-Hill Education.

Thornton, W. A. (1992). Strength and Serviceability of Hanger Connections. *Engineering

    Journal, 29*, 145-149.

Thornton, W. A. (2017). Yield line approaches for design of end plate tension connections for

    square and rectangular HSS members using end plate tensile strengths. *Engineering

    Journal, 54*, 141-154.

Tousignant, K., & Packer, J. (2017). Numerical investigation of fillet welds in HSS-to-rigid end-

    plate connections. *Journal of Structural Engineering, 143*(12), [1-16].

    doi:https://doi.org/10.1061/(ASCE)ST.1943-541X.0001889

West, M. A., & Fisher, J. M. (2020). *AISC design guide 10: Erection bracing of low-rise

    structural steel buildings* (2nd ed.). Chicago, Illinois: AISC.

Wheeler, A. T., Clarke , M. J., & Hancock, G. J. (1997). *Bending tests of bolted end plate

    connections in cold formed rectangular hollow sections.* Department of Civil

    Engineering. Sydney, Australia: University of Sydney.

Wheeler, A. T., Clarke, M. J., & Hancock, G. J. (1995). Tests of bolted moment end plate connections in tubular members. *14th Australian Conference on Mechanics of Structures and Materials* (pp. 331-336). Hobart, Tasmania, Australia: University of Tasmania.

Wheeler, A. T., Clarke, M. J., Hancock, G. J., & Murray, T. M. (1998). Design model for bolted moment end plate connections using rectangular hollow sections. *Journal of Structural Engineering, 124*(2), 164-173. doi:https://doi.org/10.1061/(ASCE)0733-9445(1998)124:2(164)

Willibald, S., Packer, J. A., & Puthli, R. S. (2002). Experimental study of bolted HSS flange-plate connections in axial tension. *Journal of Structural Engineering, 128*(3), 328-336. doi:https://doi.org/10.1061/(ASCE)0733-9445(2002)128:3(328)

Willibald, S., Packer, J. A., & Puthli, R. S. (2003). Design recommendations for bolted rectangular HSS flange-plate connections in axial tension. *Engineering Journal, 40*, 15-24.

Wilsmann, J. (2012). *Weld behavior in a rectangular HSS base plate connection with corner anchor rods subjected to an axial tensile force* [Unpublished master's thesis]. Milwaukee School of Engineering.

Zietlow, J. A. (2022). *Evaluation of the axial capacity of steel HSS end-plate connections using nonlinear finite element simulations and analytical methods* [Unpublished master's thesis]. Milwaukee School of Engineering (MSOE).

Appendix A – Calculations

Zietlow (2022) Calculations

Calculation of HSS 7x4x5/16 strength in strong axis bending:

Given:
- Grade A500C Steel

$$\text{Yield strength, specified} \qquad F_{yh} := 50 \frac{kip}{in^2}$$

$$\text{Ultimate strength, specified} \qquad F_{uh} := 62 \frac{kip}{in^2}$$

$$\text{Ultimate strength, experimental} \qquad F_{u\_exp} := \max\left(F_{yh} \cdot 1.25 \cdot \frac{in^2}{kip}, F_{uh} \cdot \frac{in^2}{kip} \right) \cdot \frac{kip}{in^2} \rightarrow \frac{62.5 \cdot kip}{in^2}$$

Bending Limit States to check:

- Yield
- Flange Local Buckling
- Web Local Buckling
- Lateral Torsional Buckling

Limit State: Yield

$$\text{Plastic section modulus} \qquad Z_x := 13.1 in^3$$

$$\text{Nominal Moment Capacity} \qquad M_{n\_y} := F_{yh} \cdot Z_x \; float, 3 \; \rightarrow 655.0 \cdot in \cdot kip$$

Limit State: Flange Local Buckling
Since HSS7x4x5/16 is compact per AISC Tab. 1-12a, the limit state of flange local buckling does not apply.

Limit State: Web Local Buckling
Since HSS7x4x5/16 is compact, the limit state of web local buckling does not apply.

<u>Limit State: Lateral Torsional Buckling</u>

Modulus of Elasticity	$E := 29000 \dfrac{kip}{in^2}$
Radius of Gyration	$r_y := 1.61 in$
Polar Moment of Inertia	$J := 35.4 in^4$
Gross Area of Steel	$A_g := 5.85 in^2$
Nominal Plastic Moment Capacity	$M_p := M_{n\_y} \rightarrow 655.0 \cdot in \cdot kip$
Unbraced Length	$L_b := 30 in$

Inelastic Bending Limit
$$L_p := 0.13 \cdot E \cdot r_y \cdot \frac{\sqrt{\dfrac{(J \cdot A_g)}{in^6}}}{M_p} \cdot in^3 \quad float, 3 \;\rightarrow 133.0 \cdot in$$

$$if\left(\frac{L_b}{in} < \frac{L_p}{in}, \text{"LTB does not apply"}, \text{"LTB applies"}\right) \rightarrow \text{"LTB does not apply"}$$

Verification of W18x76 Support Beam:

Nominal Moment Strength	$M_n := 1.25 M_{n\_y} \quad float, 3 \;\rightarrow 819.0 \cdot in \cdot kip$
Actuator Moment Arm (see CAD file)	$d_{act} := L_b \rightarrow 30 \cdot in$
Required Actuator Force	$F_{act} := \dfrac{M_n}{d_{act}} \quad float, 3 \;\rightarrow 27.3 \cdot kip$
Thickness of base plate (assumed)	$t_{bp\_a} := 1 in$
Allowable cap eccentricity (assumed)	$e_{cp} := 6 in$
Beam depth	$d_{W18} := 18.2 in$
Total moment arm	$d_{tot} := t_{bp\_a} + e_{cp} + \dfrac{d_{W18}}{2} + d_{act} \quad float, 3 \;\rightarrow 46.1 \cdot in$
Total moment in W18x76 beam	$M_u := F_{act} \cdot d_{tot} \quad float, 3 \;\rightarrow 1258.0 \cdot in \cdot kip$

Limit states for W18x76 to be checked:
- Flexural capacity
- Web shear
- Flange bending
- Web buckling

Flexural Capacity:

Yield strength, W18 beam
$$F_{y\_W18} := 50 \frac{kip}{in^2}$$

Plastic moment capacity
$$\phi M_{p\_w18} := 611 kip \cdot ft$$

Provided moment capacity
$$\phi M_{n\_w18} := \phi M_{p\_w18} \rightarrow 611 \cdot ft \cdot kip$$

$$if\left(\frac{\phi M_{n\_w18}}{kip \cdot in} \cdot \frac{12in}{ft} > \frac{M_u}{kip \cdot in}, "Flexure\ OK", "Flexure\ NG" \right) \rightarrow "Flexure\ OK"$$

Web Shear: [G2]

Bolt spacing provided
$$S_{bolt} := 15in$$

Total number of bolts provided
$$n_{W18} := 4$$

Shear force per bolt
$$F_{bolt} := \frac{M_n}{S_{bolt} \cdot \frac{n_{W18}}{2}} \quad float, 3 \rightarrow 27.3 \cdot kip$$

Web shear strength reduction factor
$$\phi_{ws} := 1.0$$

Web thickness
$$t_w := 0.425in$$

Area of beam web
$$A_w := t_w \cdot d_{W18} \rightarrow 7.735 \cdot in^2$$

Shear constant
$$c_{v1} := 1.0$$

Available shear capcity
$$\phi V_n := 0.6 \cdot \phi_{ws} \cdot F_{y\_W18} \cdot A_w \cdot c_{v1} \quad float, 3 \rightarrow 232.0 \cdot kip$$

Ultimate shear force
$$V_u := 2 \cdot F_{bolt} \rightarrow 54.6 \cdot kip$$

$$if\left(\frac{\phi V_n}{kip} > \frac{V_u}{kip}, "web\ shear\ OK", "web\ shear\ NG" \right) \rightarrow "web\ shear\ OK"$$

Flange Local Bending: [J10]

Flange local bending reduction factor $\qquad \phi_{FLB} := 0.9$

Flange thickness $\qquad t_f := 0.68\text{in}$

Available capacity $\qquad \phi R_{n\_FLB} := 6.25 \cdot \phi_{FLB} \cdot F_{y\_W18} \cdot t_f^2 \; \text{float}, 3 \; \to 130.0 \cdot \text{kip}$

$$\text{if}\left(\frac{\phi R_{n\_FLB}}{\text{kip}} > \frac{F_{bolt}}{\text{kip}}, \text{"FLB OK"}, \text{"FLB NG"}\right) \to \text{"FLB OK"}$$

Web Local Yielding: [J10]

Web local yielding reduction factor $\qquad \phi_{WLY} := 1.0$

Web yielding factor $\qquad k_1 := 1.0625\text{in}$

Flange width $\qquad b_f := 11\text{in}$

$$k := \frac{b_f}{2} - k_1 \; \text{float}, 3 \; \to 4.44 \cdot \text{in}$$

Web yielding factor $\qquad l_b := k \to 4.44 \cdot \text{in}$

Available capacity $\qquad \phi R_{n\_WLY} := \phi_{WLY} \cdot F_{y\_W18} \cdot t_w \cdot (5k + l_b) \; \text{float}, 3 \; \to 566.0 \cdot \text{kip}$

$$\text{if}\left(\frac{\phi R_{n\_WLY}}{\text{kip}} > \frac{2 \cdot F_{bolt}}{\text{kip}}, \text{"WLY OK"}, \text{"WLY NG"}\right) \to \text{"WLY OK"}$$

Web Local Crippling: [J10]

WLC strength reduction factor $\qquad \phi_{WLC} := 0.75$

WLC constant $\qquad Q_f := 1.0$

Provided capacity

$$\phi R_{n\_WLC} := 0.8 \cdot \phi_{WLC} \cdot t_w^2 \cdot \left[1 + 3 \cdot \left(\frac{l_b}{d_{W18}}\right)\left(\frac{t_w}{t_f}\right)^{1.5}\right] \cdot \sqrt{\frac{E \cdot F_{y\_W18} \cdot t_f}{t_w} \cdot \frac{\text{in}^4}{\text{kip}^2} \cdot \frac{\text{kip}}{\text{in}^2}} \cdot Q_f$$

$\phi R_{n\_WLC} \; \text{float}, 3 \; \to 225.0 \cdot \text{kip}$

$$\text{if}\left(\frac{\phi R_{n\_WLC}}{\text{kip}} > \frac{2 \cdot F_{bolt}}{\text{kip}}, \text{"WLC OK"}, \text{"WLC NG"}\right) \to \text{"WLC OK"}$$

Web Compression Buckling: [J10]

Web compression buckling reduction factor $\qquad$ $\phi_{WCB} := 0.9$

Web height $\qquad$ $h := d_{W18} - 2 \cdot k_1 \ \text{float}, 3 \ \rightarrow 16.1 \cdot \text{in}$

Available capacity $\qquad$ $\phi R_{n\_WCB} := \phi_{WCB} \cdot \left(\dfrac{24 \cdot t_w{}^3 \cdot \sqrt{\dfrac{E \cdot F_{y\_W18} \cdot \text{in}^4}{\text{kip}^2}}}{h} \right) \cdot Q_f \cdot \dfrac{\text{kip}}{\text{in}^2}$

$\phi R_{n\_WCB} \ \text{float}, 3 \ \rightarrow 124.0 \cdot \text{kip}$

$\text{if} \left(\dfrac{\phi R_{n\_WCB}}{\text{kip}} > \dfrac{2 \cdot F_{bolt}}{\text{kip}}, \text{"WCB OK"}, \text{"WCB NG"} \right) \rightarrow \text{"WCB OK"}$

Base/Cap Plate Design (HSS7x7x5/16)

<u>Given:</u>

Strength reduction factor, weld	$\phi_w := 0.75$
Strength reduction factor, tensile yield	$\phi_y := 0.9$
Strength reduction factor, tensile rupture	$\phi_r := 0.75$
Yield strength, HSS	$F_{yh} := 50\,\dfrac{kip}{in^2}$
Rupture Strength, HSS	$F_{uh} := 62\,\dfrac{kip}{in^2}$
Length, HSS	$l_h := 7\,in$
Width, HSS	$b_h := 7\,in$
Thickness, HSS	$t := 0.3125\,in$
Length workable flat	$f_l := 5.625\,in$
Width workable flat	$f_b := 5.625\,in$
Yield strength, base plate	$F_{yp} := 50\,\dfrac{kip}{in^2}$
Length, plate	$l_p := 12\,in$
Width, plate	$b_p := 12\,in$
Electrode classification number	$F_{EXX} := 70\,\dfrac{kip}{in^2}$
Weld size	$w := 0.25\,in$
Bolt diameter	$d_b := 0.75\,in$
Hole diameter	$d_h := \dfrac{13\,in}{16}\ \text{float},4\ \rightarrow 0.8125 \cdot in$
Bolt available tensile strength (AISC Tab. 7-2)	$\phi_{rn} := 29.8\,kip$
Gross area, HSS	$A_g := 7.59\,in^2$
Net area, HSS	$A_n := 7.59\,in^2$
Shear lag factor	$U := 1$
Number of bolts	$n := 4$

Design:

60% weld electrode	$F_w := F_{EXX} \cdot 0.6 \rightarrow \dfrac{42.0 \cdot kip}{in^2}$
Design weld strength	$F_{wc} := F_w \cdot \phi_w \rightarrow \dfrac{31.5 \cdot kip}{in^2}$
Weld length	$L_w := 2\left(l_h + b_h\right) \rightarrow 28 \cdot in$
Effective Area	$A_e := A_n \cdot U \rightarrow 7.59 \cdot in^2$
Available strength, weld rupture (AISC Design Guide 24, Equation 5-25a)	$P_{u1} := \dfrac{w \cdot F_{wc} \cdot L_w}{\sqrt{2}}$ float,4 $\rightarrow 155.9 \cdot kip$
Available strength, HSS yield (AISC Manual Equation D2-1)	$P_{u2} := \phi_y \cdot F_{yh} \cdot A_g$ float,4 $\rightarrow 341.5 \cdot kip$
Available strength, HSS rupture (AISC Manual Equation D2-2)	$P_{u3} := \phi_r \cdot F_{uh} \cdot A_e$ float,4 $\rightarrow 352.9 \cdot kip$
Available strength, bolts (AISC Manual Table 7-2)	$P_{u4} := n \cdot \phi_{rn}$ float,4 $\rightarrow 119.2 \cdot kip$
Limiting available strength	$P_u := \min\left(\dfrac{P_{u1}}{kip}, \dfrac{P_{u2}}{kip}, \dfrac{P_{u3}}{kip}, \dfrac{P_{u4}}{kip}\right) \cdot kip \rightarrow 119.2 \cdot kip$

NOTE: Bolt strength governs design

HSS edge to bolt edge	$b' := \dfrac{\left(\min\left(l_p, b_p\right) - \min\left(l_h, b_h\right)\right)}{4} - \dfrac{d_b}{2}$ float,3 $\rightarrow 0.875 \cdot in$
Bolt end tributary length	$p := \max\left(l_p, b_p\right) \rightarrow 12 \cdot in$
Prying factor	$\delta := 1 - \dfrac{d_h}{p}$ float,3 $\rightarrow 0.932$
Prying factor	$a_e := \dfrac{\left(b_p - b_h\right)}{4}$ float,3 $\rightarrow 1.25 \cdot in$
Prying factor	$a' := a_e + \dfrac{d_b}{2}$ float,3 $\rightarrow 1.62 \cdot in$
Prying factor	$\rho := \dfrac{b'}{a'}$ float,3 $\rightarrow 0.54$
Prying factor (LRFD Design)	$\beta := \dfrac{\left(\phi_{rn} \cdot \dfrac{n}{P_u} - 1\right)}{\rho}$ float,3 $\rightarrow -4.67e\text{-}29$
Prying factor	$\alpha' := if\left[\beta < 1, \min\left[1, \dfrac{\left\lfloor \dfrac{\beta}{(1-\beta)} \right\rfloor}{\delta}\right], 1\right]$ float,3 $\rightarrow -5.01e\text{-}29$

Minimum base plate thickness
(AISC Design Guide 24, Equation 5-23a

$$t_{bp1} := \left[\sqrt{\frac{4.44 \cdot P_u}{in^2 \cdot n} \cdot \frac{b'}{\left(p \cdot F_{yp}\right)}} \cdot in \right] \text{float}, 3 \rightarrow 0.439 \cdot in$$

$$t_{bp1\_eff} := \text{ceil}\left(t_{bp1} \cdot \frac{16}{in} \right) \rightarrow 8 \quad [16\text{th inch}]$$

Minimum base plate thickness
(AISC Design Guide 24, Equation 5-26a

$$t_{bp2} := \sqrt{\frac{4.44 \cdot P_u}{in^2 \cdot n} \cdot \frac{b'}{\left[p \cdot F_{yp} \cdot (1 + \delta \cdot \alpha')\right]}} \cdot in \text{ float}, 3 \rightarrow 0.439 \cdot in$$

$$t_{bp2\_eff} := \text{ceil}\left(t_{bp2} \cdot \frac{16}{in} \right) \rightarrow 8 \quad [16\text{th inch}]$$

Minimum base plate thickness

$$t_{bp} := \min\left(t_{bp1\_eff}, t_{bp2\_eff} \right) \rightarrow 8 \quad [16\text{th inch}]$$

Minimum cap plate thickness

$$t_{cp} := \text{ceil}\left(1.5 \cdot t_{bp} \right) \rightarrow 12 \quad [16\text{th inch}]$$

Nelson Calculations
Base/Cap Plate Design (HSS7x4x5/16)

Given:

Strength reduction factor, weld	$\phi_w := 0.75$
Strength reduction factor, tensile yield	$\phi_y := 0.9$
Strength reduction factor, tensile rupture	$\phi_r := 0.75$
Yield strength, HSS	$F_{yh} := 50 \dfrac{kip}{in^2}$
Rupture Strength, HSS	$F_{uh} := 62 \dfrac{kip}{in^2}$
Length, HSS	$l_h := 7 in$
Width, HSS	$b_h := 4 in$
Thickness, HSS	$t := 0.3125 in$
Length workable flat	$f_l := 5.625 in$
Width workable flat	$f_b := 2.625 in$
Yield strength, base plate	$F_{yp} := 50 \dfrac{kip}{in^2}$
Length, plate	$l_p := 12 in$
Width, plate	$b_p := 12 in$
Weld electrode	$F_{EXX} := 70 \dfrac{kip}{in^2}$
Weld size	$w := 0.25 in$
Bolt diameter	$d_b := 0.75 in$
Hole diameter	$d_h := \dfrac{13 in}{16} \ float, 4 \ \rightarrow 0.8125 \cdot in$
Bolt available tensile strength (AISC Tab. 7-2)	$\phi_{rn} := 29.8 kip$
Gross area, HSS	$A_g := 5.85 in^2$
Net area, HSS	$A_n := 5.85 in^2$
Shear lag factor	$U := 1$
Number of bolts	$n := 4$

Design:

60% weld electrode	$F_w := F_{EXX} \cdot 0.6 \rightarrow \dfrac{42.0 \cdot kip}{in^2}$
Design weld strength	$F_{wc} := F_w \cdot \phi_w \rightarrow \dfrac{31.5 \cdot kip}{in^2}$
Weld length	$L_w := 2(l_h + b_h) \rightarrow 22 \cdot in$
Effective Area	$A_e := A_n \cdot U \rightarrow 5.85 \cdot in^2$
Available strength, weld rupture (AISC Design Guide 24, Equation 5-25a)	$P_{u1} := \dfrac{w \cdot F_{wc} \cdot L_w}{\sqrt{2}}$ float, 4 $\rightarrow 122.5 \cdot kip$
Available strength, HSS yield (AISC Manual Equation D2-1)	$P_{u2} := \phi_y \cdot F_{yh} \cdot A_g$ float, 4 $\rightarrow 263.2 \cdot kip$
Available strength, HSS rupture (AISC Manual Equation D2-2)	$P_{u3} := \phi_r \cdot F_{uh} \cdot A_e$ float, 4 $\rightarrow 272.0 \cdot kip$
Available strength, bolts (AISC Manual Table 7-2)	$P_{u4} := n \cdot \phi_{rn}$ float, 4 $\rightarrow 119.2 \cdot kip$
Limiting available strength	$P_u := min\left(\dfrac{P_{u1}}{kip}, \dfrac{P_{u2}}{kip}, \dfrac{P_{u3}}{kip}, \dfrac{P_{u4}}{kip}\right) \cdot kip \rightarrow 119.2 \cdot kip$

Note: Bolt strength governs design

HSS edge to bolt edge	$b' := \dfrac{\left(min\left(\dfrac{l_p}{in}, \dfrac{b_p}{in}\right) - min\left(\dfrac{l_h}{in}, \dfrac{b_h}{in}\right)\right)}{4} \cdot in - \dfrac{d_b}{2}$
	b' float, 4 $\rightarrow 1.625 \cdot in$
Bolt end tributary length	$p := max(l_p, b_p) \rightarrow 12 \cdot in$
Prying factor	$\delta := 1 - \dfrac{d_h}{p}$ float, 3 $\rightarrow 0.932$
Prying factor	$a_e := \dfrac{(b_p - b_h)}{4}$ float, 3 $\rightarrow 2.0 \cdot in$
Prying factor	$a' := a_e + \dfrac{d_b}{2}$ float, 3 $\rightarrow 2.37 \cdot in$
Prying factor	$\rho := \dfrac{b'}{a'}$ float, 3 $\rightarrow 0.686$
Prying factor (LRFD Design)	$\beta := \dfrac{\left(\phi_{rn} \cdot \dfrac{n}{P_u} - 1\right)}{\rho}$ float, 3 $\rightarrow -3.68e-29$

Prying factor $\quad \alpha' := \text{if}\left[\beta < 1, \min\left[1, \dfrac{\left\lfloor\dfrac{\beta}{(1-\beta)}\right\rfloor}{\delta}\right], 1\right] \text{ float}, 3 \rightarrow -3.95\text{e-}29$

Minimum base plate thickness
(AISC Design Guide 24, Equation 5-23a

$t_{bp1} := \left[\sqrt{\dfrac{4.44 \cdot P_u}{in^2 \cdot n} \cdot \dfrac{b'}{(p \cdot F_{yp})}} \cdot in\right] \text{ float}, 3 \rightarrow 0.599 \cdot in$

$= \text{ceil}\left(t_{bp1} \cdot \dfrac{16}{in}\right) \rightarrow 10 \quad \text{[16th inch]}$

Minimum base plate thickness
(AISC Design Guide 24, Equation 5-26a

$t_{bp2} := \sqrt{\dfrac{4.44 \cdot P_u}{in^2 \cdot n} \cdot \dfrac{b'}{\left[p \cdot F_{yp} \cdot (1 + \delta \cdot \alpha')\right]}} \cdot in \text{ float}, 3 \rightarrow 0.599 \cdot in$

$= \text{ceil}\left(t_{bp2} \cdot \dfrac{16}{in}\right) \rightarrow 10 \quad \text{[16th inch]}$

Minimum base plate thickness $\quad t_{bp} := \min\left(t_{bp1\_eff}, t_{bp2\_eff}\right) \rightarrow 10 \text{ [16th inch]}$

Minimum cap plate thickness $\quad t_{cp} := \text{ceil}\left(1.5 \cdot t_{bp}\right) \rightarrow 15 \quad \text{[16th inch]}$

Axial Calculations

A193 Bolt Strength

$f_{yb} := 105 \; \boldsymbol{ksi}$

$d_b := \dfrac{3}{4} \; \boldsymbol{in}$

$A_b := \boldsymbol{\pi} \cdot \left(\dfrac{d_b}{2}\right)^2 = 0.442 \; \boldsymbol{in}^2$

$r_n := A_b \cdot f_{yb} = 46.388 \; \boldsymbol{kip}$

$\phi := 0.75$

$\phi r_n := \phi \cdot r_n = 34.791 \; \boldsymbol{kip}$

$n := 4$

$R_n := n \cdot r_n = 185.55 \; \boldsymbol{kip}$

$\phi R_n := n \cdot \phi r_n = 139.163 \; \boldsymbol{kip}$

$T_r := \dfrac{\phi R_n}{n} = 34.791 \; \boldsymbol{kip}$

AISC Design Guide 24 (2010) Prying Action

$f_{yp} := 57.1 \; \boldsymbol{ksi}$ $\qquad$ $f_{up} := 82.9 \; \boldsymbol{ksi}$

$d_h := \dfrac{13}{16} \; \boldsymbol{in}$

$b := 1.25 \; \boldsymbol{in}$

$p := 12 \; \boldsymbol{in}$

$a := 1.25 \; \boldsymbol{in}$

$a_e := 1.25 \; \boldsymbol{in}$

$a' := a_e + \dfrac{d_b}{2} = 1.625 \; \boldsymbol{in}$

$b' := b - \dfrac{d_b}{2} = 0.875 \; \boldsymbol{in}$

$$t_{min} := \sqrt{\frac{4.44 \cdot \left(T_r\right) b'}{p \cdot f_{yp}}} = 0.444 \; in$$

Calculate Force Using Actual Plate Thickness of 1/2"

$$t := \frac{1}{2} \; in$$

$$P_n := \frac{t^2 \cdot p \cdot f_{yp}}{4.44 \cdot b'} \cdot n = 176.371 \; kip$$

Corner Specimen Capacity - HSS Connections Manual (1997) and Christensen (2010)

$$L := \sqrt{\left(1.25 \; in\right)^2 + \left(1.25 \; in\right)^2} = 1.768 \; in$$

$$b_e := 2 \cdot L = 3.536 \; in$$

$$R_n := \frac{b_e \cdot t^2 \; f_{yp}}{L} = 28.55 \; kip \qquad\qquad \text{Equation (29)}$$

$$P_n := 4 \cdot R_n = 114.2 \; kip$$

$$t_{HSS} := \frac{1}{4} \; in$$

$$R_{HSS} := 0.6$$

$$P_n := R_{HSS} \cdot 4 \cdot R_n = 68.52 \; kip$$

$$t_{HSS} := \frac{3}{8} \; in$$

$$R_{HSS} := 0.7$$

$$P_n := R_{HSS} \cdot 4 \cdot R_n = 79.94 \; kip$$

Prying Actions for Side Bolts with Adjusted Tributary Width - Thornton (2017) and AISC *Manual,* 16th Ed., Equations

$$P_u := 100 \; \textbf{\textit{kip}}$$ (100-kip Capacity of Load Cell)

$$w_i := 7 \; \textbf{\textit{in}}$$

$$h_i := 7 \; \textbf{\textit{in}}$$

$$p_c := \frac{2 \cdot (w_i + h_i + \pi \cdot b)}{n} = 8.963 \; \textbf{\textit{in}}$$ Equation (32)

$$p_{imax} := 4 \cdot \sqrt{b' \cdot (a+b)} = 5.916 \; \textbf{\textit{in}}$$ Equation (33)

$$\phi_b := 0.9$$

$$t_{min} := \sqrt{\frac{4.44 \cdot (T_r) \; b'}{\phi_b \cdot p_{imax} \cdot f_{up}}} = 0.553 \; \textbf{\textit{in}}$$ No Prying Action - Equation (3)

$$t := \frac{1}{2} \; \textbf{\textit{in}}$$

$$P_n := \frac{t^2 \cdot \phi_b \cdot p_{imax} \cdot f_{up}}{4.44 \cdot b'} \cdot n = 113.616 \; \textbf{\textit{kip}}$$

$$\delta := 1 - \frac{d_h}{p_{imax}} = 0.863$$

$$\rho := \frac{b'}{a'} = 0.538$$

$$\beta := \left[\frac{\phi r_n}{\left(\dfrac{P_u}{n} \right)} - 1 \right] \cdot \frac{1}{\rho} = [0.727]$$

$$\alpha' := min\left(1.0, \frac{1}{\delta} \cdot \left(\frac{\beta}{1-\beta} \right) \right) = 1$$

$$t_{min} := \sqrt{\frac{4.44 \cdot (T_r) \cdot b'}{\phi_b \cdot p_{imax} \cdot f_{up} \cdot (1 + \delta \cdot \alpha')}} = 0.405 \; \textbf{\textit{in}}$$ Prying Action - Equation (5)

$$P_n := \frac{t^2 \cdot \phi_b \cdot p_{imax} \cdot f_{up} \cdot (1 + \delta \cdot \alpha')}{4.44 \cdot b'} \cdot n = 211.629 \; \textbf{kip}$$

Prying Action for Corner Bolts with p=be

$$p := b_e = 3.536 \; \textbf{in}$$

$$a' := a + \frac{d_b}{2} = 1.625 \; \textbf{in}$$

$$b' := b - \frac{d_b}{2} = 0.875 \; \textbf{in}$$

$$t_{min} := \sqrt{\frac{4.44 \cdot (T_r) \; b'}{\phi_b \cdot p \cdot f_{up}}} = 0.716 \; \textbf{in}$$ No Prying Action - Equation (3)

$$t := \frac{1}{2} \; \textbf{in}$$

$$P_n := \frac{t^2 \cdot \phi_b \cdot p \cdot f_{up}}{4.44 \cdot b'} \cdot n = 67.899 \; \textbf{kip}$$

$$\delta := 1 - \frac{d_h}{p} = 0.77$$

$$\rho := \frac{b'}{a'} = 0.538$$

$$\beta := \left[\frac{\phi r_n}{\left(\frac{P_u}{n} \right)} - 1 \right] \cdot \frac{1}{\rho} = [0.727]$$

$$\alpha' := min\left(1.0, \frac{1}{\delta} \cdot \left(\frac{\beta}{1 - \beta} \right) \right) = 1$$

$$t_{min} := \sqrt{\frac{4.44 \cdot (T_r) \cdot b'}{\phi_b \cdot p \cdot f_{up} \cdot (1 + \delta \cdot \alpha')}} = 0.538 \ in$$ Prying Action - Equation (5)

$$P_n := \frac{t^2 \cdot \phi_b \cdot p \cdot f_{up} \cdot (1 + \delta \cdot \alpha')}{4.44 \cdot b'} \cdot n = 120.193 \ kip$$

Prying Action for Corner Bolts with Adjusted a and b Dimensions

$$p := p_{imax} = 5.916 \ in$$

$$b := \sqrt{(1.25 \ in)^2 + (1.25 \ in)^2} = 1.768 \ in$$

$$a := \sqrt{(1.25 \ in)^2 + (1.25 \ in)^2} = 1.768 \ in$$

$$a' := a + \frac{d_b}{2} = 2.143 \ in$$

$$b' := b - \frac{d_b}{2} = 1.393 \ in$$

$$t_{min} := \sqrt{\frac{4.44 \cdot (T_r) \ b'}{\phi_b \cdot p \cdot f_{up}}} = 0.698 \ in$$ No Prying Action - Equation (3)

$$t := \frac{1}{2} \ in$$

$$P_n := \frac{t^2 \cdot \phi_b \cdot p \cdot f_{up}}{4.44 \cdot b'} \cdot n = 71.379 \ kip$$

$$\delta := 1 - \frac{d_h}{p} = 0.863$$

$$\rho := \frac{b'}{a'} = 0.65$$

$$\beta := \left[\frac{\phi r_n}{\left(\frac{P_u}{n} \right)} - 1 \right] \cdot \frac{1}{\rho} = [0.603]$$

$$\alpha' := min\left(1.0, \frac{1}{\delta} \cdot \left(\frac{\beta}{1-\beta} \right) \right) = 1$$

$$t_{min} := \sqrt{\frac{4.44 \cdot (T_r) \cdot b'}{\phi_b \cdot p \cdot f_{up} \cdot (1 + \delta \cdot \alpha')}} = 0.512 \ \pmb{in}$$ Prying Action - Equation (5)

$$P_n := \frac{t^2 \cdot \phi_b \cdot p \cdot f_{up} \cdot (1 + \delta \cdot \alpha')}{4.44 \cdot b'} \cdot n = 132.955 \ \pmb{kip}$$

Prying Action for Corner Bolts with Adjusted a and b Dimensions and p= be

$$p := b_e = 3.536 \ \pmb{in}$$

$$b := \sqrt{(1.25 \ \pmb{in})^2 + (1.25 \ \pmb{in})^2} = 1.768 \ \pmb{in}$$

$$a := \sqrt{(1.25 \ \pmb{in})^2 + (1.25 \ \pmb{in})^2} = 1.768 \ \pmb{in}$$

$$a' := a + \frac{d_b}{2} = 2.143 \ \pmb{in}$$

$$b' := b - \frac{d_b}{2} = 1.393 \ \pmb{in}$$

$$t_{min} := \sqrt{\frac{4.44 \cdot (T_r) \ b'}{\phi_b \cdot p \cdot f_{up}}} = 0.903 \ \pmb{in}$$ No Prying Action - Equation (3)

$$P_n := \frac{t^2 \cdot \phi_b \cdot p \cdot f_{up}}{4.44 \cdot b'} \cdot n = 42.657 \ \pmb{kip}$$

$$\delta := 1 - \frac{d_h}{p} = 0.77$$

$$\rho := \frac{b'}{a'} = 0.65$$

$$\beta := \left[\frac{\phi r_n}{\left(\frac{P_u}{n} \right)} - 1 \right] \cdot \frac{1}{\rho} = [0.603]$$

$$\alpha' := min\left(1.0, \frac{1}{\delta} \cdot \left(\frac{\beta}{1-\beta} \right) \right) = 1$$

$$t_{min} := \sqrt{\frac{4.44 \cdot (T_r) \cdot b'}{\phi_b \cdot p \cdot f_{up} \cdot (1 + \delta \cdot \alpha')}} = 0.679 \; \boldsymbol{in}$$

Prying Action - Equation (5)

$$P_n := \frac{t^2 \cdot \phi_b \cdot p \cdot f_{up} \cdot (1 + \delta \cdot \alpha')}{4.44 \cdot b'} \cdot n = 75.511 \; \boldsymbol{kip}$$

Strong Axis - AISC Design Guide 24 (LRFD)

HSS7x4x5/16

$F_{yHSS} := 53.2 \ ksi$
$F_{uHSS} := 66.8 \ ksi$

$S_x := 10.4 \ in^3$

$M_u := F_{yHSS} \cdot S_x = 46.107 \ kip \cdot ft$

$E := 29000 \ ksi$

Base Plate

$F_{yp} := 57.1 \ ksi$
$F_{up} := 82.9 \ ksi$

From AISC *Manual* Table 1-12, the HSS geometric properties are as follows:

HSS7x4x5/16
$H := 4.00 \ in$
$B := 7.00 \ in$

$t := \dfrac{5}{16} \ in = 0.313 \ in$

Gage
$g := 9.5 \ in$

Geometric properties of end-plate and bolts are as follows:

Base Plate
$L := 12.0 \ in$
$W := 12.0 \ in$

$t_p := \dfrac{5}{8} \ in = 0.625 \ in$

A193 B7 Rods

$F_{nt} := 125 \ ksi$

$d_b := \dfrac{3}{4} \ in = 0.75 \ in$

Tensile load in bolt

$$M_u = 553.28 \; kip \cdot in$$

$$T_u := \frac{M_u}{\dfrac{g}{2}} \cdot \frac{1}{2} = 58.24 \; kip$$

Effect of prying action - end-plate minimum thickness

$$b := \frac{(g - B)}{2} = 1.25 \; in$$

$$b' := b - \frac{d_b}{2} = 0.875 \; in$$

$$p := \frac{W}{2} = 6 \; in$$

$$t_{min} := \sqrt{\frac{4.44 \cdot T_u \cdot b'}{p \cdot F_{up}}} = 0.674 \; in$$

Effect of prying action - capacity using actual 5/8" end-plate thickness

$$T_n := \frac{t_p^{\;2} \cdot p \cdot F_{up}}{4.44 \cdot b'} = 50.012 \; kip$$

$$M_n := T_n \cdot \frac{g}{2} \cdot 2 = 39.593 \; kip \cdot ft$$

$$P_n := \frac{M_n}{35.5 \; in} = 13.384 \; kip$$

$$\phi_p := 0.9$$

$$\phi_p M_n := \phi_p \cdot M_n = 35.634 \; kip \cdot ft$$

$$\phi_p P_n := \phi_p \cdot P_n = 12.045 \; kip$$

Bolt available tensile strength

$$\phi r_n := 0.75 \cdot F_{nt} \cdot \pi \cdot \left(\frac{d_b}{2}\right)^2 = 41.417 \; kip$$

Weld size between the HSS and end-plate

$$2 \ g = 19 \ \boldsymbol{in} \ > B$$

$$2 \cdot \left(d_b + 2 \cdot b \right) = 6.5 \ \boldsymbol{in}$$

$$B = 7 \ \boldsymbol{in}$$

$$\frac{2 \cdot T_u}{B} = 16.64 \ \frac{\boldsymbol{kip}}{\boldsymbol{in}}$$

$$D := \frac{\dfrac{2 \cdot T_u}{B}}{1.392 \ \dfrac{\boldsymbol{kip}}{\boldsymbol{in}}} = 11.954$$

Force using actual 1/4" weld size (D=4)

$$D := 4$$

$$T_u := \frac{D \cdot 1.392 \ \dfrac{\boldsymbol{kip}}{\boldsymbol{in}} \cdot (B)}{2} = 19.488 \ \boldsymbol{kip}$$

$$\phi M_u := \left(T_u \cdot 12 \right) \cdot \frac{g}{2} \cdot \frac{1}{2} = 46.284 \ \boldsymbol{kip} \cdot \boldsymbol{ft}$$

$$\phi := 0.75$$

$$M_u := \frac{\phi M_u}{\phi} = 61.712 \ \boldsymbol{kip} \cdot \boldsymbol{ft}$$

$$P := \frac{M_u}{35.5 \ \boldsymbol{in}} = 20.86 \ \boldsymbol{kip}$$

Weak Axis - AISC Design Guide 24 (LRFD)

HSS7x4x5/16

$F_{yHSS} := 53.2 \ ksi$
$F_{uHSS} := 66.8 \ ksi$

$S_y := 5.16 \ in^3$

$M_u := F_{yHSS} \cdot S_y = 22.876 \ kip \cdot ft$

$E := 29000 \ ksi$

Base Plate

$F_{yp} := 57.1 \ ksi$
$F_{up} := 82.9 \ ksi$

From AISC *Manual* Table 1-12, the HSS geometric properties are as follows:

HSS7x4x5/16
$H := 7.00 \ in$
$B := 4.00 \ in$

$t := \dfrac{5}{16} \ in = 0.313 \ in$

Gage
$g := 9.5 \ in$

Geometric properties of end-plate plate and bolts are as follows:

Base Plate
$L := 12.0 \ in$
$W := 12.0 \ in$

$t_p := \dfrac{5}{8} \ in = 0.625 \ in$

A193 B7 Rods

$F_{nt} := 90 \ ksi$

$d_b := \dfrac{3}{4} \ in = 0.75 \ in$

Tensile load in bolt

$$M_u = 274.512 \ \boldsymbol{kip \cdot in}$$

$$T_u := \frac{M_u}{\frac{g}{2}} \cdot \frac{1}{2} = 28.896 \ \boldsymbol{kip}$$

Effect of prying action - end-plate minimum thickness

$$b := \frac{(g - B)}{2} = 2.75 \ \boldsymbol{in}$$

$$b' := b - \frac{d_b}{2} = 2.375 \ \boldsymbol{in}$$

$$p := \frac{W}{2} = 6 \ \boldsymbol{in}$$

$$t_{min} := \sqrt{\frac{4.44 \cdot T_u \cdot b'}{p \cdot F_{up}}} = 0.783 \ \boldsymbol{in}$$

Effect of prying action - capacity using actual 5/8" end-plate thickness

$$T_n := \frac{t_p^{\ 2} \cdot p \cdot F_{up}}{4.44 \cdot b'} = 18.425 \ \boldsymbol{kip}$$

$$M_n := T_n \cdot \frac{g}{2} \cdot 2 = 14.587 \ \boldsymbol{kip \cdot ft}$$

$$P_n := \frac{M_n}{35.5 \ \boldsymbol{in}} = 4.931 \ \boldsymbol{kip}$$

$$\phi_p := 0.9$$

$$\phi_p M_n := \phi_p \cdot M_n = 13.128 \ \boldsymbol{kip \cdot ft}$$

$$\phi_p P_n := \phi_p \cdot P_n = 4.438 \ \boldsymbol{kip}$$

Bolt available tensile strength

$$\phi r_n := 0.75 \cdot F_{nt} \cdot \pi \cdot \left(\frac{d_b}{2}\right)^2 = 29.821 \ \boldsymbol{kip}$$

Weld size between the HSS and end-plate

$$2\ g = 19\ in\ > B$$

$$2 \cdot (d_b + 2 \cdot b) = 12.5\ in\ > B$$

$$B = 4\ in$$

$$\frac{2 \cdot T_u}{B} = 14.448\ \frac{kip}{in}$$

$$D := \frac{\dfrac{2 \cdot T_u}{B}}{1.392\ \dfrac{kip}{in}} = 10.379$$

Force Using 1/4" Weld (D=4)

$$D := 4$$

$$T_u := \frac{D \cdot 1.392\ \dfrac{kip}{in} \cdot (B)}{2} = 11.136\ kip$$

$$\phi M_u := (T_u \cdot 12) \cdot \frac{g}{2} \cdot \frac{1}{2} = 26.448\ ft \cdot kip$$

$$\phi := 0.75$$

$$M_u := \frac{\phi M_u}{\phi} = 35.264\ ft \cdot kip$$

$$P := \frac{M_u}{35.5\ in} = 11.92\ kip$$

Strong Axis - Wheeler et al. Method

$f_y := 57.1 \ \boldsymbol{ksi}$

$f_u := 82.9 \ \boldsymbol{ksi}$

$f_p := \dfrac{f_y + 2 \cdot f_u}{3} = 74.3 \ \boldsymbol{ksi}$

$W_p := 12 \ \boldsymbol{in}$	$b := 4 \ \boldsymbol{in}$	$d_f := \dfrac{13}{16} \ \boldsymbol{in}$
$D_p := 12 \ \boldsymbol{in}$	$d := 7 \ \boldsymbol{in}$	$d_b := \dfrac{3}{4} \ \boldsymbol{in}$
$a_e := 1.25 \ \boldsymbol{in}$	$t_s := \dfrac{5}{16} \ \boldsymbol{in}$	$B_y := 105 \ \boldsymbol{ksi} \cdot \pi \cdot \left(\dfrac{d_b}{2}\right)^2 = 46.388 \ \boldsymbol{kip}$
$c := 2.75 \ \boldsymbol{in}$	$t_p := \dfrac{5}{8} \ \boldsymbol{in}$	
$s_0 := 1.25 \ \boldsymbol{in}$	$s := 0.25 \ \boldsymbol{in}$	$B_u := 125 \ \boldsymbol{ksi} \cdot \pi \cdot \left(\dfrac{d_b}{2}\right)^2 = 55.223 \ \boldsymbol{kip}$

$n := 2$

$a_p := min\left(a_e, \left(2 \cdot t_p\right)\right) = 1.25 \ \boldsymbol{in}$

$s_0' := s_0 - \dfrac{s}{\sqrt{2}} = 1.073 \ \boldsymbol{in}$

$d' := d + \dfrac{s}{\sqrt{2}} = 7.177 \ \boldsymbol{in}$

FIG. 3. End Plate Layout and Model Parameters

$w := b + 2 \cdot a_e + 2 \cdot c = 12 \ \boldsymbol{in}$

$v := d' + s_0' = 8.25 \ \boldsymbol{in}$

$u_{max} := s_0' + a_e = 2.323 \ \boldsymbol{in}$

$0 \le u < u_{max}$

$u := 0 \ \boldsymbol{in}$

FIG. 6. Analytical Model Used in Modified Stub-Tee Analysis

$q := a_e + s_0' - u = 2.323 \ \boldsymbol{in}$

$r := 2 \cdot q \cdot c - b \cdot d' = -15.929 \ \boldsymbol{in}^2$

$$d_{34} := \frac{a_e \cdot (2 \cdot q \cdot v - r) \cdot \left(\sqrt{\left(\dfrac{2}{r}\right)^2 + \left(\dfrac{1}{q \cdot v}\right)^2}\right)}{2} - d_f = 3.799 \; \textbf{in}$$

$$m_p := \frac{1}{4} \cdot t_p^{\;2} \cdot f_y = 5.576 \; \textbf{kip}$$

Mode 1

$$M_{y1} := \left(\frac{(d' + 2 \cdot (s_0' + a_e)) \cdot w}{(s_0' + a_e) \cdot d'} \cdot m_p + \frac{n \cdot B_y \cdot a_e}{s_0' + a_e}\right) \cdot (d - t_s) = 54.3 \; \textbf{kip} \cdot \textbf{ft}$$

Mode 2

$$M_{y2} := \left(\frac{2 \cdot (d' + s_0') \cdot w}{s_0' \cdot d'} - \frac{n \cdot d_f}{s_0'}\right) \cdot m_p \cdot (d - t_s) = 75.2 \; \textbf{kip} \cdot \textbf{ft}$$

Mode 3

$$M_{y3} := \left(\frac{w}{d'} + \frac{\dfrac{v \cdot w}{b} \cdot (b^2 + 4 \cdot q^2) + \left(\sqrt{r^2 + 4 \cdot v^2 \; q^2}\right) \cdot d_{34} + 4 \cdot u \cdot q \cdot v}{(2 \cdot q \cdot c + s_0' \cdot b) \cdot d'}\right) \cdot d \cdot m_p = 34.3 \; \textbf{kip} \cdot \textbf{ft}$$

Failure Mode

$$M_y := min\left(M_{y1}, M_{y2}, M_{y3}\right) = 34.326 \; \textbf{kip} \cdot \textbf{ft}$$

Design Model

$$w_{eq} := \left(\frac{4 \cdot M_{y3}}{d \cdot t_p^{\;2} \cdot f_p} + \frac{n \cdot d_f}{s_0'}\right) \cdot \left(\frac{d' \cdot s_0'}{2 \cdot (d' + s_0')}\right) = 4.493 \; \textbf{in}$$

$$\phi_b := 0.8$$

$$\phi_p := 0.9$$

Bolt Failure

$$f_{yb} := \frac{B_y}{\pi \cdot \left(\frac{d_b}{2}\right)^2} = 0.724 \ \frac{kN}{mm^2}$$

$$M_{cb} := \left(\frac{4 \cdot n \cdot \left(B_u \cdot a_p + \frac{\pi \cdot d_b^3 \cdot f_{yb}}{32}\right) \cdot d' + w_{eq} \cdot \left(d' + 2 \cdot \left(s_0' + a_p\right)\right) \cdot t_p^2 \cdot f_p}{4 \cdot \left(a_p + s_0'\right) \cdot d'}\right) \cdot \left(d - t_s\right) = 48.086 \ \textbf{kip} \cdot \textbf{ft}$$

$$\phi_b \cdot M_{cb} = 38.469 \ \textbf{kip} \cdot \textbf{ft}$$

$$P_{cb} := \frac{M_{cb}}{35.5 \ \textbf{in}} = 16.254 \ \textbf{kip}$$

$$t_{bu} := \sqrt{\frac{4 \cdot \left(\frac{\left(M_{cb} \cdot \left(a_p + s_0'\right)\right)}{\phi_b \cdot \left(d - t_s\right)} - n \cdot \left(B_u \cdot a_p + \frac{\pi \cdot d_b^3 \cdot f_{yb}}{32}\right)\right) \cdot d'}{w_{eq} \cdot \left(d' + 2 \cdot \left(s_0' + a_p\right)\right) \cdot f_p}} = 0.869 \ \textbf{in}$$

$$t_{pmax} := \sqrt{\frac{4 \cdot n \cdot B_u \cdot s_0'}{w_{eq} \cdot f_p}} = 1.192 \ \textbf{in}$$

Plate Failure

$$M_{cp} := \left(\frac{t_p^2 \cdot f_p \cdot \left(w_{eq} \cdot \left(d' + 2 \cdot s_0'\right) + \left(w_{eq} - n \cdot d_f\right) \cdot d'\right) + n \cdot \frac{\pi \cdot d_b^3 \cdot f_{yb}}{8} \cdot d'}{4 \cdot d' \cdot s_0'}\right) \cdot \left(d - t_s\right) = 37.31 \ \textbf{kip} \cdot \textbf{ft}$$

$$\phi_p \cdot M_{cp} = 33.579 \ \textbf{kip} \cdot \textbf{ft}$$

$$P_{cp} := \frac{M_{cp}}{35.5 \ \textbf{in}} = 12.612 \ \textbf{kip}$$

$$t_{pu} := 2 \cdot \sqrt{\frac{\left(\frac{M_{cb} \cdot s_0'}{\phi_p \cdot \left(d + t_s\right)} - n \cdot \frac{\pi \cdot d_b^3 \cdot f_{yb}}{32}\right) \cdot d'}{\left(w_{eq} \cdot \left(d' + 2 \cdot s_0'\right) + \left(w_{eq} - n \cdot d_f\right) \cdot d'\right) \cdot f_p}} = 0.727 \ \textbf{in}$$

Serviceability

Bolt Yielding

$$M_{cbs} := \left(\frac{\left(d' + 2 \cdot \left(s_0' + a_e \right) \right) \cdot w_{eq} \cdot t_p^{\ 2} \cdot f_y}{4 \cdot \left(s_0' + a_e \right) \cdot d'} + \frac{n \cdot B_y \cdot a_e}{s_0' + a_e} \right) \cdot \left(d - t_s \right) = 37.718 \ \textbf{kip} \cdot \textbf{ft}$$

$$\phi_b \cdot M_{cbs} = 30.175 \ \textbf{kip} \cdot \textbf{ft}$$

$$P_{cbs} := \frac{M_{cbs}}{35.5 \ \textbf{in}} = 12.75 \ \textbf{kip}$$

Plate Yielding

$$M_{cps} := \left(\frac{\left(\left(d' + s_0' \right) \cdot w_{eq} - n \cdot d_f \cdot d' \right) \cdot t_p^{\ 2} \cdot f_y}{2 \cdot d' \cdot s_0'} \right) \cdot \left(d - t_s \right) = 20.497 \ \textbf{kip} \cdot \textbf{ft}$$

$$\phi_p \cdot M_{cps} = 18.447 \ \textbf{kip} \cdot \textbf{ft}$$

$$P_{cps} := \frac{M_{cps}}{35.5 \ \textbf{in}} = 6.929 \ \textbf{kip}$$

Weak Axis - Wheeler et al. Method

$$f_y := 57.1 \; \textbf{\textit{ksi}}$$

$$f_u := 82.9 \; \textbf{\textit{ksi}}$$

$$f_p := \frac{f_y + 2 \cdot f_u}{3} = 74.3 \; \textbf{\textit{ksi}}$$

$W_p := 12 \; \textbf{\textit{in}}$	$b := 7 \; \textbf{\textit{in}}$	$d_f := \dfrac{13}{16} \; \textbf{\textit{in}}$
$D_p := 12 \; \textbf{\textit{in}}$	$d := 4 \; \textbf{\textit{in}}$	$d_b := \dfrac{3}{4} \; \textbf{\textit{in}}$
$a_e := 1.25 \; \textbf{\textit{in}}$	$t_s := \dfrac{5}{16} \; \textbf{\textit{in}}$	$B_y := 105 \; \textbf{\textit{ksi}} \cdot \pi \cdot \left(\dfrac{d_b}{2}\right)^2 = 46.388 \; \textbf{\textit{kip}}$
$c := 1.25 \; \textbf{\textit{in}}$	$t_p := \dfrac{5}{8} \; \textbf{\textit{in}}$	$B_u := 125 \; \textbf{\textit{ksi}} \cdot \pi \cdot \left(\dfrac{d_b}{2}\right)^2 = 55.223 \; \textbf{\textit{kip}}$
$s_0 := 2.75 \; \textbf{\textit{in}}$	$s := 0.25 \; \textbf{\textit{in}}$	$n := 2$

$$a_p := min\left(a_e, \left(2 \cdot t_p\right)\right) = 1.25 \; \textbf{\textit{in}}$$

$$s_0' := s_0 - \frac{s}{\sqrt{2}} = 2.573 \; \textbf{\textit{in}}$$

$$d' := d + \frac{s}{\sqrt{2}} = 4.177 \; \textbf{\textit{in}}$$

$$w := b + 2 \cdot a_e + 2 \cdot c = 12 \; \textbf{\textit{in}}$$

$$v := d' + s_0' = 6.75 \; \textbf{\textit{in}}$$

$$u_{max} := s_0' + a_e = 3.823 \; \textbf{\textit{in}}$$

$$0 \leq u < u_{max}$$

$$u := 0 \; \textbf{\textit{in}}$$

$$q := a_e + s_0' - u = 3.823 \; \textbf{\textit{in}}$$

$$r := 2 \cdot q \cdot c - b \cdot d' = -19.679 \; \textbf{\textit{in}}^2$$
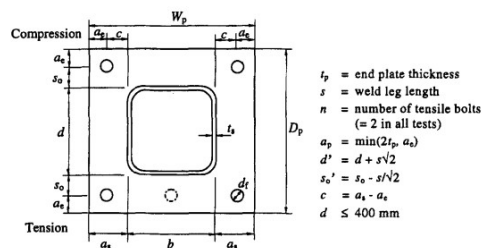
FIG. 3. End Plate Layout and Model Parameters
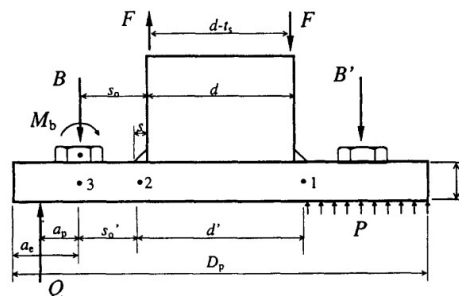
FIG. 6. Analytical Model Used in Modified Stub-Tee Analysis
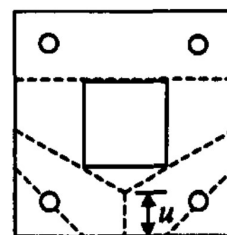
$$d_{34} := \frac{a_e \cdot (2 \cdot q \cdot v - r) \cdot \left(\sqrt{\left(\frac{2}{r}\right)^2 + \left(\frac{1}{q \cdot v}\right)^2} \right)}{2} - d_f = 4.034 \ \textbf{\textit{in}}$$

$$m_p := \frac{1}{4} \cdot t_p^{\ 2} \cdot f_y = 5.576 \ \textbf{\textit{kip}}$$

Mode 1

$$M_{y1} := \left(\frac{\left(d' + 2 \cdot (s_0' + a_e)\right) \cdot w}{(s_0' + a_e) \cdot d'} \cdot m_p + \frac{n \cdot B_y \cdot a_e}{s_0' + a_e} \right) \cdot (d - t_s) = 24.5 \ \textbf{\textit{kip}} \cdot \textbf{\textit{ft}}$$

Mode 2

$$M_{y2} := \left(\frac{2 \cdot (d' + s_0') \cdot w}{s_0' \cdot d'} - \frac{n \cdot d_f}{s_0'} \right) \cdot m_p \cdot (d - t_s) = 24.7 \ \textbf{\textit{kip}} \cdot \textbf{\textit{ft}}$$

Mode 3

$$M_{y3} := \left(\frac{w}{d'} + \frac{\frac{v \cdot w}{b} \cdot (b^2 + 4 \cdot q^2) + \left(\sqrt{r^2 + 4 \cdot v^2 \ q^2} \right) \cdot d_{34} + 4 \cdot u \cdot q \cdot v}{(2 \cdot q \cdot c + s_0' \cdot b) \cdot d'} \right) \cdot d \cdot m_p = 29 \ \textbf{\textit{kip}} \cdot \textbf{\textit{ft}}$$

Failure Mode

$$M_y := min \left(M_{y1}, M_{y2}, M_{y3} \right) = 24.545 \ \textbf{\textit{kip}} \cdot \textbf{\textit{ft}}$$

Design Model

$$w_{eq} := \left(\frac{4 \cdot M_{y3}}{d \cdot t_p^{\ 2} \cdot f_p} + \frac{n \cdot d_f}{s_0'} \right) \cdot \left(\frac{d' \cdot s_0'}{2 \cdot (d' + s_0')} \right) = 10.052 \ \textbf{\textit{in}}$$

$$\phi_b := 0.8$$

$$\phi_p := 0.9$$

Bolt Failure

$$f_{yb} := \frac{B_y}{\pi \cdot \left(\frac{d_b}{2}\right)^2} = 0.724 \ \frac{kN}{mm^2}$$

$$M_{cb} := \left(\frac{4 \cdot n \cdot \left(B_u \cdot a_p + \frac{\pi \cdot d_b^3 \cdot f_{yb}}{32}\right) \cdot d' + w_{eq} \cdot \left(d' + 2 \cdot \left(s_0' + a_p\right)\right) \cdot t_p^2 \cdot f_p}{4 \cdot \left(a_p + s_0'\right) \cdot d'}\right) \cdot \left(d - t_s\right) = 28.389 \ kip \cdot ft$$

$$\phi_b \cdot M_{cb} = 22.711 \ kip \cdot ft$$

$$P_{cb} := \frac{M_{cb}}{35.5 \ in} = 9.596 \ kip$$

$$t_{bu} := \sqrt{\frac{4 \cdot \left(\frac{\left(M_{cb} \cdot \left(a_p + s_0'\right)\right)}{\phi_b \cdot \left(d - t_s\right)} - n \cdot \left(B_u \cdot a_p + \frac{\pi \cdot d_b^3 \cdot f_{yb}}{32}\right)\right) \cdot d'}{w_{eq} \cdot \left(d' + 2 \cdot \left(s_0' + a_p\right)\right) \cdot f_p}} = 0.747 \ in$$

$$t_{pmax} := \sqrt{\frac{4 \cdot n \cdot B_u \cdot s_0'}{w_{eq} \cdot f_p}} = 1.234 \ in$$

Plate Failure

$$M_{cp} := \left(\frac{t_p^2 \cdot f_p \cdot \left(w_{eq} \cdot \left(d' + 2 \cdot s_0'\right) + \left(w_{eq} - n \cdot d_f\right) \cdot d'\right) + n \cdot \frac{\pi \cdot d_b^3 \cdot f_{yb}}{8} \cdot d'}{4 \cdot d' \cdot s_0'}\right) \cdot \left(d - t_s\right) = 27.781 \ kip \cdot ft$$

$$\phi_p \cdot M_{cp} = 25.003 \ kip \cdot ft$$

$$P_{cp} := \frac{M_{cp}}{35.5 \ in} = 9.391 \ kip$$

$$t_{pu} := 2 \cdot \sqrt{\frac{\left(\frac{M_{cb} \cdot s_0'}{\phi_p \cdot \left(d + t_s\right)} - n \cdot \frac{\pi \cdot d_b^3 \cdot f_{yb}}{32}\right) \cdot d'}{\left(w_{eq} \cdot \left(d' + 2 \cdot s_0'\right) + \left(w_{eq} - n \cdot d_f\right) \cdot d'\right) \cdot f_p}} = 0.615 \ in$$

Serviceability

Bolt Yielding

$$M_{cbs} := \left(\frac{\left(d' + 2 \cdot \left(s_0' + a_e \right) \right) \cdot w_{eq} \cdot t_p^2 \cdot f_y}{4 \cdot \left(s_0' + a_e \right) \cdot d'} + \frac{n \cdot B_y \cdot a_e}{s_0' + a_e} \right) \cdot \left(d - t_s \right) = 22.073 \ \boldsymbol{kip \cdot ft}$$

$$\phi_b \cdot M_{cbs} = 17.659 \ \boldsymbol{kip \cdot ft}$$

$$P_{cbs} := \frac{M_{cbs}}{35.5 \ \boldsymbol{in}} = 7.461 \ \boldsymbol{kip}$$

Plate Yielding

$$M_{cps} := \left(\frac{\left(\left(d' + s_0 \right) \cdot w_{eq} - n \cdot d_f \cdot d' \right) \cdot t_p^2 \cdot f_y}{2 \cdot d' \cdot s_0'} \right) \cdot \left(d - t_s \right) = 19.47 \ \boldsymbol{kip \cdot ft}$$

$$\phi_p \cdot M_{cps} = 17.523 \ \boldsymbol{kip \cdot ft}$$

$$P_{cps} := \frac{M_{cps}}{35.5 \ \boldsymbol{in}} = 6.581 \ \boldsymbol{kip}$$

Appendix B – Axial Tests Plots

Load versus Displacement Plots

Figure B1

Load versus Average Displacement for Corner Bolt Specimens
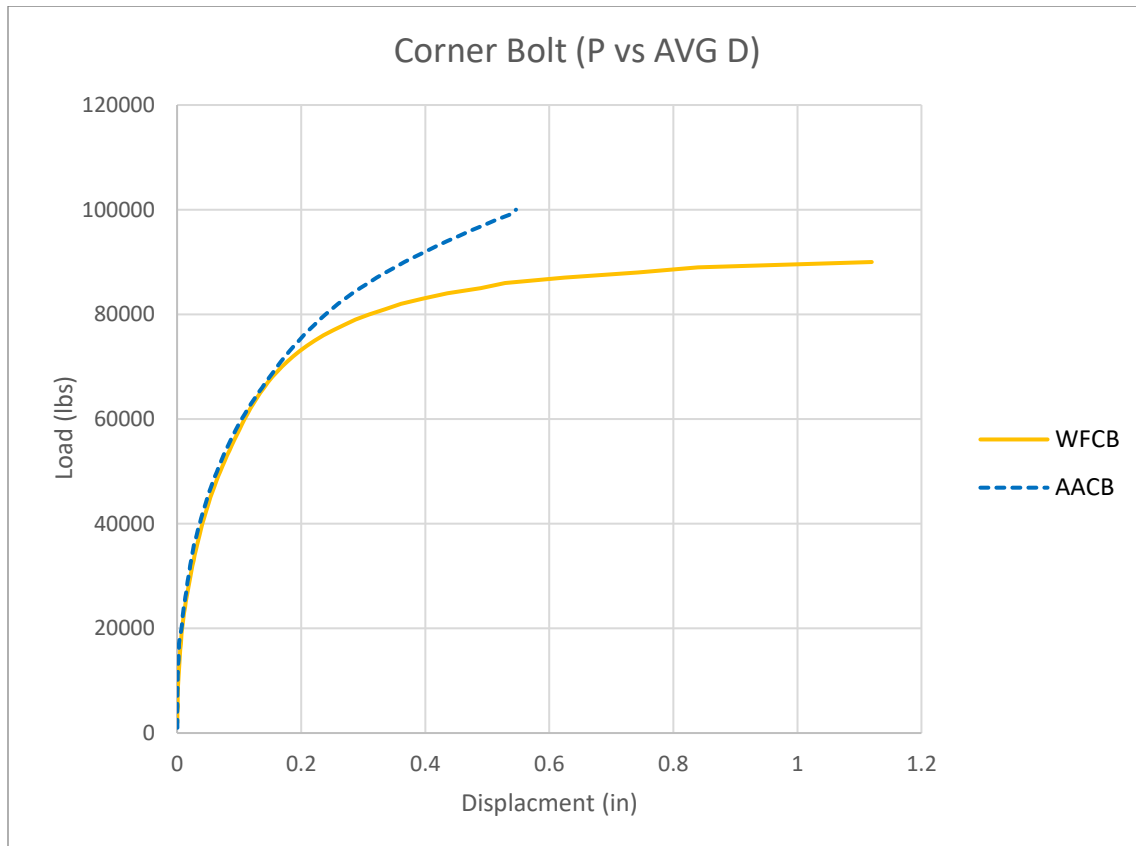
Figure B2

Load versus Average Displacement for Side Bolt Specimens
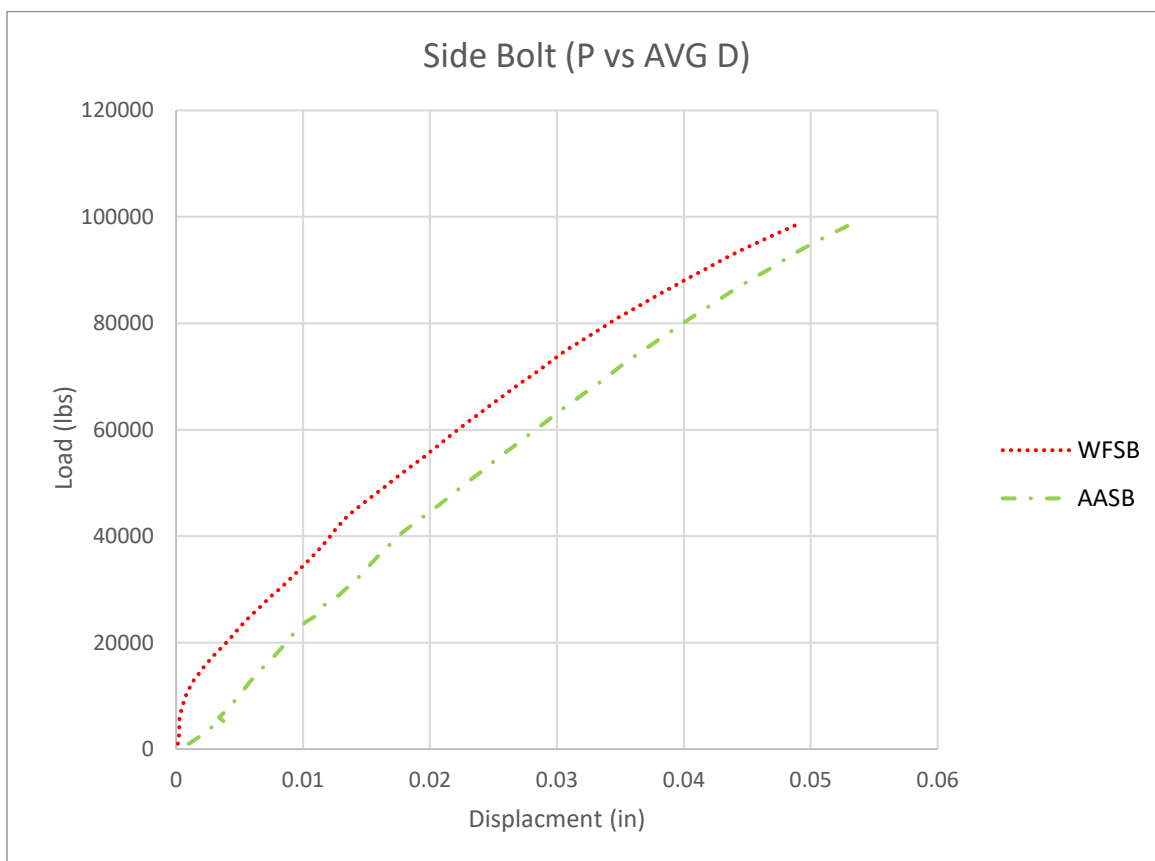
Figure B3

Load versus Average Displacement for All Specimens
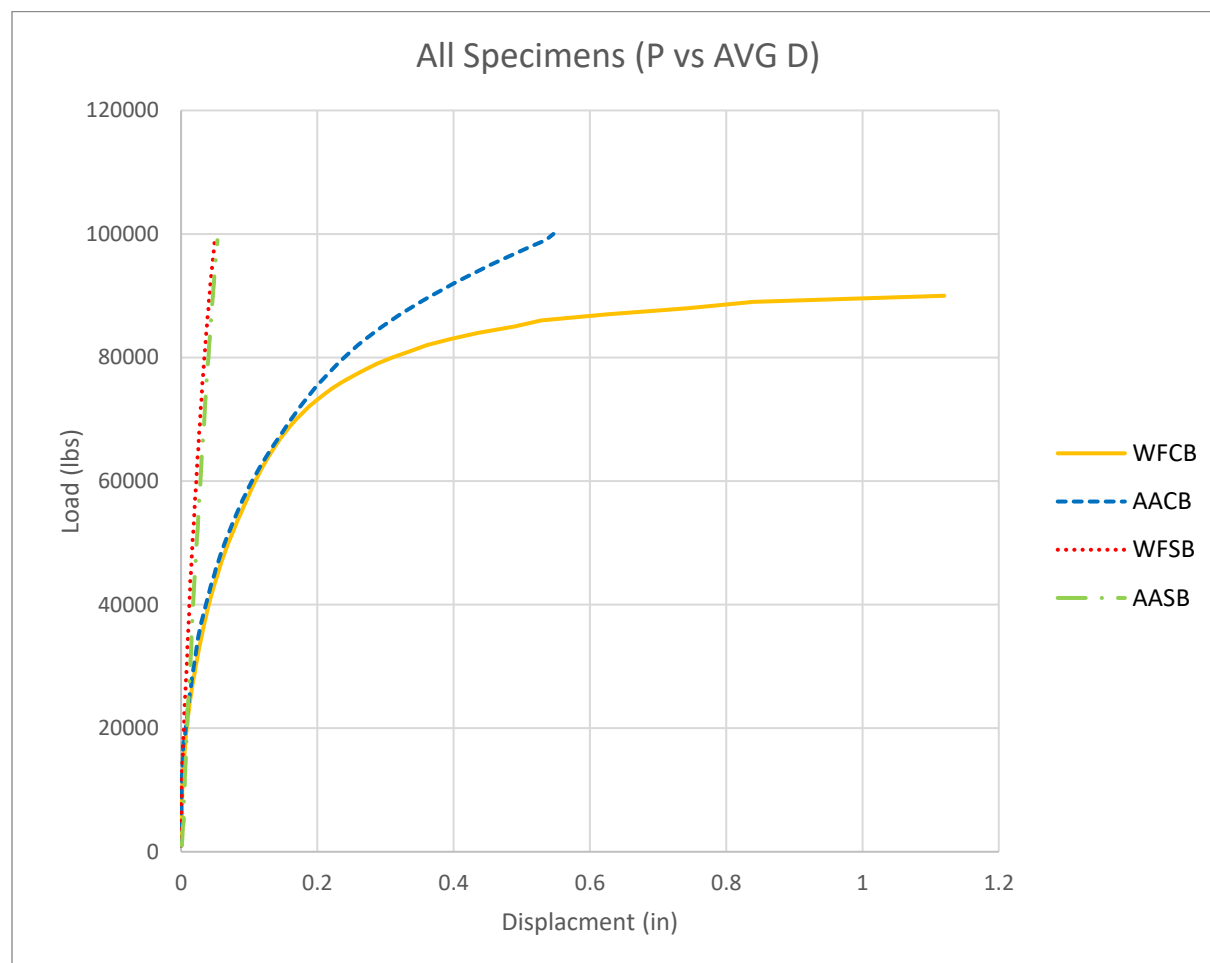
Load versus Strain Plots

All-Around Weld and Corner Bolt Specimens (AACB)

Figure B4

Load versus Strain for Specimen AACB01
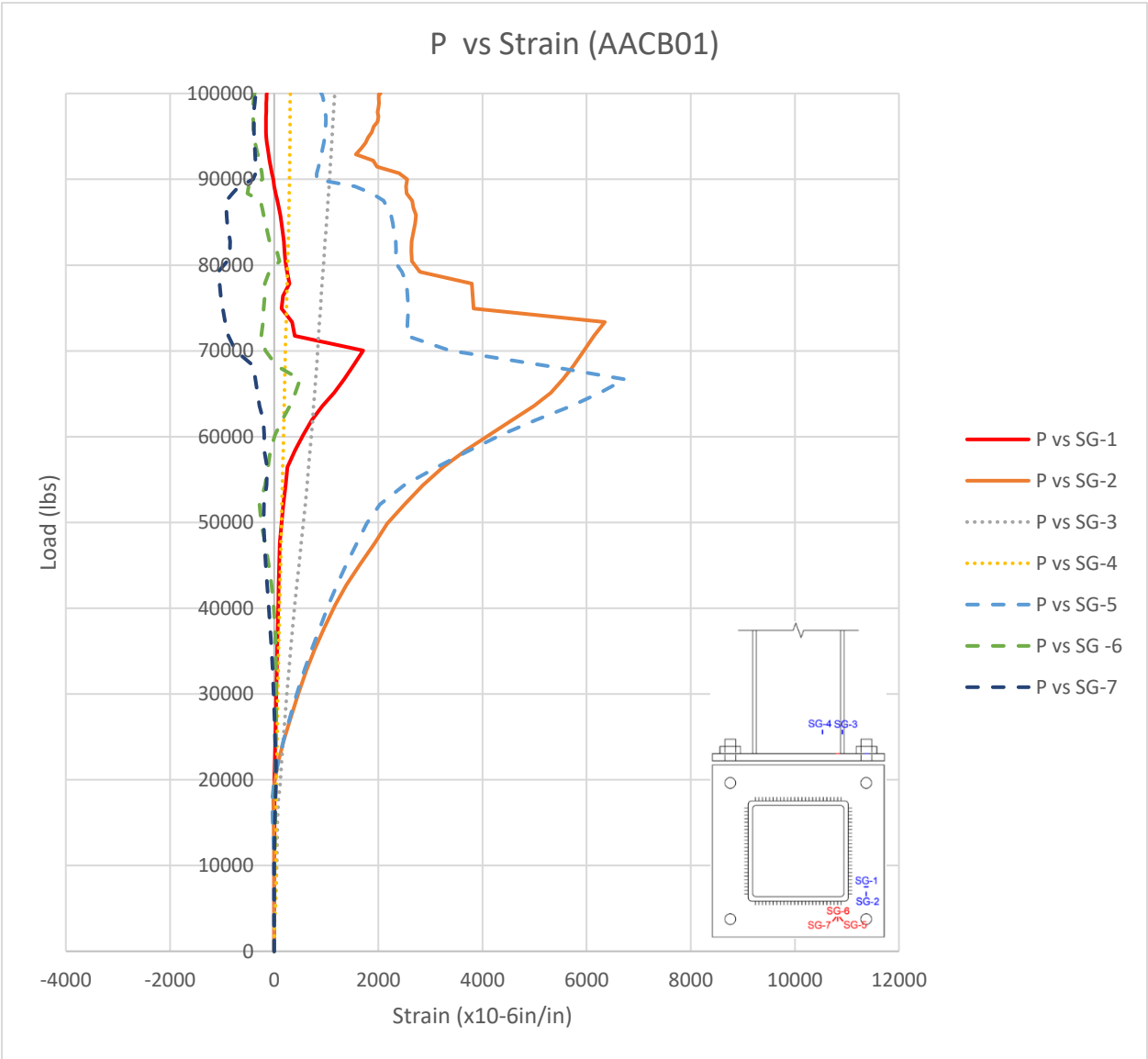
Figure B5

Load versus Strain for Specimen AACB02
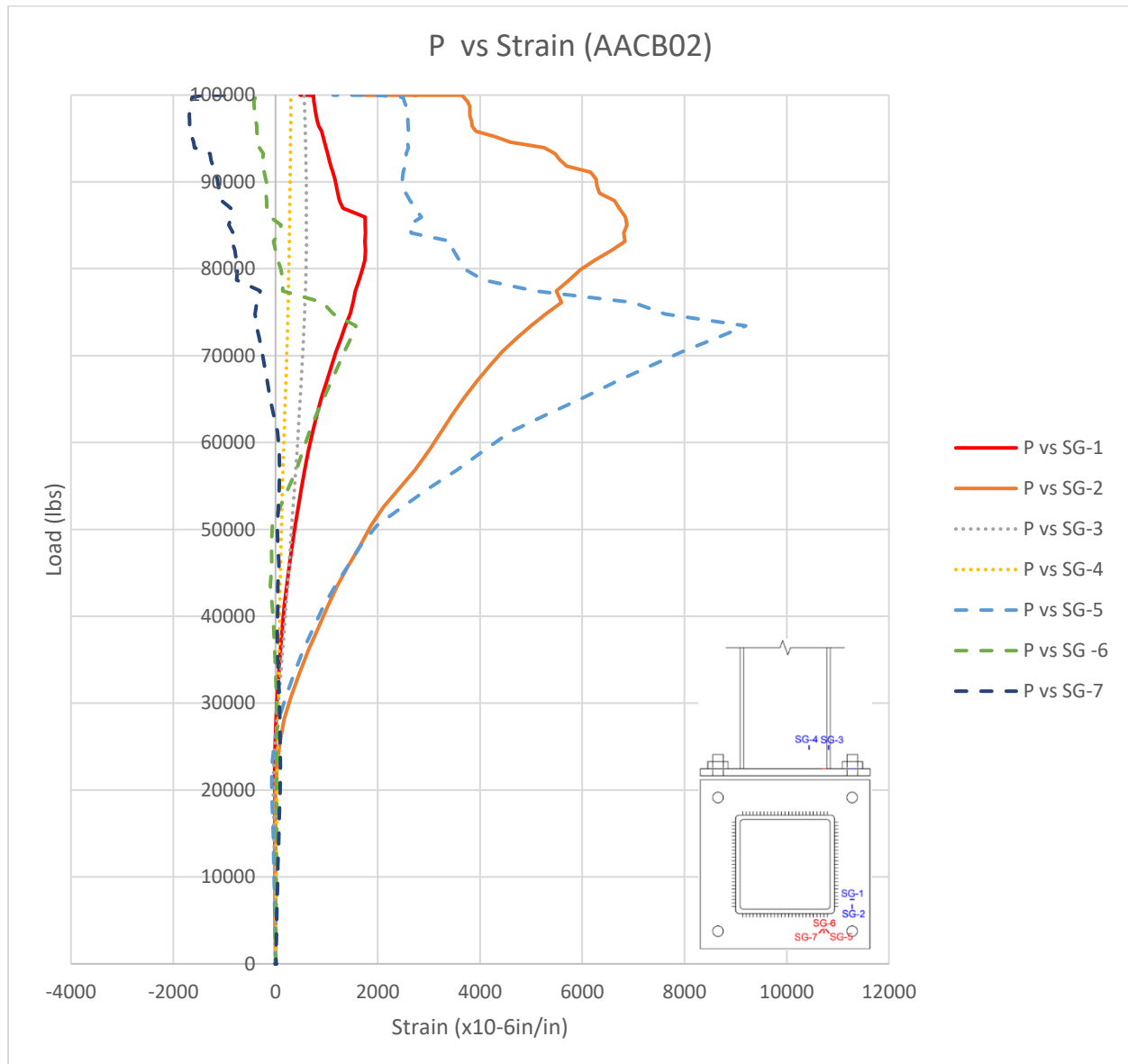
Figure B6

Load versus Strain for Specimen AACB03
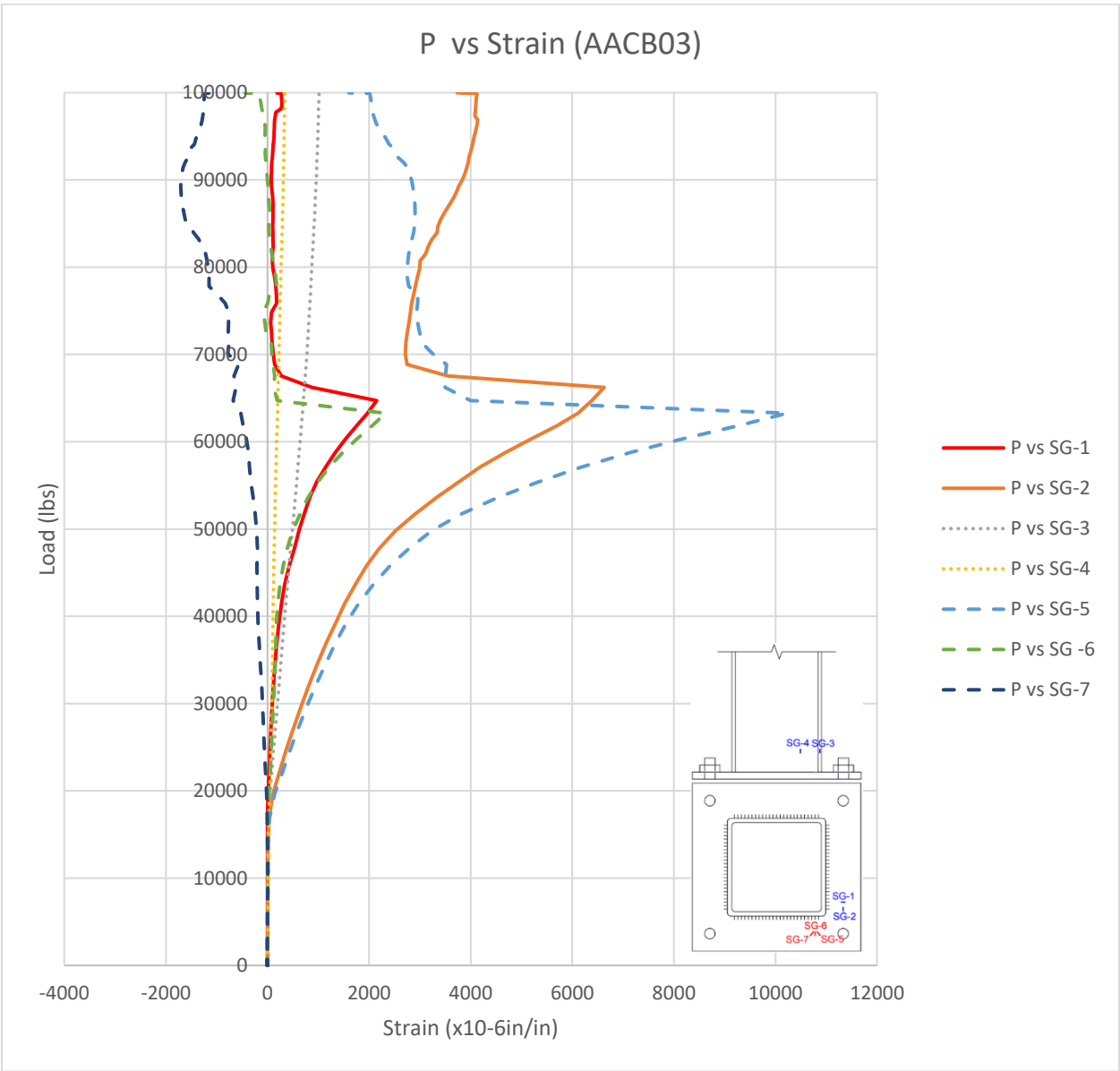
Workable-Flat Welds and Corner Bolt Specimens (WFCB)

Figure B7

Load versus Strain for Specimen WFCB01
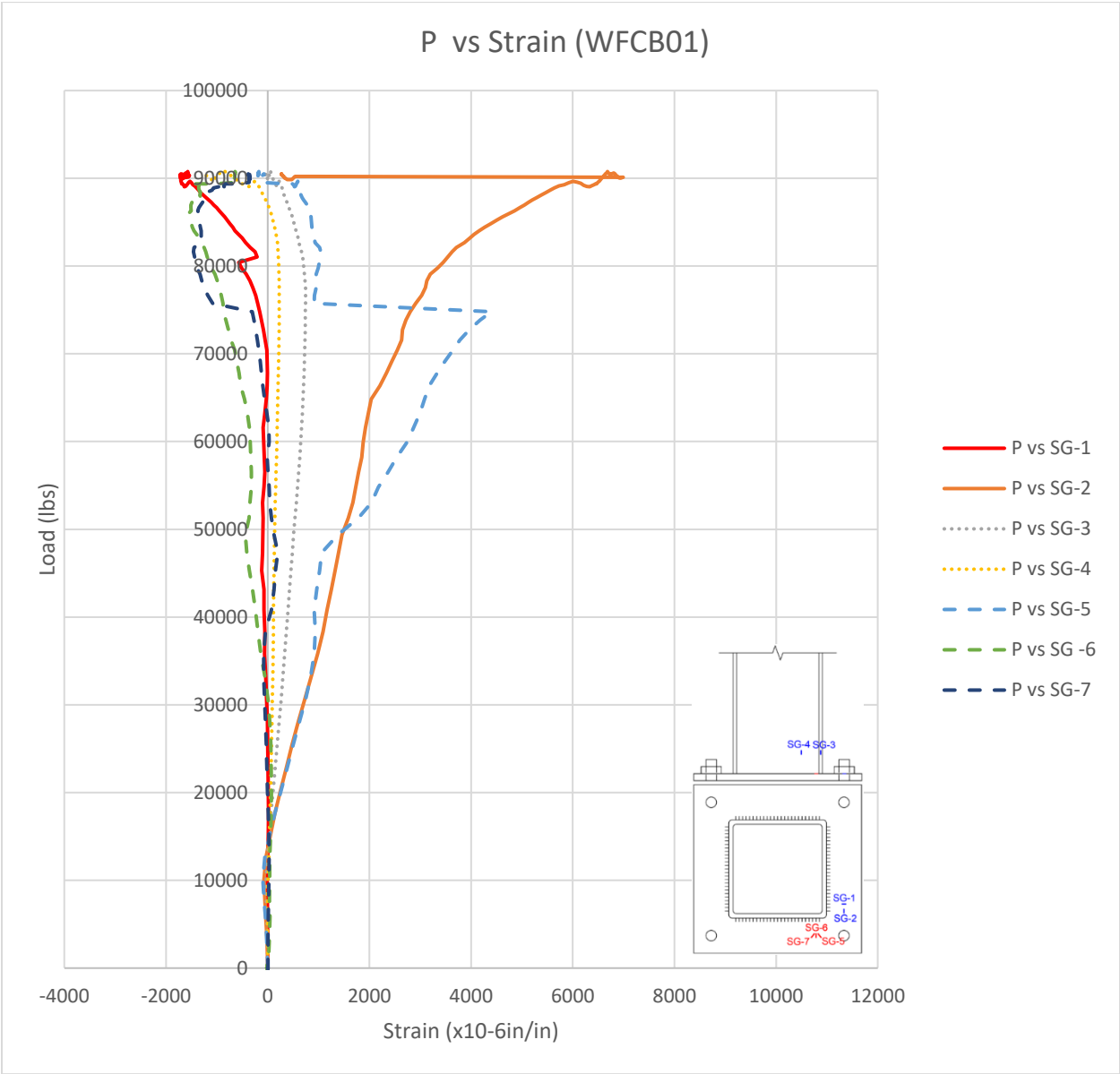
Figure B8

Load versus Strain for Specimen WFCB02
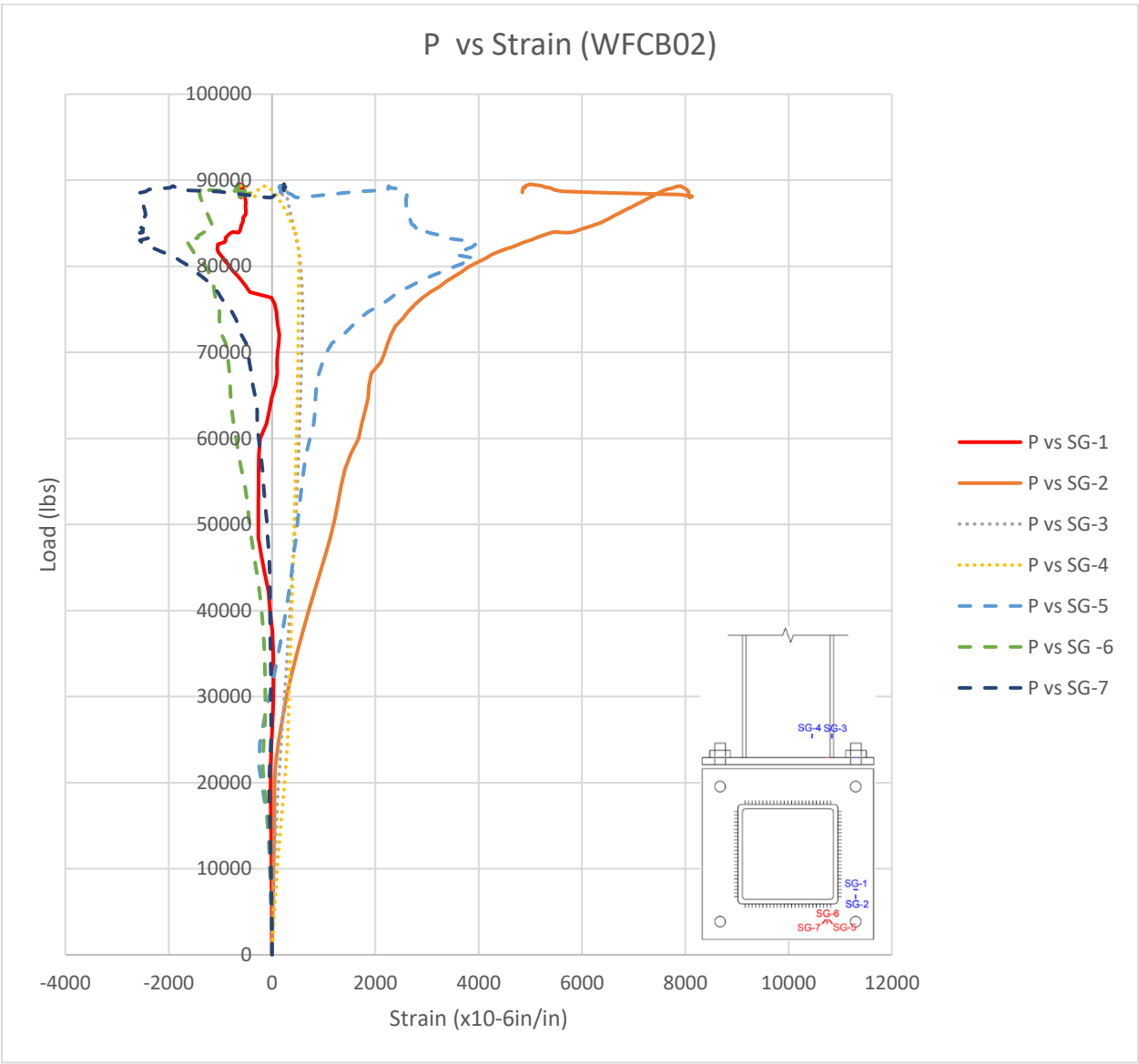
Figure B9

Load versus Strain for Specimen WFCB03
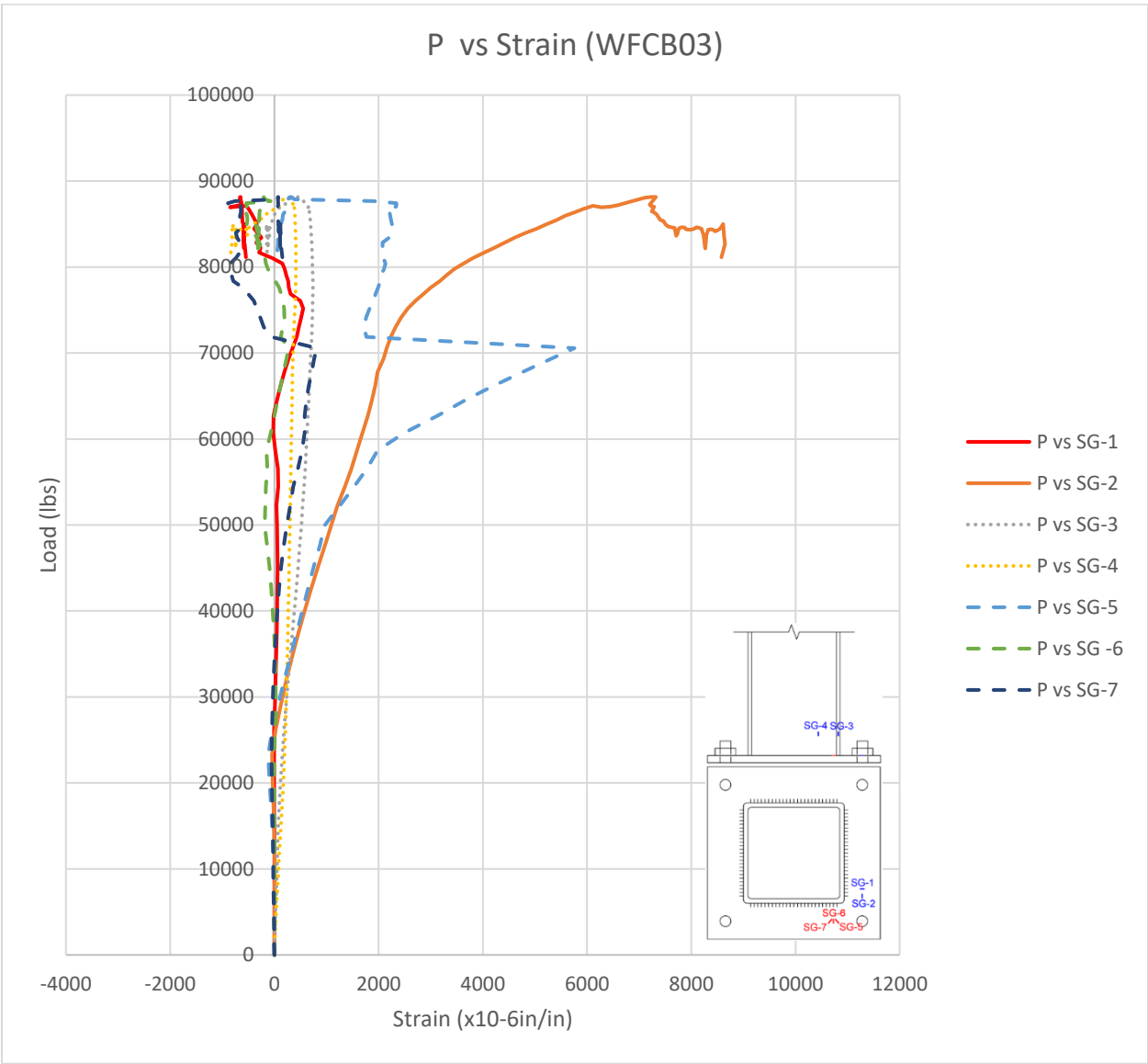
All-Around Weld and Side Bolt Specimens (AASB)

Figure B10

Load versus Strain for Specimen AASB01

Figure B11

Load versus Strain for Specimen AASB02
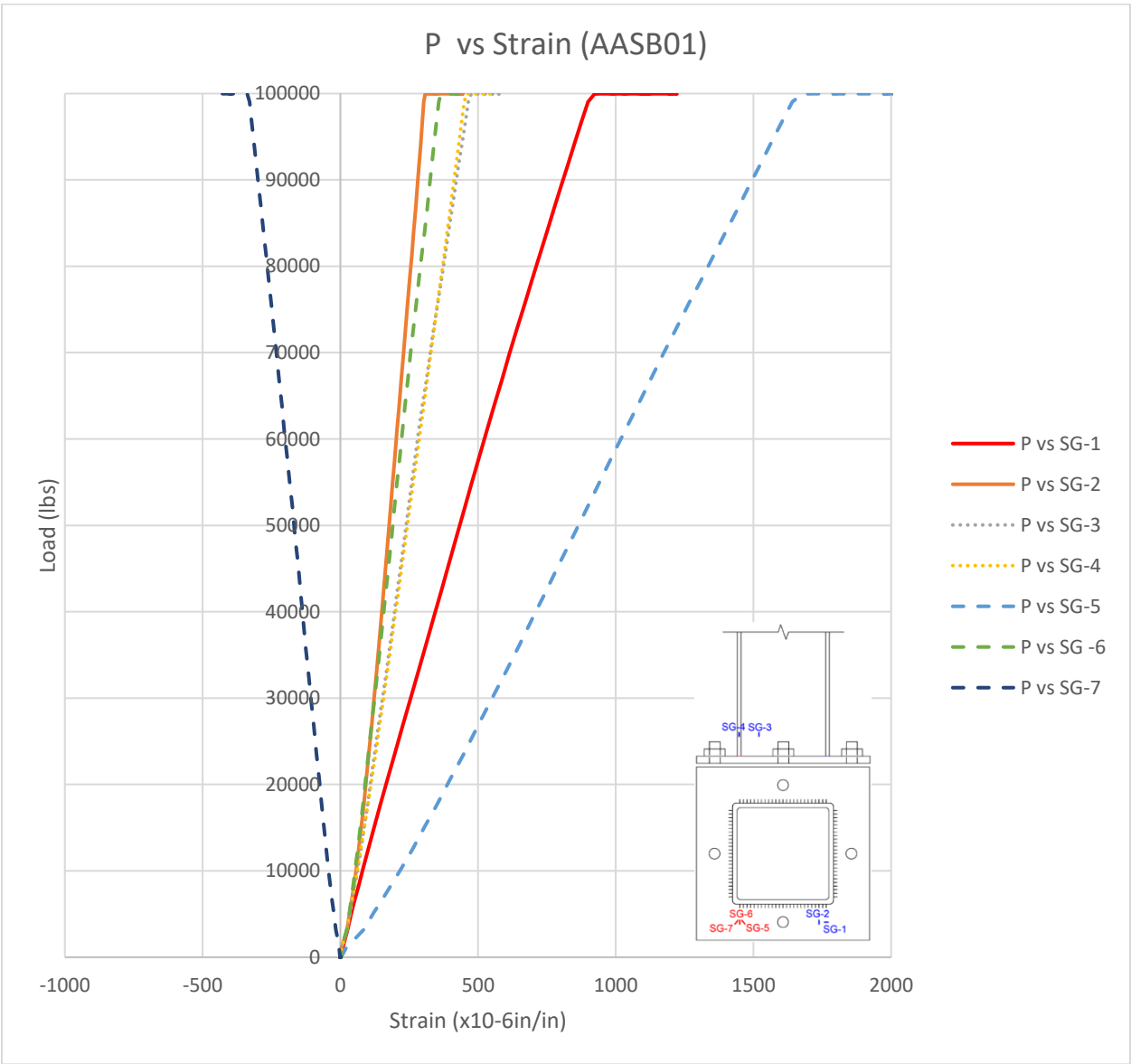
Figure B12

Load versus Strain for Specimen AASB03
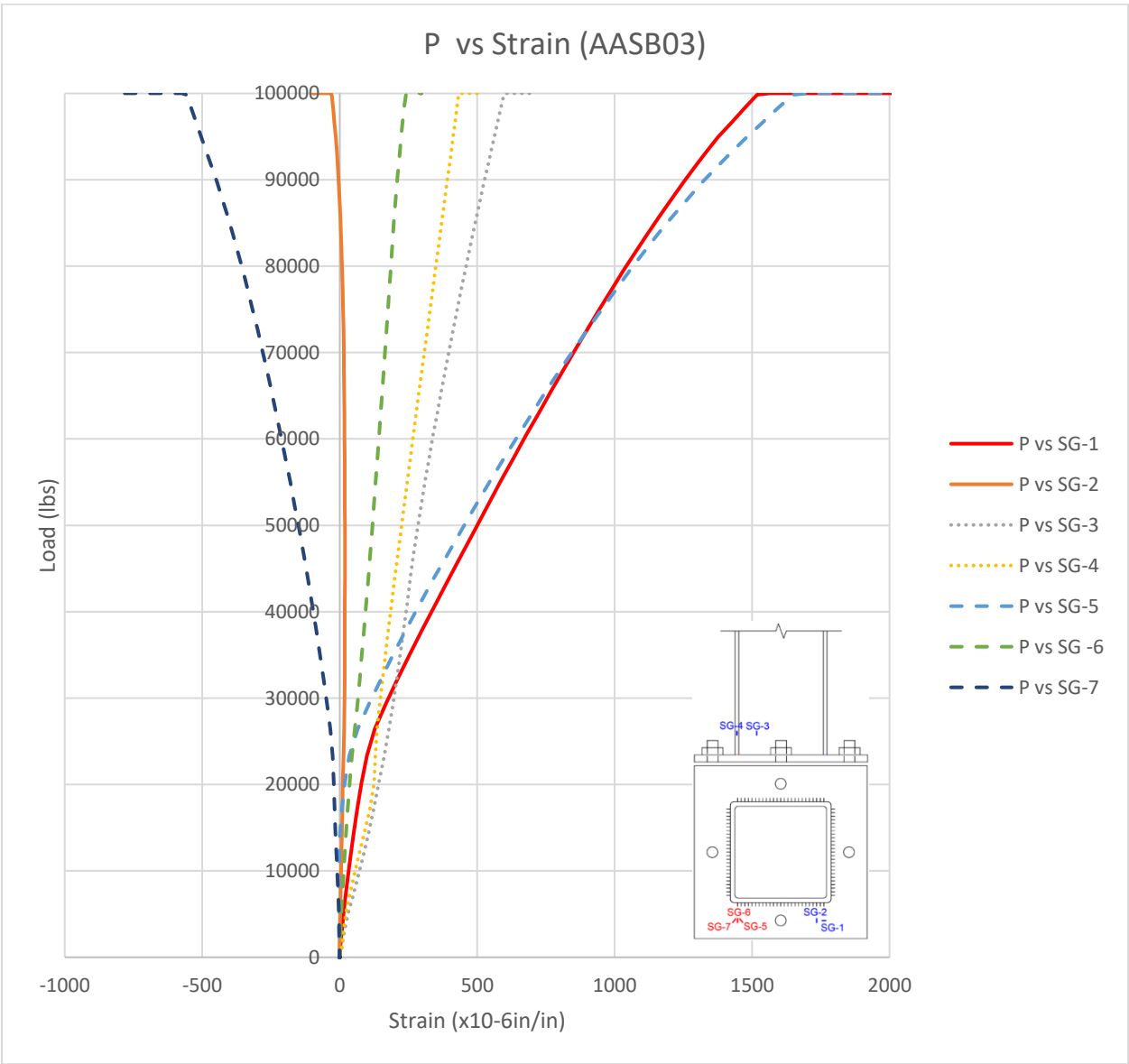
Figure B13

Load versus Strain for Specimen AASB04
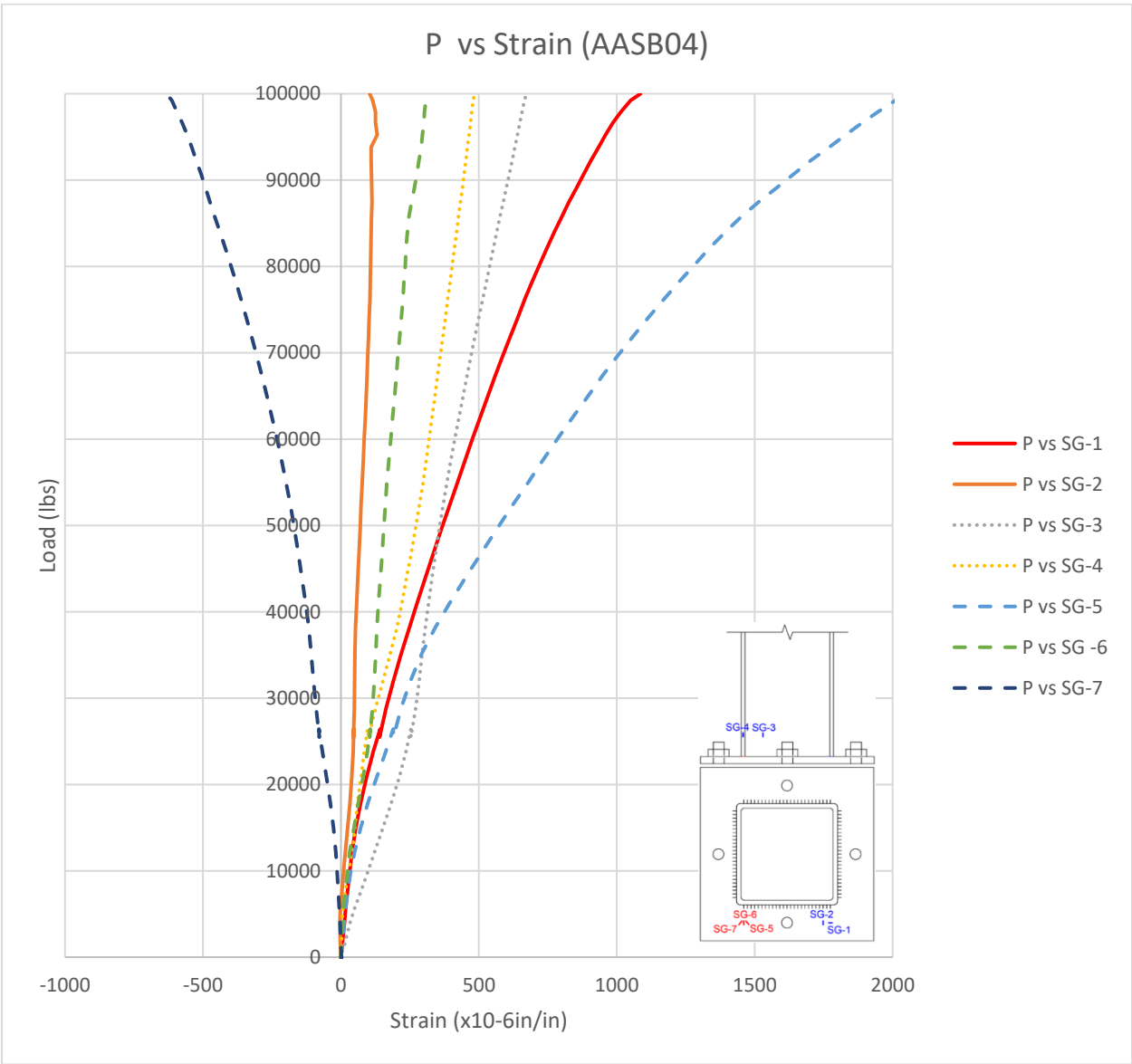
Workable-Flat Welds and Side Bolt Specimens (WFSB)

Figure B14

Load versus Strain for Specimen WFSB01
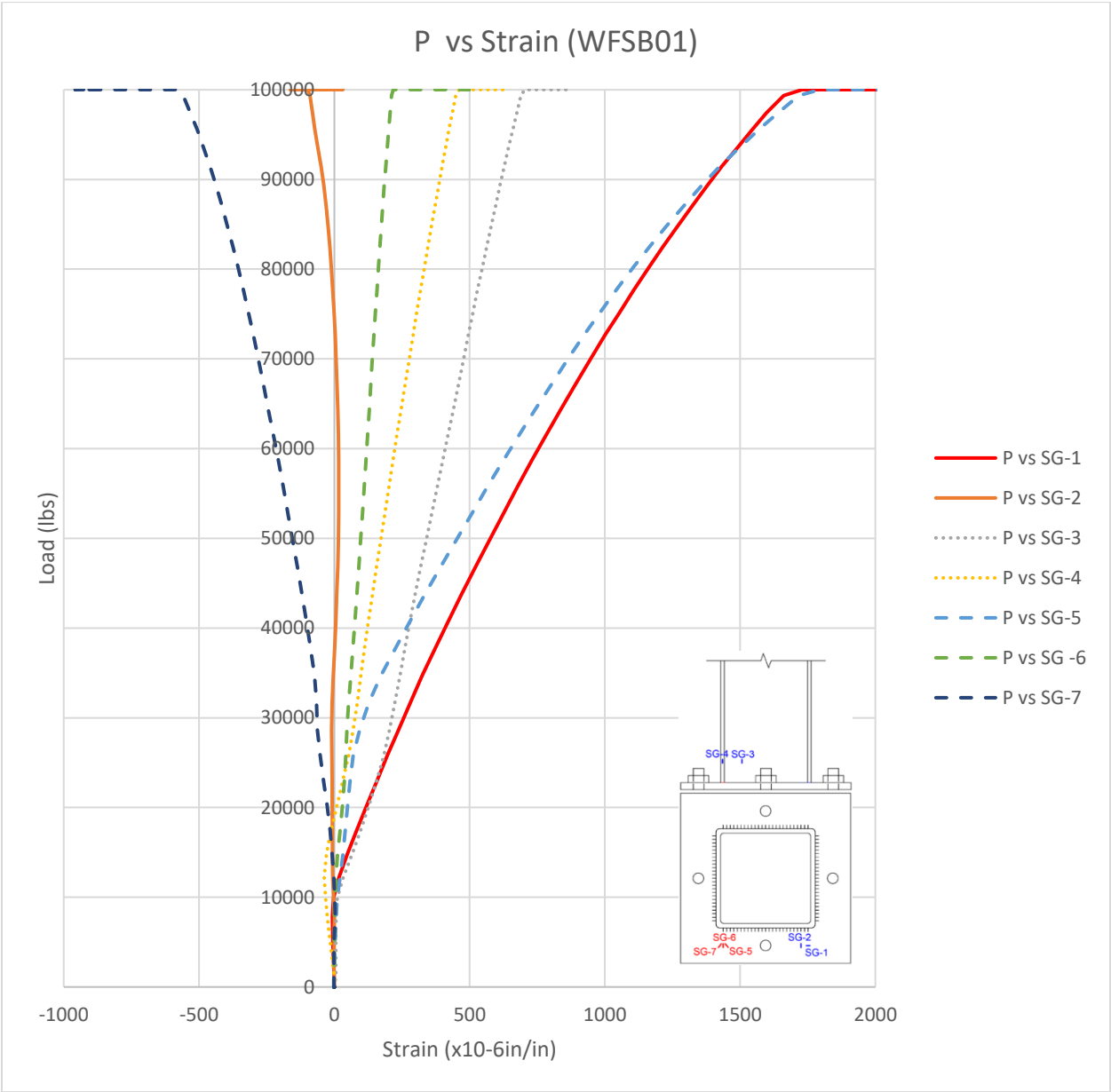
Figure B15

Load versus Strain for Specimen WFSB02
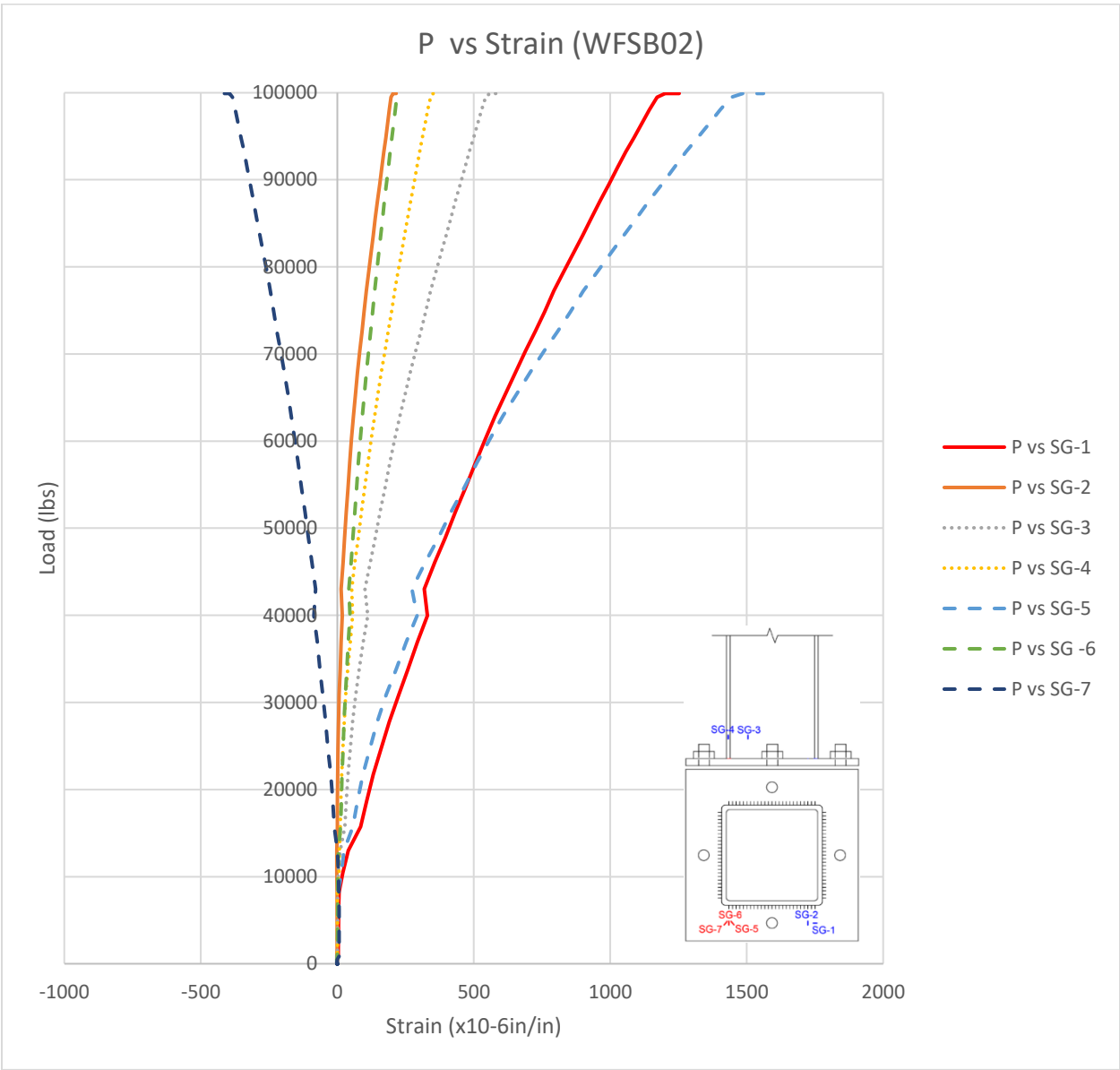
Appendix C – Flexural Tests Plots

Load versus Displacement Plots

Figure C1

Raw Load versus LVDT 1 Displacement for Specimen WFST Specimens
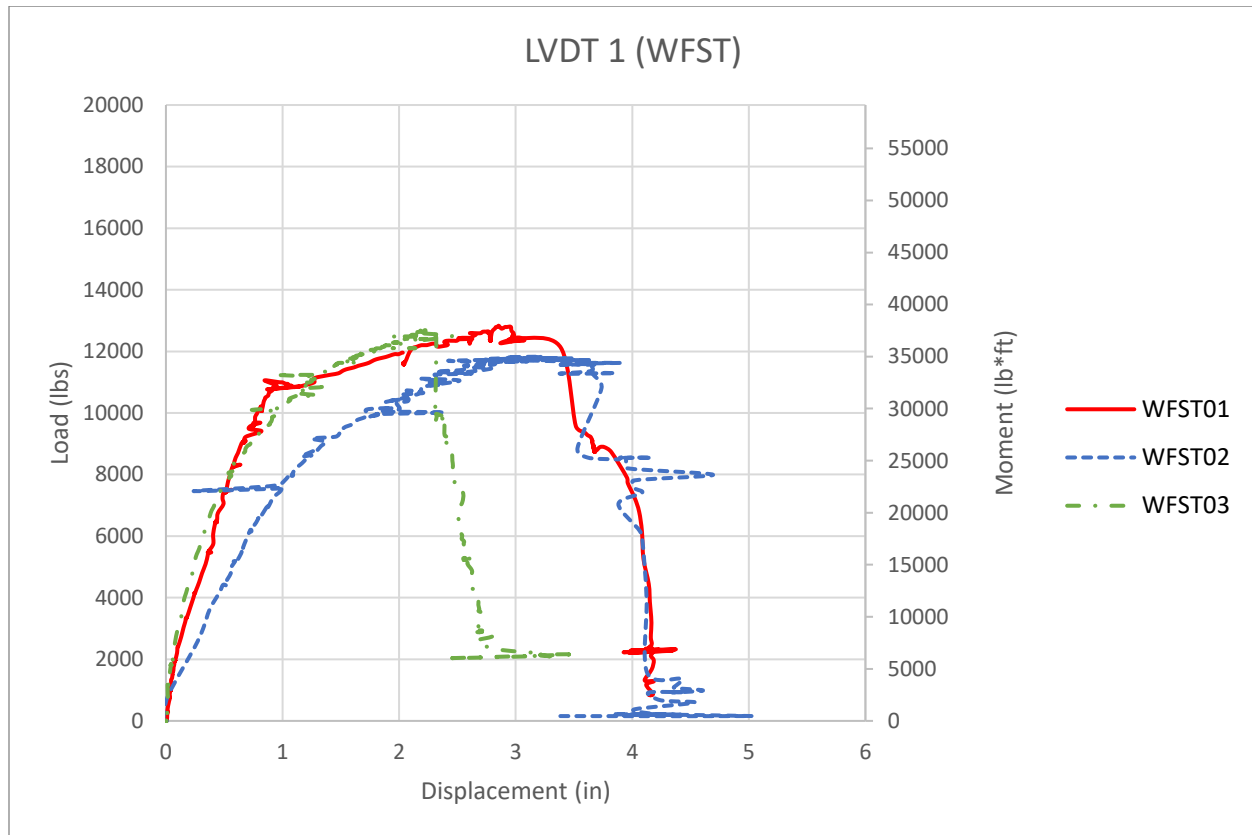
Figure C2

Raw Load versus LVDT 2 Displacement for Specimens WFST Specimens
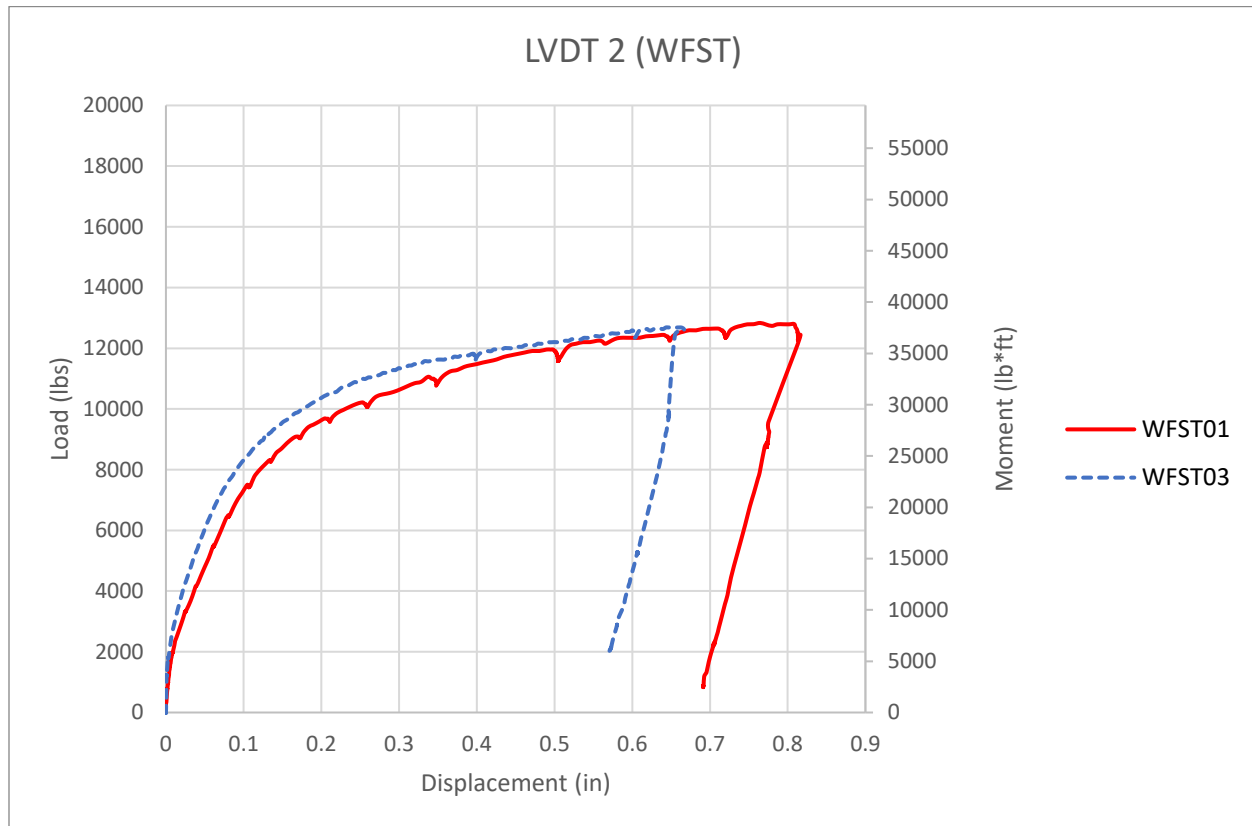
Figure C3

Raw Load versus LVDT 1 Displacement for Specimens AAST Specimens
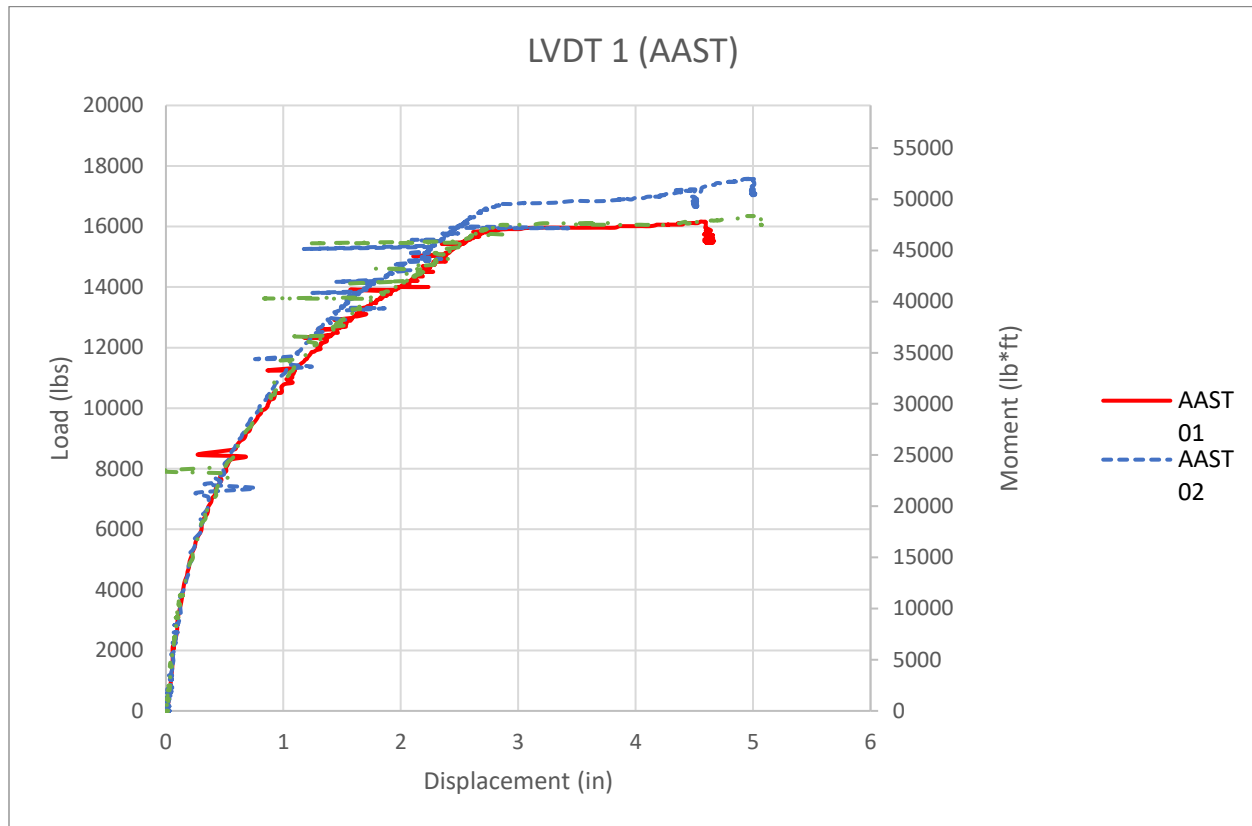
Figure C4

Raw Load versus LVDT 2 Displacement for Specimens AAST Specimens
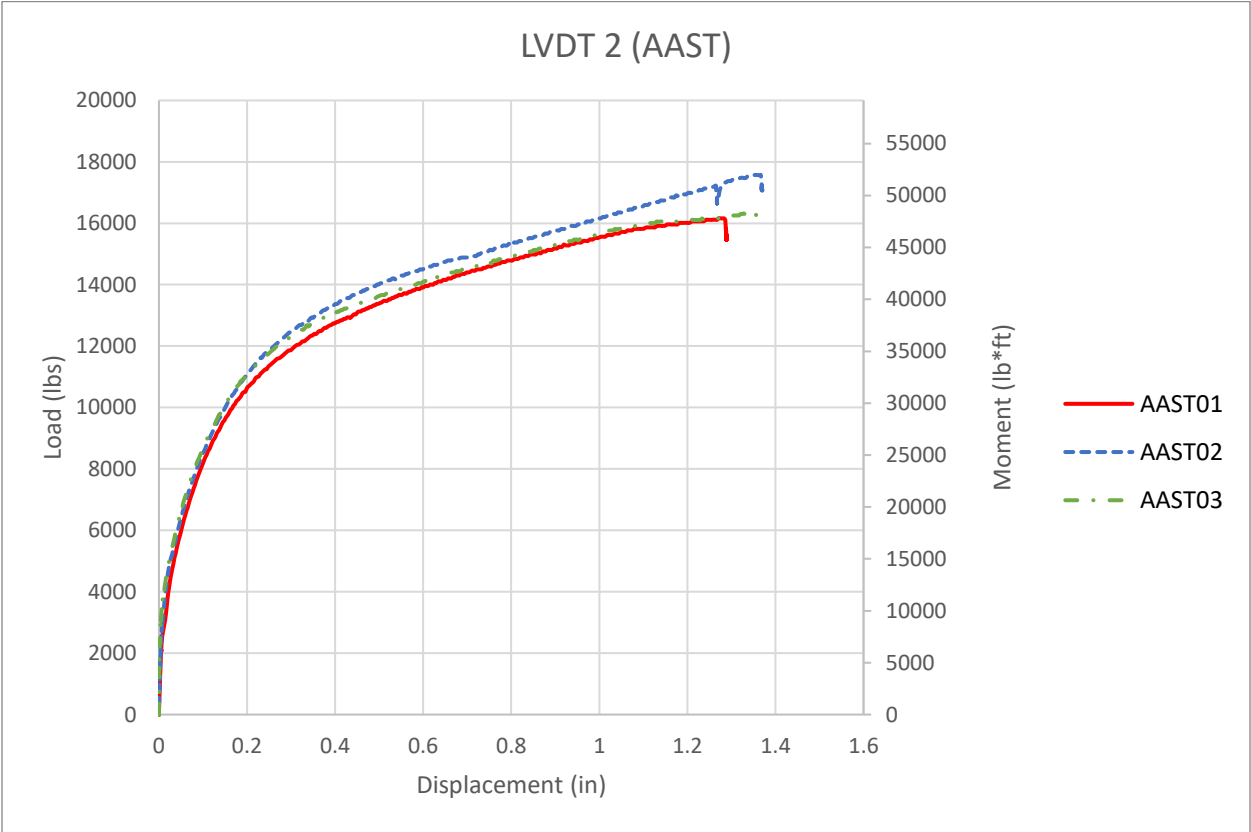
Figure C5

Raw Load versus LVDT 1 Displacement for Specimens WFWK Specimens
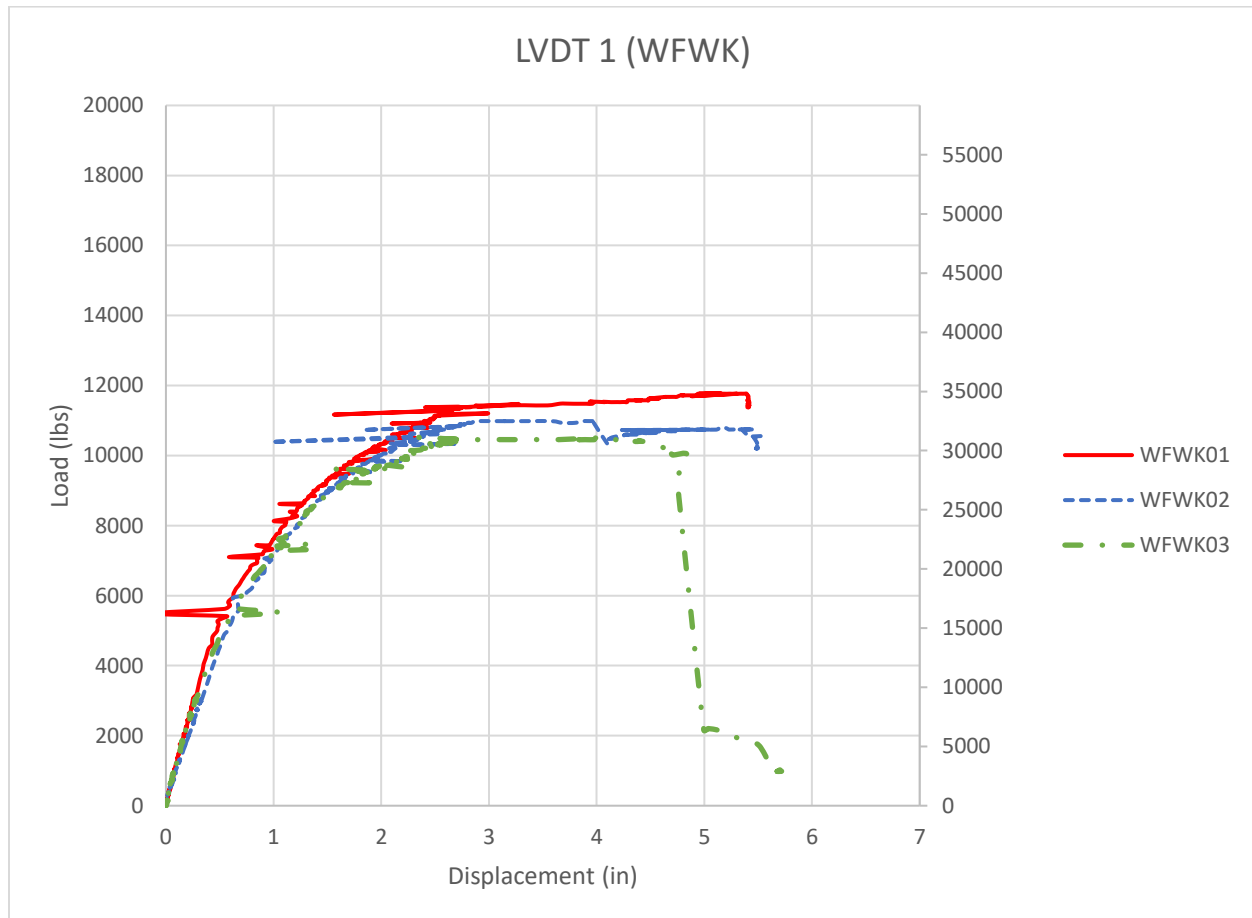
Figure C6

Raw Load versus LVDT 2 Displacement for Specimens WFWK Specimens
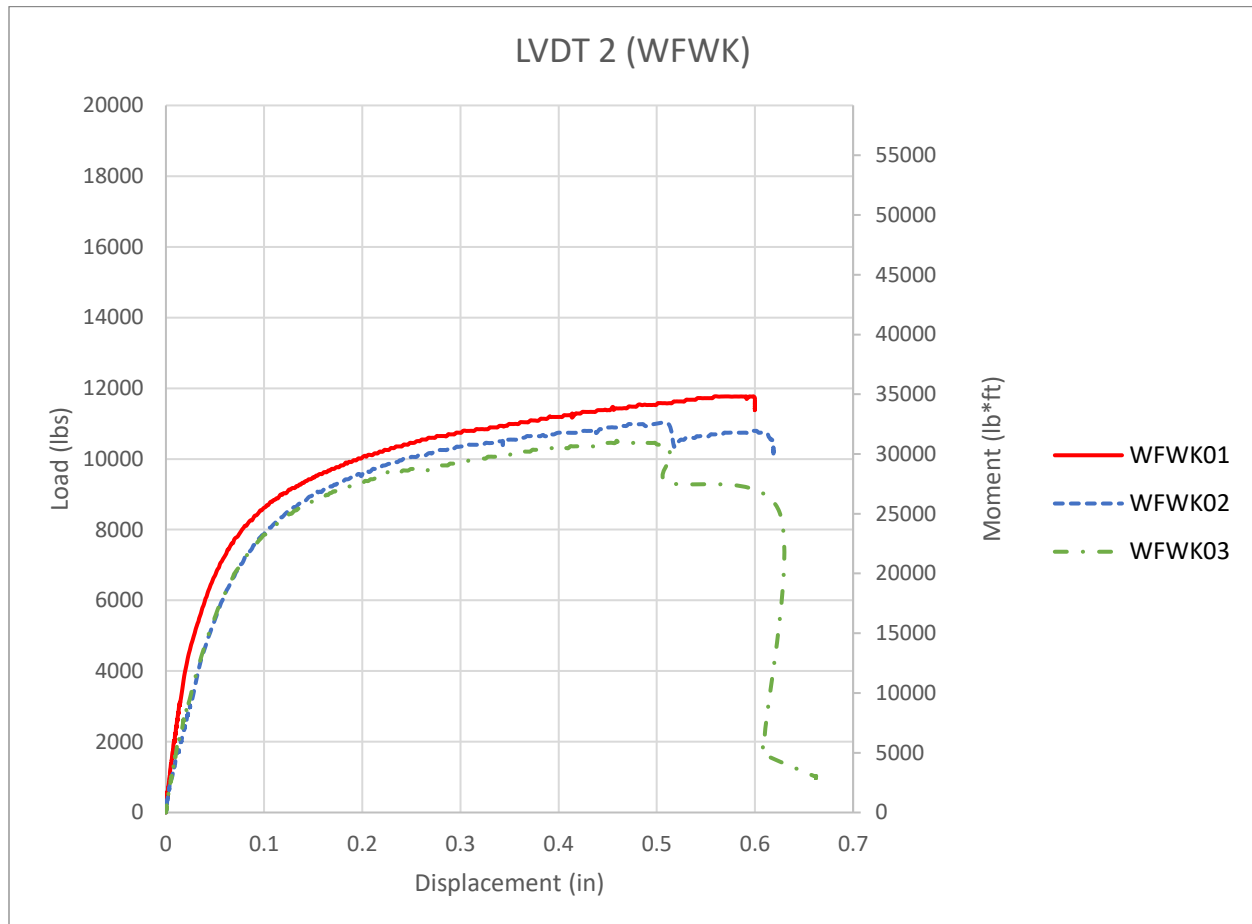
Figure C7

Raw Load versus LVDT 1 Displacement for Specimens AAWK Specimens
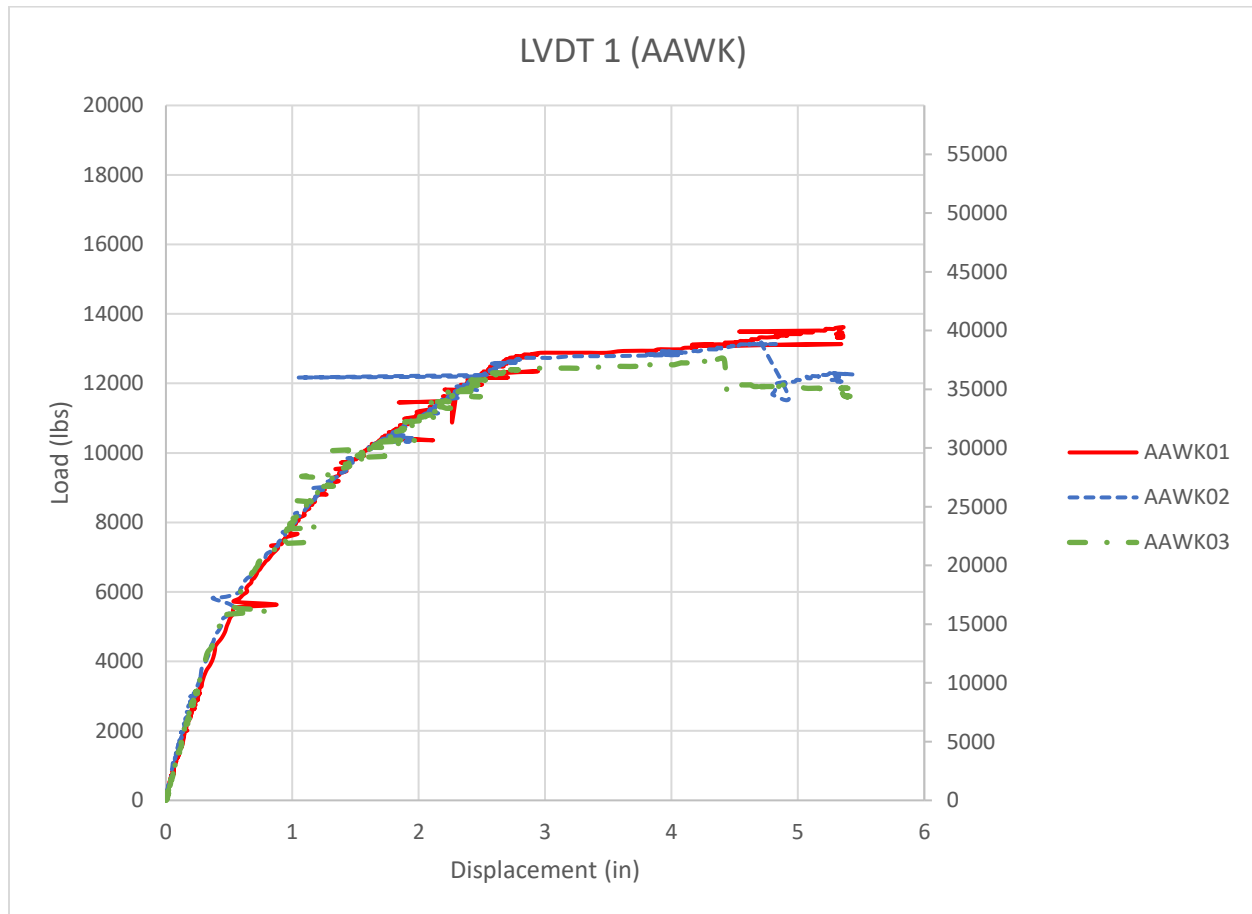
Figure C8

Raw Load versus LVDT 2 Displacement for Specimens AAWK Specimens
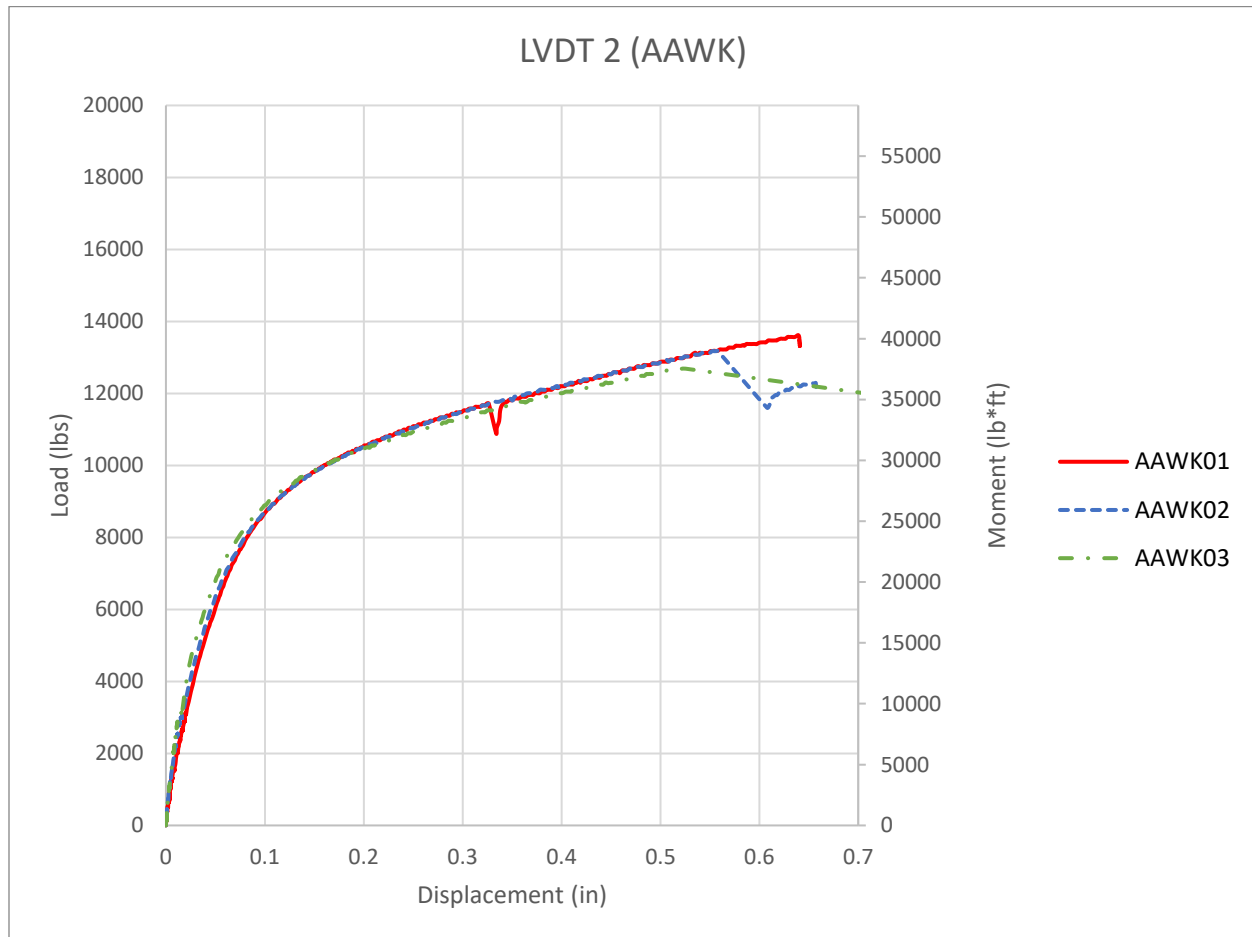
Load versus Strain Plots

Figure C9

Load versus Strain for Specimen WFST01
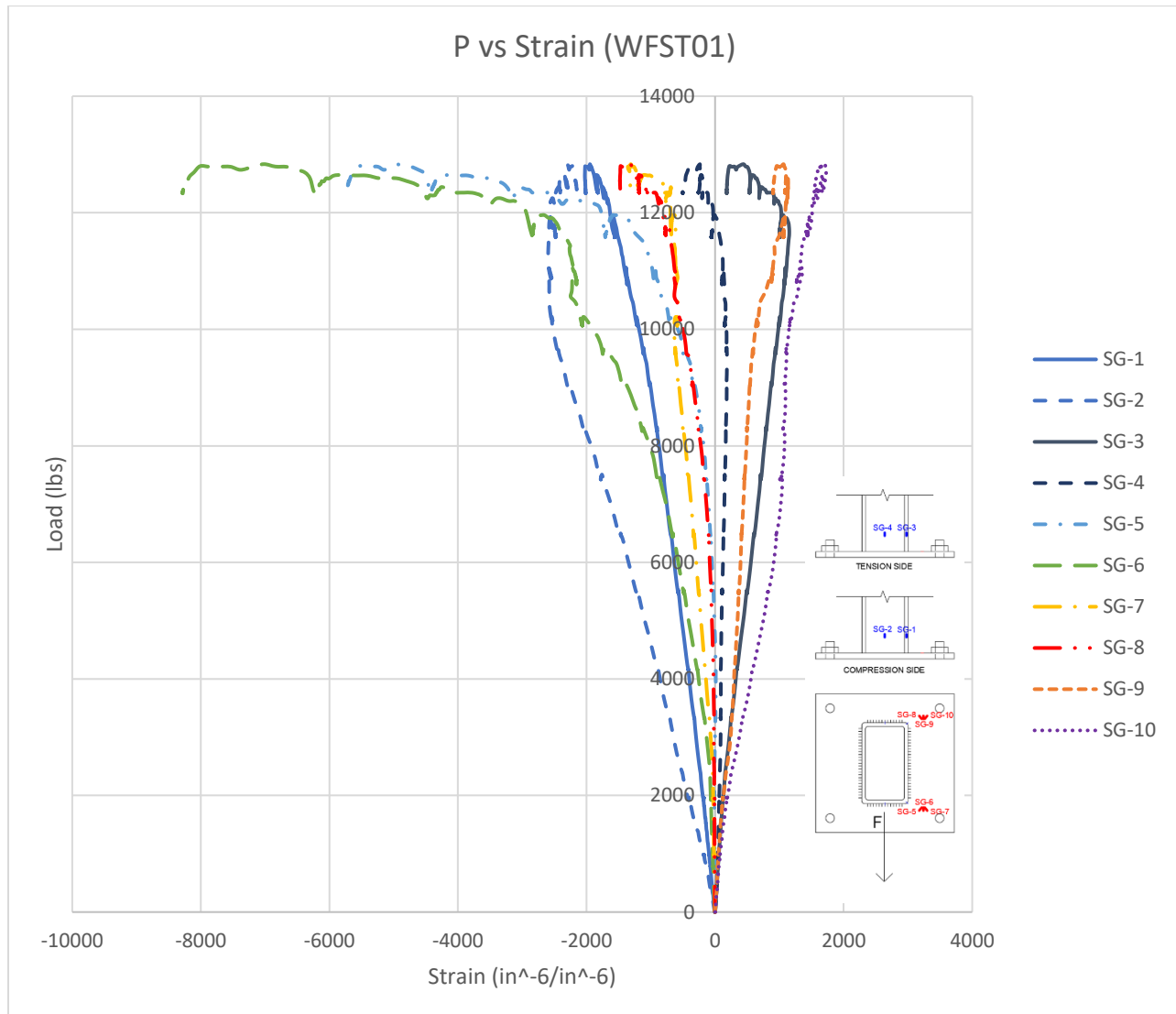
Figure C10

Load versus Strain for Specimen WFST02
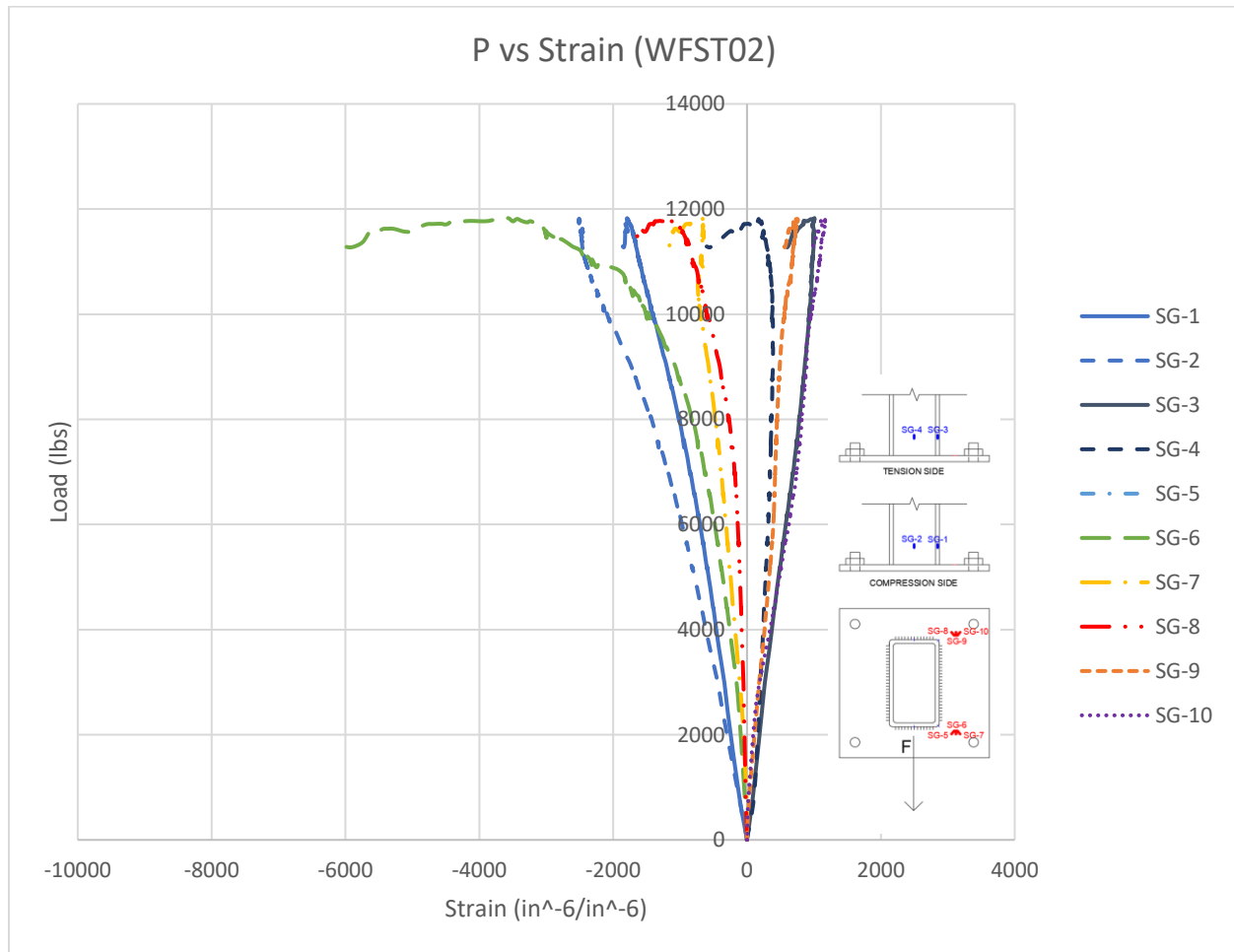
Figure C11

Load versus Strain for Specimen WFST03
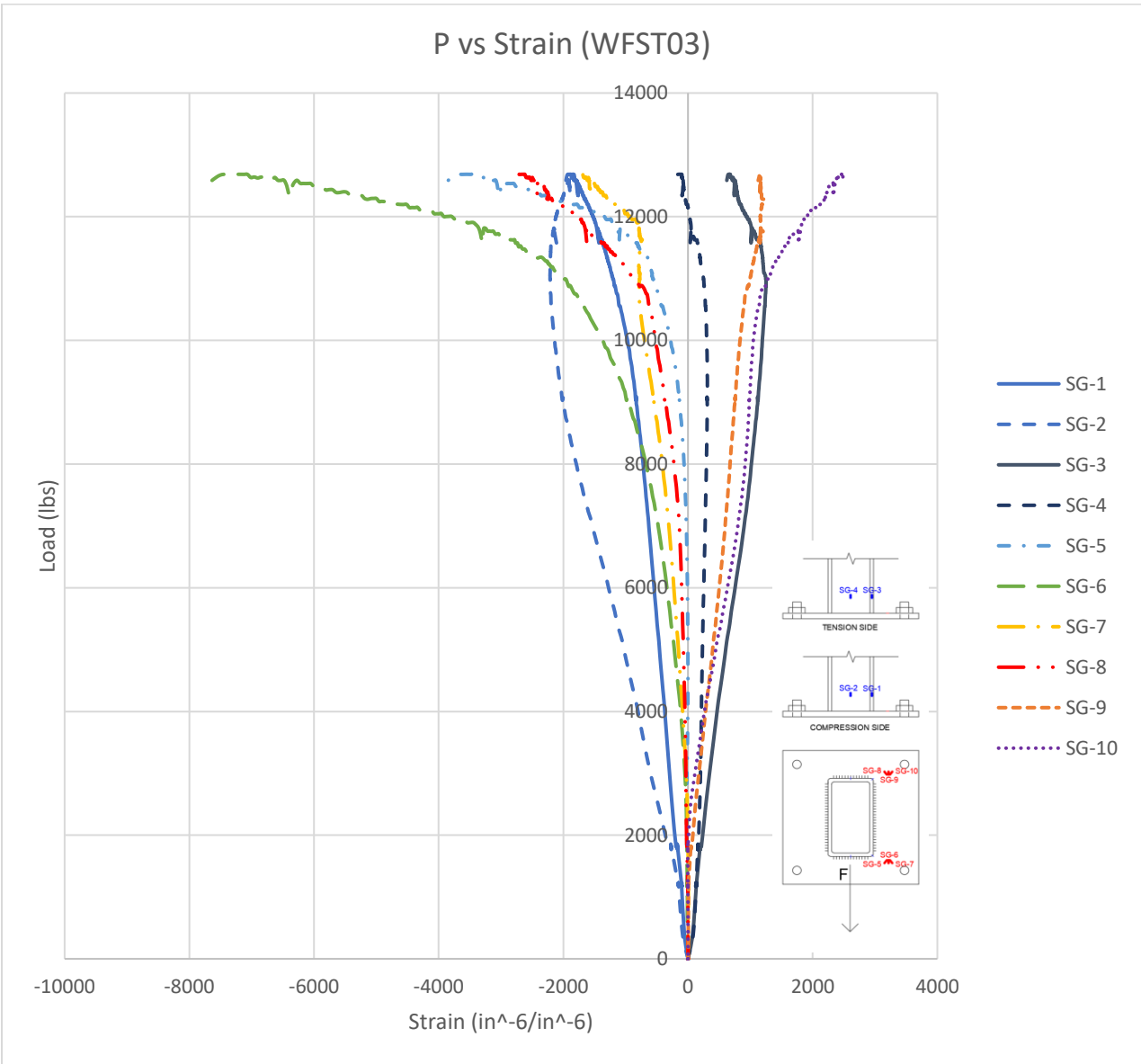
Figure C12

Load versus Strain for Specimen AAST01
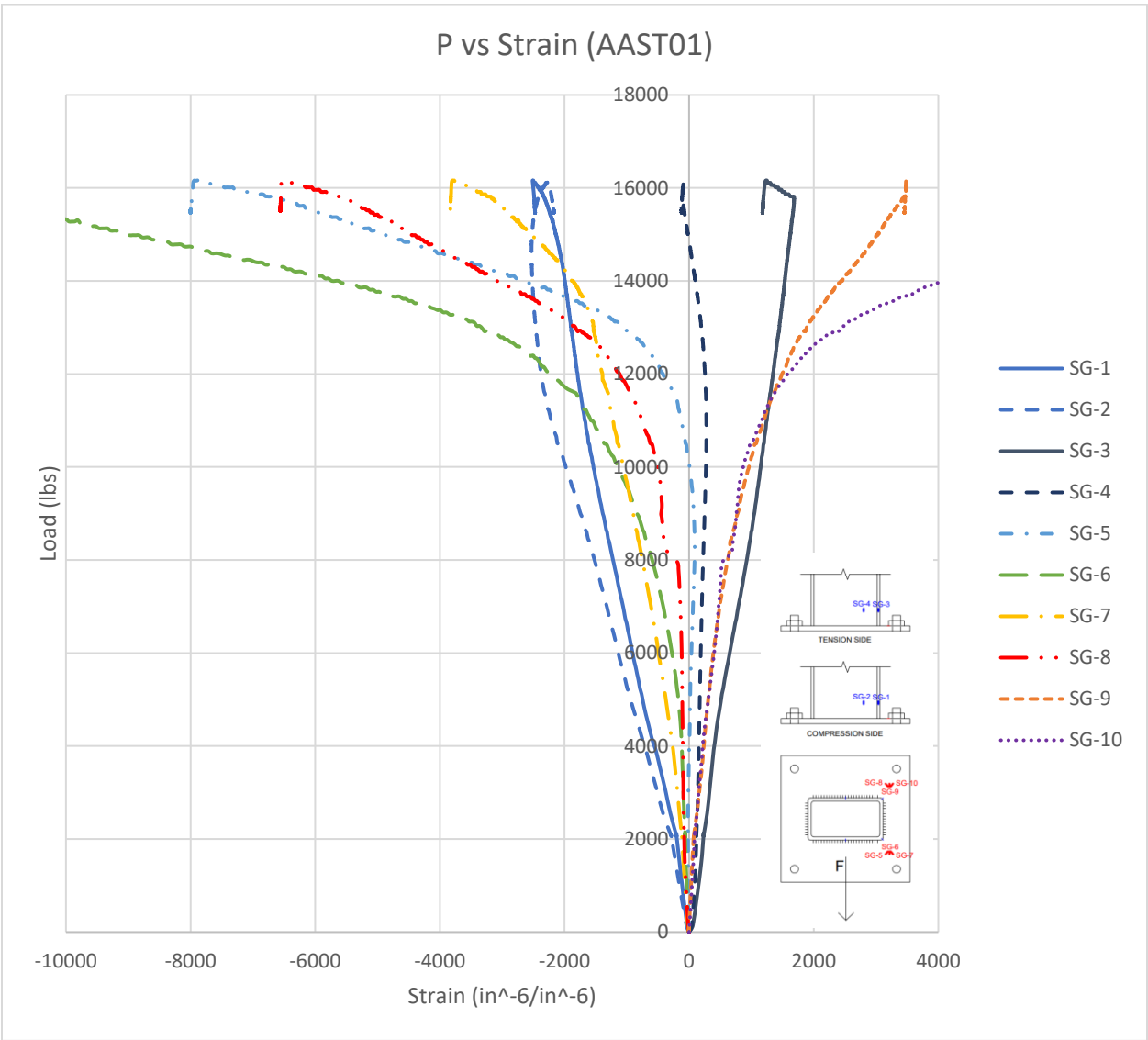
Figure C13

Load versus Strain for Specimen AAST02
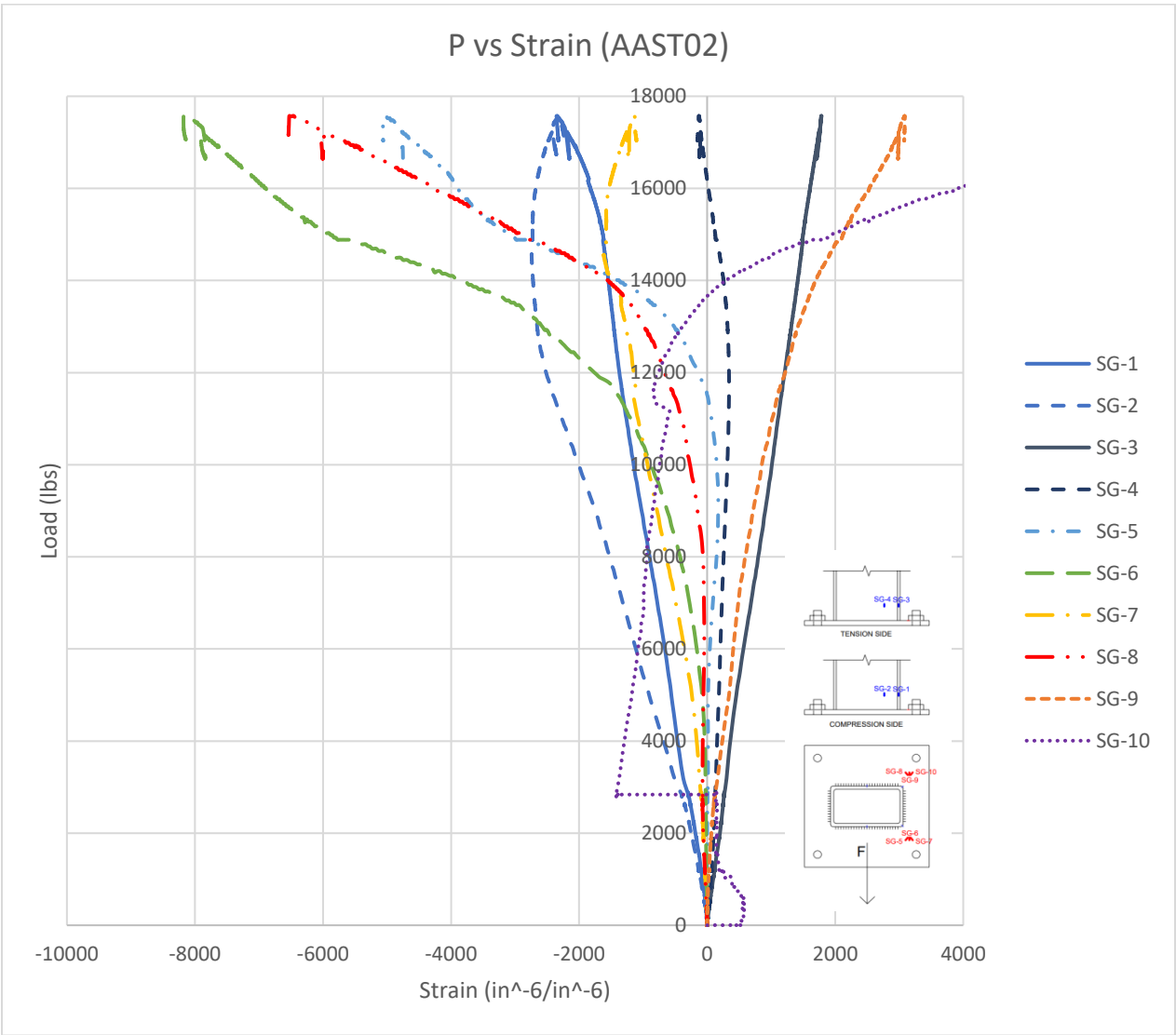
Figure C14

Load versus Strain for Specimen AAST03
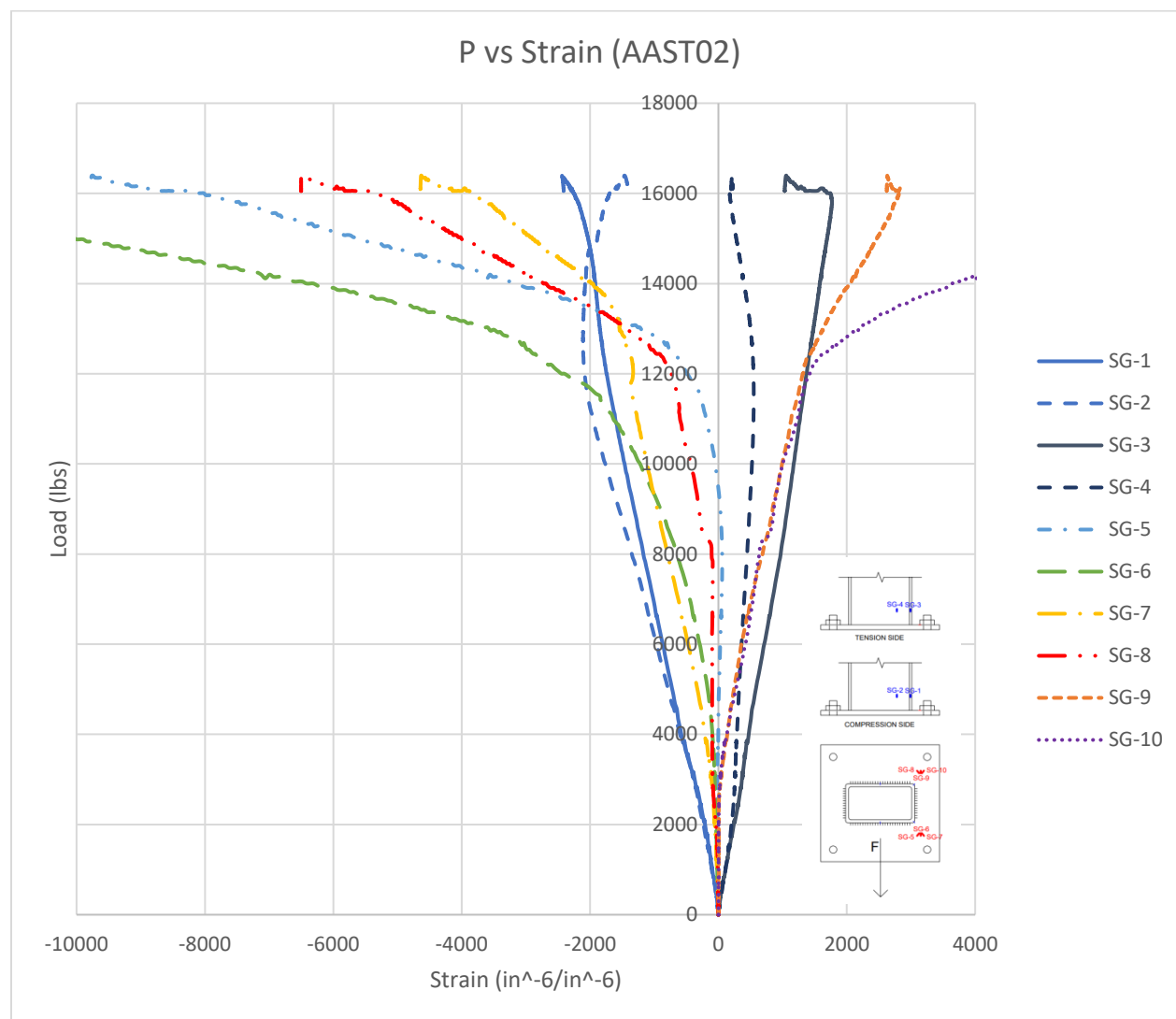
Figure C15

Load versus Strain for Specimen WFWK01
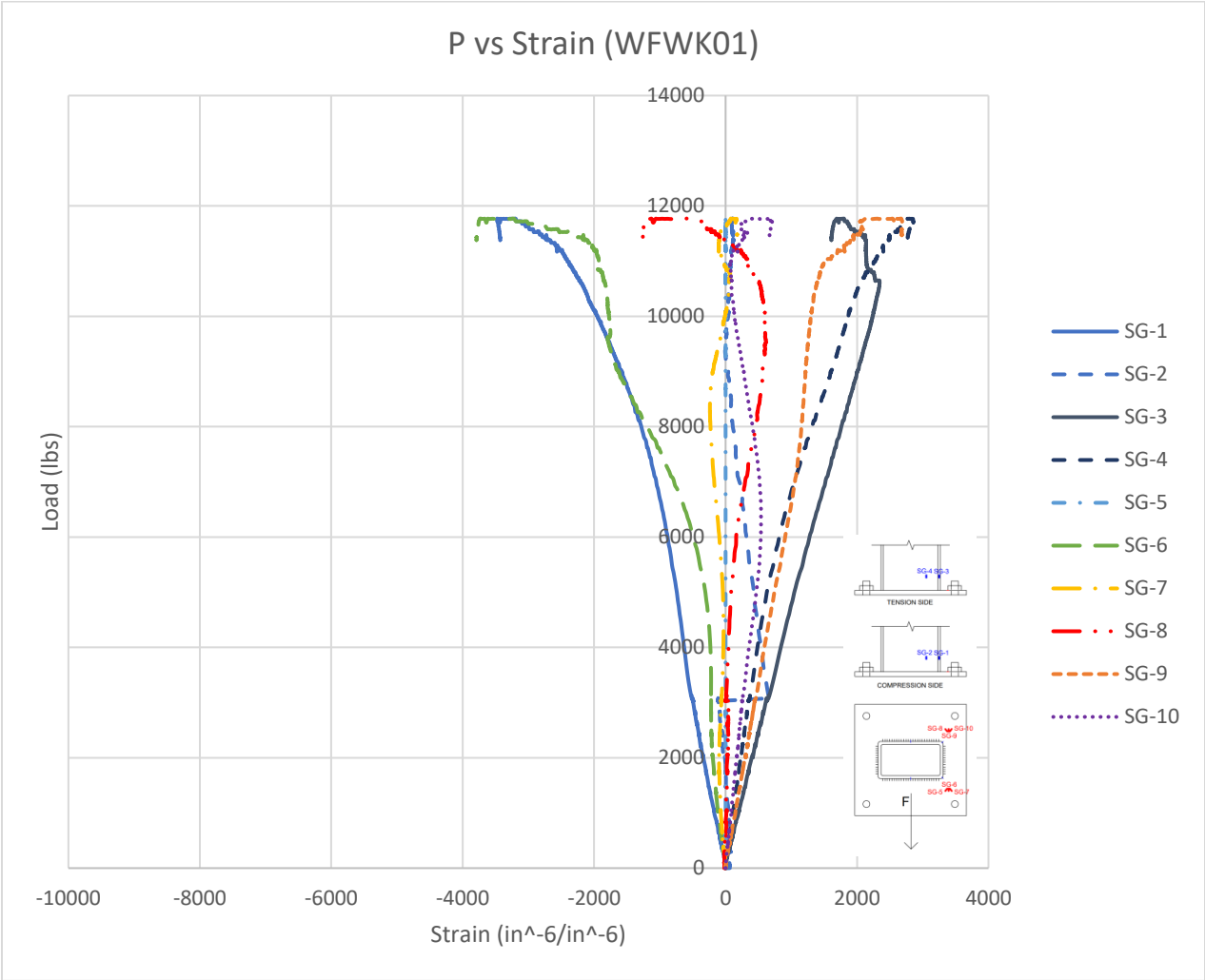
Figure C16

Load versus Strain for Specimen WFWK02
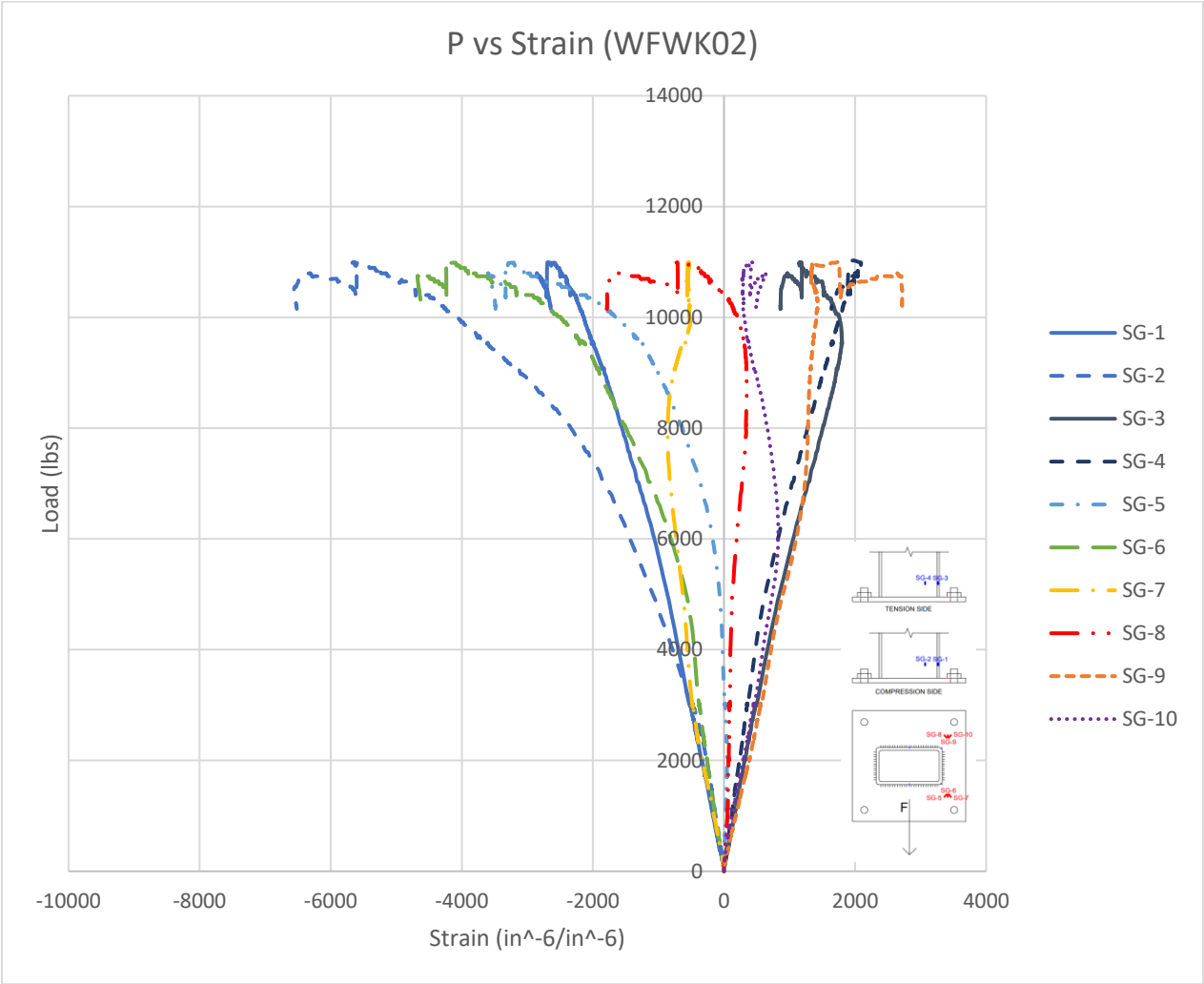
Figure C17

Load versus Strain for Specimen WFWK03
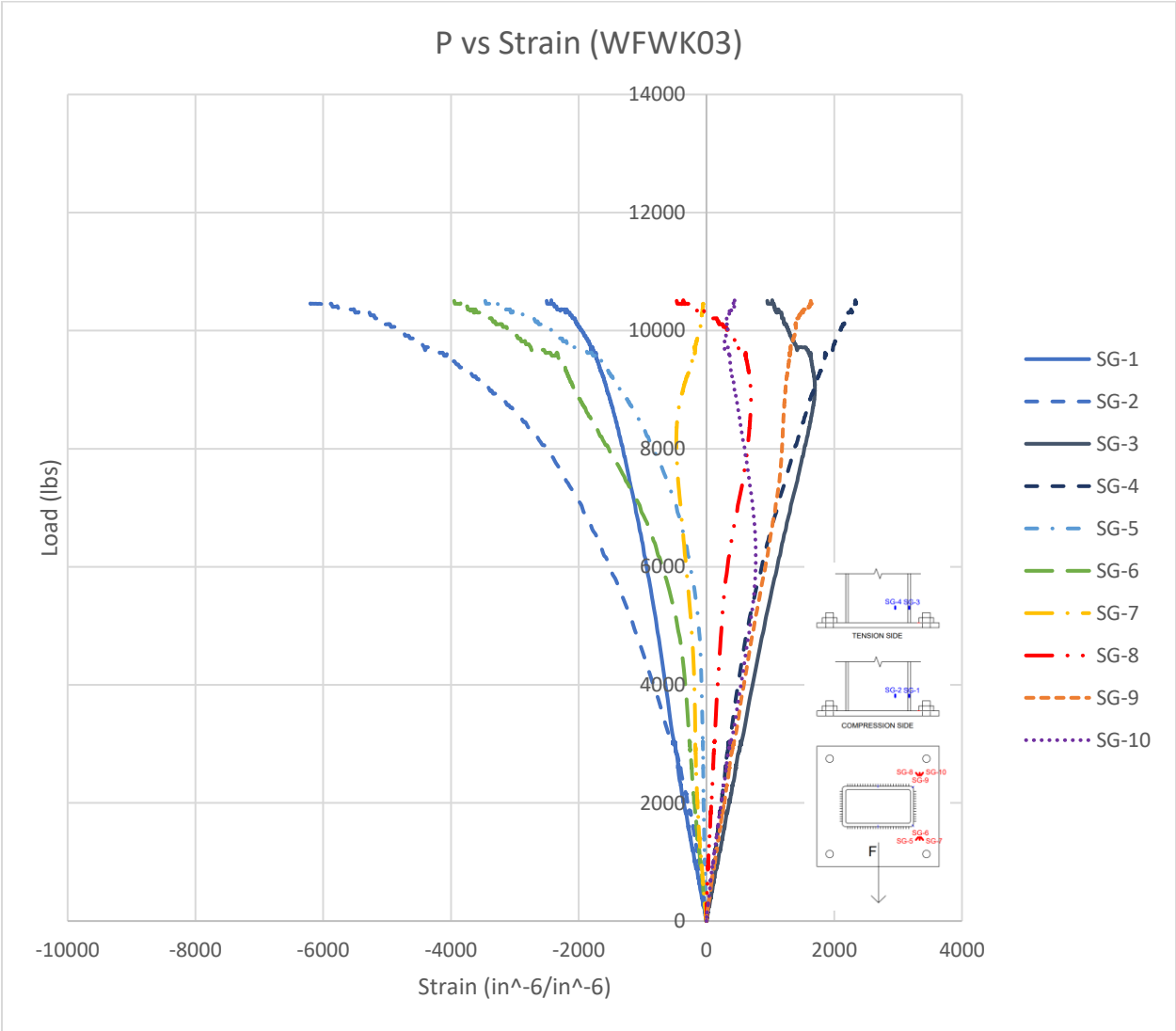
Figure C18

Load versus Strain for Specimen AAWK01
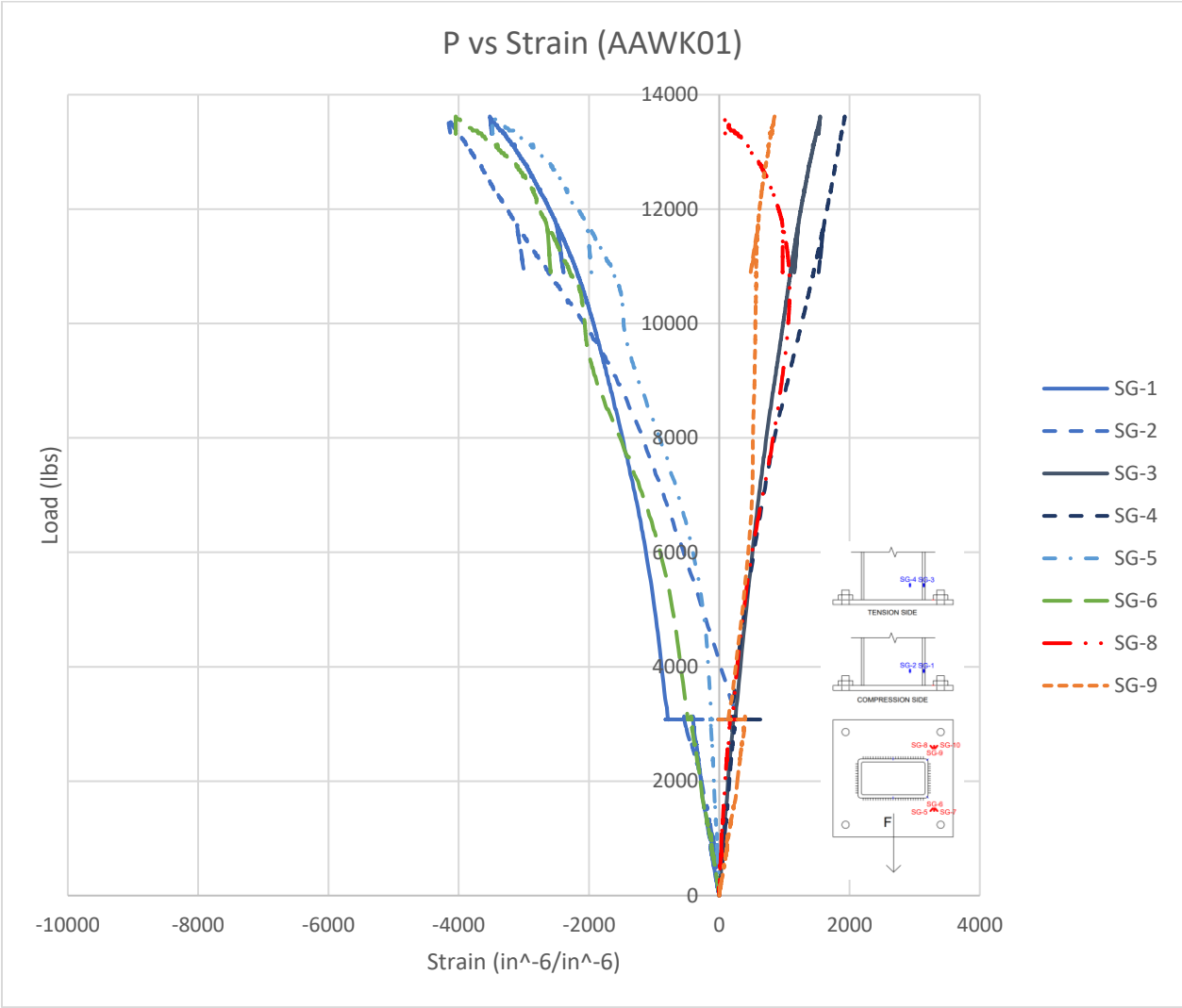
Figure C19

Load versus Strain for Specimen AAWK02
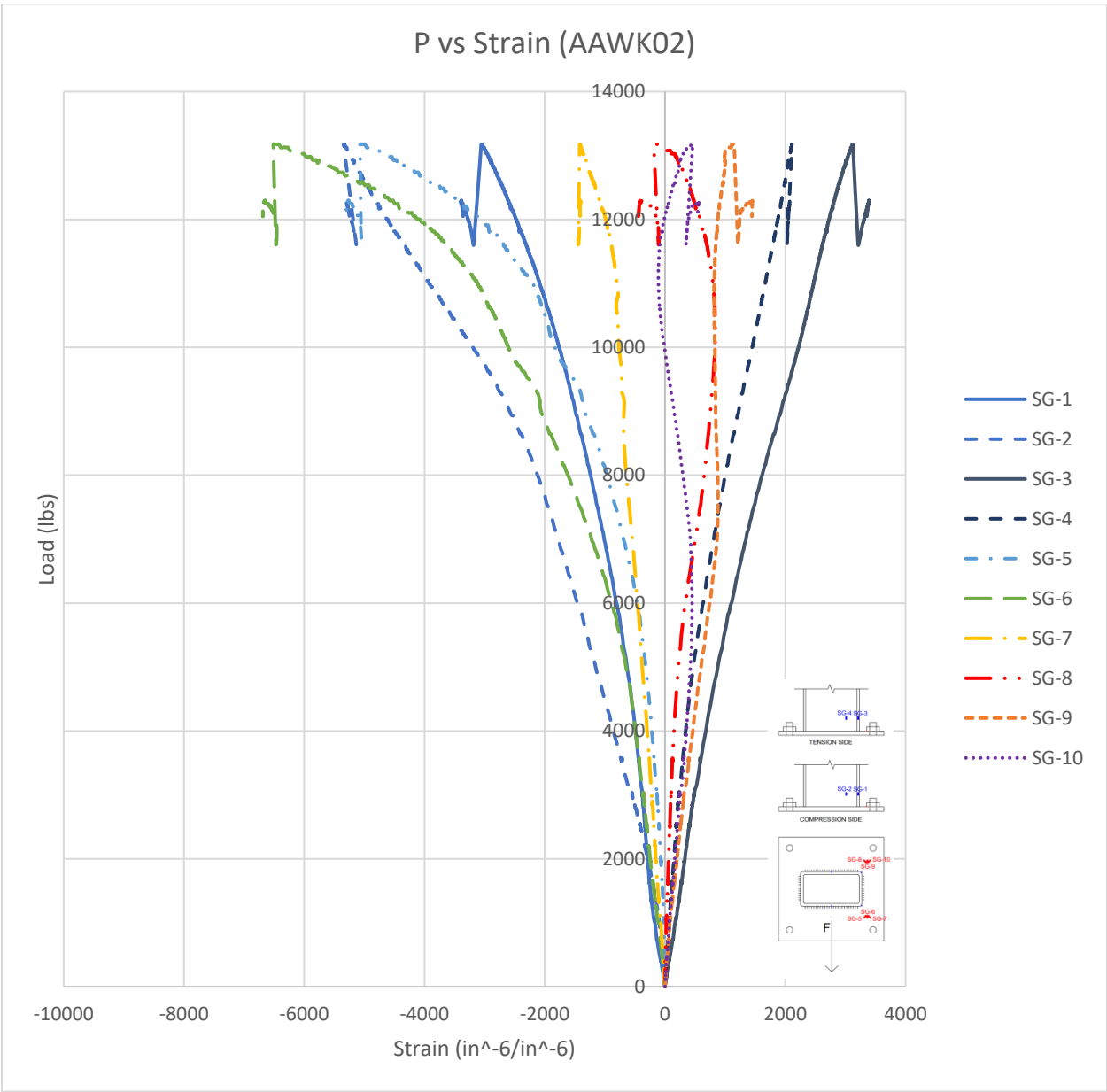
Figure C20

Load versus Strain for Specimen AAWK03
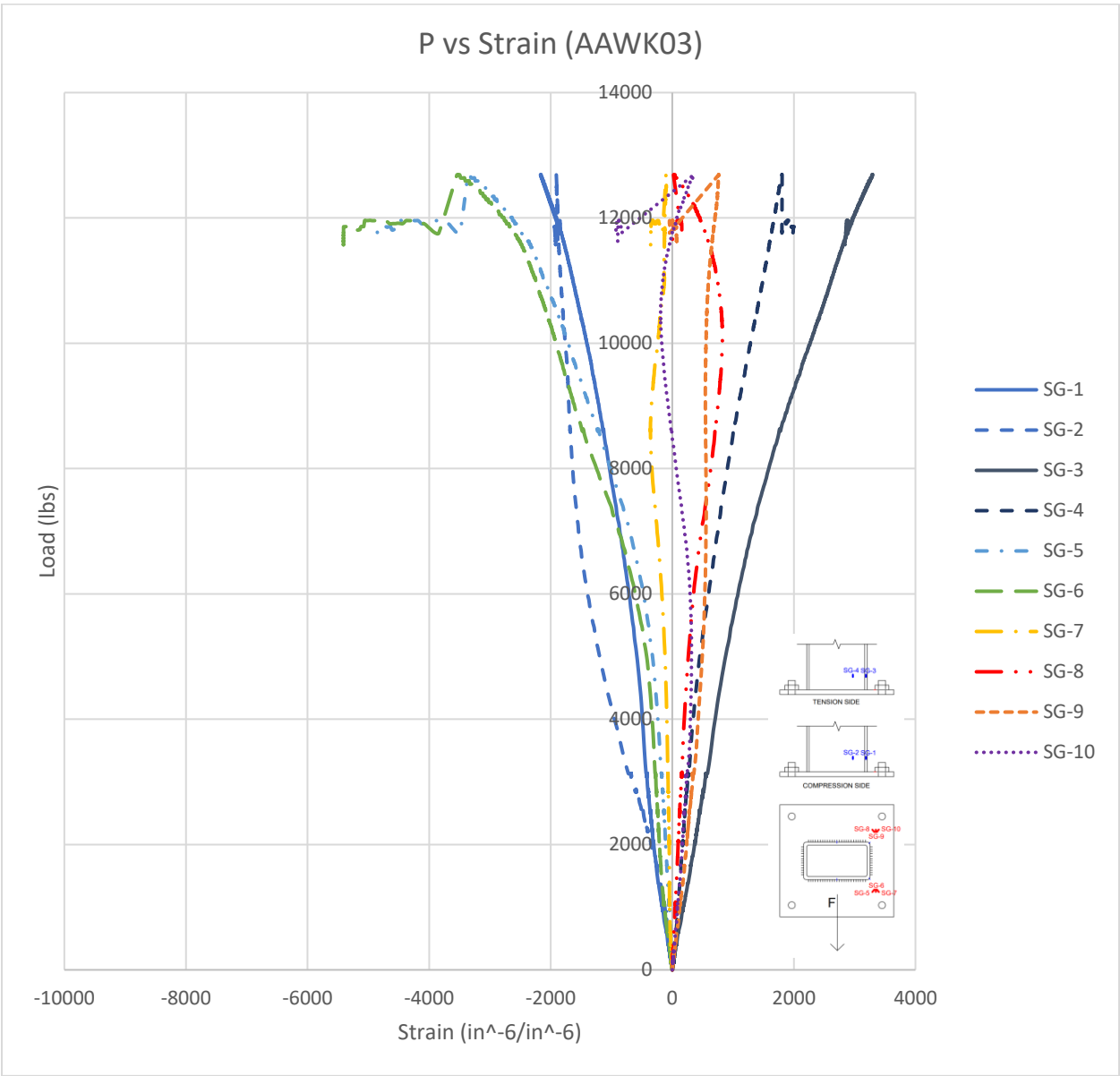
Appendix D – Structural Drawings

BASE PLATE AND CAP PLATE CONFIGURATIONS

NOTE: ALL HOLES 13/16" OD
ALL PLATE MATERIAL GRADE 50
(3) OF EACH ASSEMBLY - (24) TOTAL ASSEMBLIES

HSS 7x7x5/16" CENTERED ON 12"x12"x1/2" BASE PL. W/ (4) 3/4" A325 BOLTS AT PLATE SIDES

HSS 7x7x5/16" CENTERED ON 12"x12"x1/2" BASE PL. W/ (4) 3/4" A325 BOLTS AT PLATE CORNERS

HSS 7x4x5/16" CENTERED ON 12"x12"x5/8" BASE PL. W/ (4) 3/4" A325 BOLTS AT PLATE CORNERS

TYP BASE PL CONN U.N.O.

TYP ALL CAP PLATES

SHORT SIDES
LONG SIDES
4 SIDES

2 PLATES

(2) - 3/4" PLATES, EACH
4"x1'-7", 1 3/4" DIA HOLES

2"
1'-3"
1'-7"
7/8"
2"
2"
4"

AXIAL SPECIMEN CAP PLATE ASSEMBLY
1 ASSEMBLY

(2) - 1" PLATES, EACH
8"x12", CENTERED ON
12"x12"x1" PLATE,
SEPARATED BY 2" GAP

PJP
1/4
1/4
3/8
4 3/4"
4 3/4"
1 1/4"
9 1/2"
1 1/4"

1'-0"
6"
6"
1"
2"
4"
2"
9"

1'-0"
4"
4"
1"
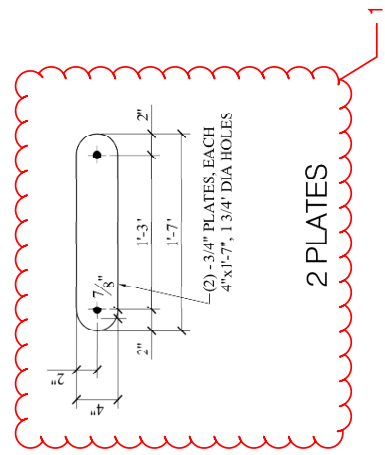
CONNECTION ASSEMBLIES

NOTE: ALL HOLES 13/16" DIA UNO
ALL PLATE MATERIAL GRADE 50

MSOE UNIVERSITY

| Client | MILWAUKEE SCHOOL OF ENGINEERING |
| Milwaukee, WI | |

| Project | CV8000 - RESEARCH AND PRESENTATION |
| JAKE ZIETLOW | |

1	07/19	RELEASED
2	08/16	REVISIONS
Ver	Date	Description

Course ID	CV 8000
Section No.	101
Date	08/16/21
Drawn	JAZ
Checked	PB
Scale	1" = 1'-0"

Sheet Title
CONN ASSEMBLIES

Sheet No
S2

This drawing is part of a Milwaukee School of Engineering University academic project.

Appendix E – Shop Drawings

BILL OF MATERIAL

SEQ. NO.	SEQ. QTY	PC MARK	QTY	DESCRIPTION	LENGTH FT. IN.	PC. WT.	TOTAL WEIGHT	REMARKS	A/B
1	3	100C001	3	COLUMN	3 0	132.9	398.6	32	
		100C001	3	HSS7x7x5/16		82.8	248.3	M2E A500B	
		cp1	3	PL3/4x12	1 0	30.0	89.9	A572-50	
		07p56	3	PL1/2x12	1 0	20.1	60.4	A572-50	

FOR APPROVAL ONLY 3 COLUMNS 100C001

NOT CERTIFIED FOR FABRICATION OR FIELD USE

(1-HSS7x7x5/16x3-0) A500B 3-11¼ (P/P 3-11¼)

MARK FACE "A" "WEST"

MILL CUT

1-cp1

Wp EL 3-11¼

EL 0-0

4 SIDES

5⅝

1-07p56

BILL OF MATERIAL

SEQ. NO.	SEQ. QTY	PC MARK	QTY	DESCRIPTION	LENGTH FT. IN.	PC. WT.	TOTAL WEIGHT	REMARKS	A/B
1	3	100C002	3	COLUMN		132.9	398.6	32	
		100C002	3	HSS7x7x5/16	3 0	82.8	248.3	M2E A500B	
		cp1	3	PL3/4x12	1 0	30.0	89.9	A572-50	
		07p56	3	PL1/2x12	1 0	20.1	60.4	A572-50	

PLOTTED Aug 18 2021

ZALK JOSEPHS
FABRICATORS L.L.C.
STOUGHTON, WISCONSIN

MSOE
CV8000-RESEARCH AND PRESSENTATION

DR. DATE	MMM 8-18-21
CKD DATE	BLF 8-21
CODE	XX

CONTR. NO.11201407 | DWG. NO. 100C002 | REV.

PAINT:
NONE
SSPC-SP1

SHOP NOTE:
ALL RE-ENTRANT CORNERS
SHALL BE SHAPED NOTCH
FREE TO A RADIUS AT LEAST 1/2"

ALL MATERIAL: AS NOTED

HOLES: 13/16"Dia
(U.N.O)

FOR APPROVAL ONLY 3 COLUMNS 100C002

NOT CERTIFIED FOR FABRICATION OR FIELD USE

MARK FACE "A"
"WEST"

MILL CUT

EL 0-0

(1-HSS7X7X5/16X3-0) A500B 3-1¹/₄ (P/P 3-1¹/₄)

BILL OF MATERIAL

SEQ. NO.	SEQ. QTY	PC MARK	QTY	DESCRIPTION	LENGTH FT. IN.	PC. WT.	TOTAL WEIGHT	REMARKS	A/B
1	3	100C003	3	COLUMN		132.9	398.6	32	
		100C003	3	HSS7x7x5/16	3 0	82.8	248.3	M2E A500B	
		cp1	3	PL3/4x12	1 0	30.0	89.9	A572-50	
		bp3	3	PL1/2x12	1 0	20.1	60.4	A572-50	

PLOTTED Aug 18 2021

ZALK JOSEPHS
STOUGHTON, WISCONSIN
FABRICATORS L.L.C.

MSOE
CV8000-RESEARCH AND PRESSENTATION

CONTR. NO.11201407 DWG. NO. 100C003

DR. DATE	MMM 8-18-21
CKD DATE	BLF 8-21
CODE	XX

PAINT:
NONE
SSPC-SP1

SHOP NOTE:
ALL RE-ENTRANT CORNERS
SHALL BE SHAPED NOTCH
FREE TO A RADIUS AT LEAST 1/2"

ALL MATERIAL: AS NOTED

HOLES: 13/16"Dia
(U.N.O)

3 COLUMNS 100C003

MARK FACE "A"
"WEST"

MILL CUT

Wp EL 3-1¹/₄

EL 0-0

(1-HSS7x7x5/16x3-0) A500B 3-1¹/₄ (p/p 3-1¹/₄)

4 SIDES

1-cp1

1-bp3

FOR APPROVAL ONLY

BILL OF MATERIAL

SEQ. NO.	SEQ. QTY	PC MARK	QTY	DESCRIPTION	LENGTH FT. IN.		PC. WT.	TOTAL WEIGHT	REMARKS	A/B
1	3	100C004	3	COLUMN			132.9	398.6	32	
		100C004	3	HSS7x7x5/16	3	0	82.8	248.3	M2E A500B	
		cp1	3	PL3/4x12	1	0	30.0	89.9	A572-50	
		bp3	3	PL1/2x12	1	0	20.1	60.4	A572-50	

PLOTTED Aug 18 2021

ZALK JOSEPHS FABRICATORS L.L.C.
STOUGHTON, WISCONSIN

MSOE
CV8000-RESEARCH AND PRESSENTATION

CONTR. NO.11201407 DWG. NO. 100C004

DR. DATE	MMM 8-18-21
CKD DATE	BLF 8-21
CODE	XX

PAINT:
NONE
SSPC-SP1

SHOP NOTE:
ALL RE-ENTRANT CORNERS
SHALL BE SHAPED NOTCH
FREE TO A RADIUS AT LEAST 1/2"

ALL MATERIAL: AS NOTED

HOLES: 13/16"Dia
(U.N.O)

FOR APPROVAL ONLY
NOT CERTIFIED FOR FABRICATION OR FIELD USE

3 COLUMNS 100C004

1-cp1

MARK FACE "A"
"WEST"

MILL CUT 3/4

WP EL 3-1¹/₄

1/4

3¹/₂ 3¹/₂

Ⓑ

MILL CUT 1/2

EL 0-0

Ⓐ

(1-HSS7X7X⁵/₁₆X3-0) A500B 3-1¹/₄ (P/P 3-1¹/₄)

1-bp3

1/4

BILL OF MATERIAL

SEQ. NO.	SEQ. QTY	PC MARK	QTY	DESCRIPTION	LENGTH FT.	LENGTH IN.	PC. WT.	TOTAL WEIGHT	REMARKS	A/B
1	3	100C005	3	COLUMN			113.7	341.2	32	
		100C005	3	HSS7x4x$^5/_{16}$	2	6	53.0	159.1	M2E A500B	
		cp2	3	PL1x8$^1/_2$	1	3	35.6	106.7	A572-50	
		bp4	3	PL$^5/_8$x12	1	0	25.2	75.5	A572-50	

PLOTTED Aug 18 2021

ZALK JOSEPHS
FABRICATORS L.L.C.
STOUGHTON, WISCONSIN

MSOE
CV8000-RESEARCH AND PRESSENTATION

CONTR. NO.11201407 | DWG. NO. 100C005

DR. DATE	MMM 8-18-21
CKD DATE	BLF 8-21
CODE	XX

PAINT:
NONE
SSPC-SP1

SHOP NOTE:
ALL RE-ENTRANT CORNERS
SHALL BE SHAPED NOTCH
FREE TO A RADIUS AT LEAST 1/2"

ALL MATERIAL: AS NOTED

HOLES: $^{13}/_{16}$"Dia
(U.N.O)

FOR APPROVAL ONLY 3 COLUMNS 100C005

NOT CERTIFIED FOR FABRICATION OR FIELD USE

(1-HSS7x4x$^5/_{16}$x2-6) A500B 2-7$^5/8$ (P/P 2-7$^5/8$)

MARK FACE "A"
"WEST"

MILL CUT
MILL CUT
EL 0-0
Wp EL 2-7$^5/8$

BILL OF MATERIAL

SEQ. NO.	SEQ. QTY	PC MARK	QTY	DESCRIPTION	LENGTH FT.	LENGTH IN.	PC. WT.	TOTAL WEIGHT	REMARKS	A/B
1	3	100C006	3	COLUMN			113.5	340.4	32	
		100C006	3	HSS7x4x5/16	2	6	53.0	159.1	M2E A500B	
		cp3	3	PL1x8¹/₂	1	3	35.3	105.8	A572-50	
		bp4	3	PL⁵/₈x12	1	0	25.2	75.5	A572-50	

PLOTTED Aug 18 2021

ZALK JOSEPHS
STOUGHTON, WISCONSIN
FABRICATORS L.L.C.

DR. DATE	MMM	8-18-21
CK'D DATE	BLF	8-21
CODE	XX	

MSOE
CV8000-RESEARCH AND PRESSENTATION

CONTR. NO.11201407 | DWG. NO. 100C006

PAINT:
NONE
SSPC-SP1

SHOP NOTE:
ALL RE-ENTRANT CORNERS
SHALL BE SHAPED NOTCH
FREE TO A RADIUS AT LEAST 1/2"

ALL MATERIAL: AS NOTED

HOLES: 13/16"Dia
(U.N.O)

REVISION   NO.   REV.   DATE   DR. CK'D.

3 COLUMNS 100C006

FOR APPROVAL ONLY

NOT CERTIFIED FOR FABRICATION OR FIELD USE

MARK FACE "A"
"WEST"

MILL CUT

EL 0-0

Wp EL 2-7⁵/₈

(1-HSS7x4x5/₁₆x2-6) A500B 2-7⁵/₈ (P/P 2-7⁵/₈)

1-cp3

1-bp4

BILL OF MATERIAL

SEQ. NO.	SEQ. QTY	PC MARK	QTY	DESCRIPTION	LENGTH FT.	LENGTH IN.	PC. WT.	TOTAL WEIGHT	REMARKS	A/B
1	3	100C007	3	COLUMN			113.7	341.2	32	
		100C007	3	HSS7x4x5/16	2	6	53.0	159.1	M2E A500B	
		cp2	3	PL1x8 1/2	1	3	35.6	106.7	A572-50	
		bp4	3	PL5/8x12	1	0	25.2	75.5	A572-50	

PLOTTED Aug 18 2021

ZALK JOSEPHS FABRICATORS L.L.C.
STOUGHTON, WISCONSIN

MSOE
CV8000-RESEARCH AND PRESSENTATION

CONTR. NO.11201407 DWG. NO. 100C007   REV.

DR. DATE	MMM 8-18-21
CKD DATE	BLF 8-21
CODE	XX

PAINT:
NONE
SSPC-SP1

SHOP NOTE:
ALL RE-ENTRANT CORNERS
SHALL BE SHAPED NOTCH
FREE TO A RADIUS AT LEAST 1/2"

ALL MATERIAL : AS NOTED

HOLES: 13/16"Dia
(U.N.O)

FOR APPROVAL ONLY 3 COLUMNS 100C007

NOT CERTIFIED FOR FABRICATION OR FIELD USE

1-cp2

1/4

4 1/4 4 1/4 1 1/2 1 1/2
5 1/2
1 1/2
1 1/2 1-0 1 1/2
7 1/2 7 1/2

MARK FACE "A"
"WEST"

3 1/2 3 1/2

Ⓐ   Ⓑ

MILL CUT
MILL CUT

5/8
EL 0-0
WP EL 2-7 5/8

(1-HSS7x4x5/16x2-6) A500B 2-7 5/8 (P/P 2-7 5/8)

1/4

1-bp4

1 1/2 6 6
4 3/4 4 3/4
1 1/4 4 3/4 4 3/4 1 1/4
6 6

BILL OF MATERIAL

SEQ. NO.	SEQ. QTY	PC MARK	QTY	DESCRIPTION	LENGTH FT.	LENGTH IN.	PC. WT.	TOTAL WEIGHT	REMARKS	A/B
1	3	100C008	3	COLUMN			113.5	340.4	32	
		100C008	3	HSS7x4x5/16	2	6	53.0	159.1	M2E A500B	
		cp3	3	PL1x8 1/2	1	3	35.3	105.8	A572-50	
		bp4	3	PL5/8x12	1	0	25.2	75.5	A572-50	

PLOTTED Aug 18 2021

ZALK JOSEPHS
STOUGHTON, WISCONSIN
FABRICATORS L.L.C.

DR. DATE	MMM	8-18-21
CKD DATE	BLF	8-21
CODE	XX	

MSOE
CV8000-RESEARCH AND PRESSENTATION

CONTR. NO.11201407 DWG. NO. 100C008

PAINT:
NONE
SSPC-SP1

SHOP NOTE:
ALL RE-ENTRANT CORNERS
SHALL BE SHAPED NOTCH
FREE TO A RADIUS AT LEAST 1/2"

ALL MATERIAL: AS NOTED

HOLES: 13/16"Dia
(U.N.O)

REVISION

3 COLUMNS 100C008

FOR APPROVAL ONLY

NOT CERTIFIED FOR FABRICATION OR FIELD USE

MARK FACE "A"
"WEST"

MILL CUT

MILL CUT

EL 0-0

WP EL 2-7 5/8

(1-HSS7x4x5/16x2-6) A500B 2-7 5/8 (P/P 2-7 5/8)

1-cp3

1-bp4

BILL OF MATERIAL

SEQ. NO.	SEQ. QTY	PC MARK	QTY	DESCRIPTION	LENGTH FT. IN.	PC. WT.	TOTAL WEIGHT	REMARKS	A/B
1	1	100P009	ONE	PLATE		90.6	90.6	32	
		100P009	1	PL1x12	1 0	40.0	40.0	A572-50	
		07p63	1	PL1x8	1 0	25.2	25.2	A572-50	
		07p62	1	PL1x8	1 0	25.4	25.4	A572-50	

PLOTTED Aug 18 2021

ZALK JOSEPHS FABRICATORS L.L.C.
STOUGHTON, WISCONSIN

MSOE
CV8000-RESEARCH AND PRESSENTATION

DR. DATE	MMM 8-18-21
CKD DATE	BLF 8-21
CODE	XX

CONTR. NO.11201407 DWG. NO. 100P009 REV.

| NO. | REVISION | DATE | DR. | CKD. |

PAINT:
NONE
SSPC-SP1

SHOP NOTE:
ALL RE-ENTRANT CORNERS
SHALL BE SHAPED NOTCH
FREE TO A RADIUS AT LEAST 1/2"

ALL MATERIAL: A572-50

HOLES: $^{13}/_{16}$"Dia
(U.N.O)

ONE PLATE 100P009

1-07p63 (NS)
1-07p62 (FS)

FOR APPROVAL ONLY

NOT CERTIFIED FOR FABRICATION OR FIELD USE

BILL OF MATERIAL

SEQ. NO.	SEQ. QTY	PC MARK	QTY	DESCRIPTION	LENGTH FT. IN.	PC. WT.	TOTAL WEIGHT	REMARKS	A/B
1	2	100P010	2	PLATE		14.4	28.8	32	
		100P010	2	PL3/4x4	1 7	14.4	28.8	A572-50	

RAD=2" TYP

1-7
1-3
2
2
13/4 ∅
2 2
4

2 PLATES 100P010

PAINT:
NONE
SSPC-SP1

SHOP NOTE:
ALL RE-ENTRANT CORNERS
SHALL BE SHAPED NOTCH
FREE TO A RADIUS AT LEAST 1/2"

ALL MATERIAL: A572-50

HOLES: 13/16"Dia
(U.N.O)

PLOTTED Aug 18 2021

ZALK JOSEPHS
STOUGHTON, WISCONSIN
FABRICATORS L.L.C.

DR. DATE	MMM 8-18-21
CKD DATE	BLF 8-21
CODE	XX

MSOE
CV8000-RESEARCH AND PRESSENTATION

CONTR. NO.11201407 | DWG. NO. 100P010

REV.

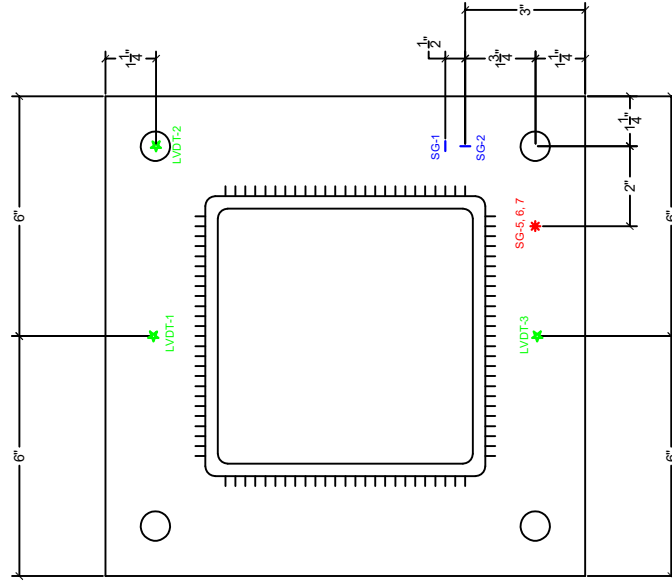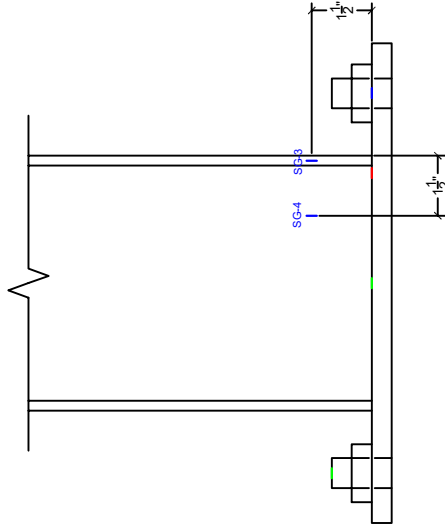|			DATE	DR.	CKD.

NO. REVISION DATE DR. CKD.

FOR APPROVAL ONLY

NOT CERTIFIED FOR FABRICATION OR FIELD USE
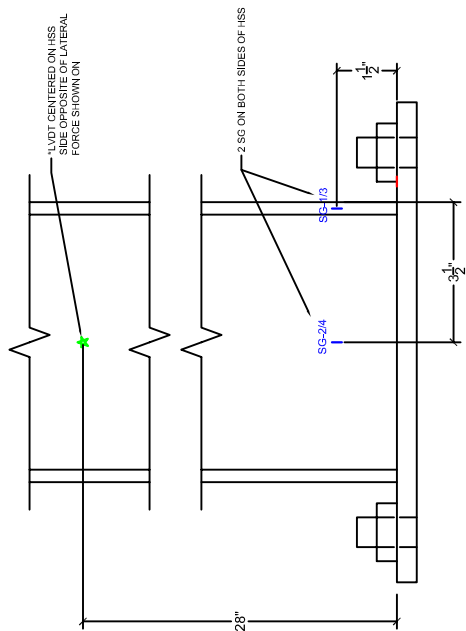
Appendix F – Instrumentation Plans

Corner Bolts

SG-3
SG-4

$1\frac{1}{2}$"
$1\frac{1}{2}$"
6"

LVDT-2
LVDT-1
LVDT-3
SG-1
SG-2
SG-5, 6, 7

$1\frac{1}{4}$"
$1\frac{1}{2}$"
$1\frac{3}{4}$"
$1\frac{1}{4}$"
3"
6"
6"
$1\frac{1}{4}$"
2"

★ = LVDT Location
▌ = Linear Strange Gage Location
✹ = Rosette Strain Gage Location

Side Bolts

SG-3
SG-4

$1\frac{1}{2}$"
$1\frac{1}{2}$"

LVDT-1
LVDT-2
LVDT-3
SG-1
SG-2
SG-5, 6, 7

$1\frac{1}{4}$"
$1\frac{1}{4}$"
3"
$1\frac{1}{2}$"
6"
6"
3"
$1\frac{1}{4}$"
$1\frac{1}{4}$"
6"
6"

★ = LVDT Location
▌ = Linear Strange Gage Location
✹ = Rosette Strain Gage Location

Strong Axis

*LVDT CENTERED ON HSS SIDE OPPOSITE OF LATERAL FORCE SHOWN ON

SG-1/3

SG-2/4

28"

1½"

2"

6"

6"

2"

2¾"

1¼"

SG-8, 9, 10

SG-5, 6, 7

F

✶ = LVDT Location

| = Linear Strange Gage Location

✳ = Rosette Strain Gage Location

Weak Axis

*LVDT CENTERED ON HSS SIDE OPPOSITE OF LATERAL FORCE SHOWN ON

2 SG ON BOTH SIDES OF HSS

SG-1/3

SG-2/4

28"

1½"

3½"

6"

6"

2"

2¾"

1¼"

SG-8, 9, 10

SG-5, 6, 7

F

✶ = LVDT Location

| = Linear Strange Gage Location

✳ = Rosette Strain Gage Location

Appendix G – Material Testing

Tensile Test Report (Page 1 of 2)

MAI Report No:	222-2-196	**Date:** June 27, 2022
Client:	Milwaukee School of Engineering	**Contact:** Pouria Bahmani
P.O. No:	Verbal	**Date Rec'd:** June 16, 2022
Description:	Plate and Tube Sections	

Property	Plate 1	Plate 2	Plate 3	ASTM A36	ASTM A572, Grade 50
Test Bar Dimensions, Diameter, inch	0.496	0.495	0.496	D	D
Gage Length, inches	2.0	2.0	2.0	4D	4D
Tensile Strength, psi	82,900	82,900	82,900	58,000 - 80,000	65,000 min.
Yield Strength, psi (1)	57,300	56,900	57,200	36,000 min.	50,000 min.
Elongation, %	30	30	29	23 min.	21 min.
Elongation, %	67	66	67	Not Specified	Not Specified

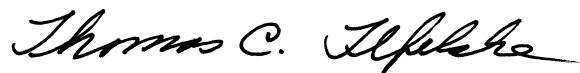| Property	Tube 1	Tube 2	Tube 3	ASTM A500, Grade B	ASTM A1085
Test Bar Dimensions Width, inch	0.493	0.489	0.493	0.50	0.50
Thickness, inch	0.295	0.293	0.293	Material Thickness	Material Thickness
Gage Length, inches	2.0	2.0	2.0	2.0	2.0
Tensile Strength, psi	65,500	67,200	67,700	58,000 min.	65,000 min.
Yield Strength, psi (1)	53,100	53,300	53,300	46,000 min.	50,000 - 70,000
Elongation, %	35	32	32	23 min.	21 min.

(1): at 0.2% offset

Notes: The tensile properties of the three plate samples are in conformance with both ASTM A36, "Standard Specification for Carbon Structural Steel," and ASTM A572, Grade 50, "Standard Specification for High-Strength Low-Alloy Columbium-Vanadium Structural Steels."

The tensile properties of the three tubes are in conformance with both ASTM A500, Grade B, "Standard Specification for Cold-Formed Welded and Seamless Carbon Steel Structural Tubing in Rounds and Shapes," and ASTM A1085, "Standard Specification for Cold-Formed Welded Carbon Steel Hollow Structural Sections (HSS)." It should be noted, however, that this specification also has specified Charpy V-Notch impact properties that were not determined.

MAI ▪ 1515 Paramount Drive ▪ Suite 1 ▪ Waukesha, WI 53186
Phone: 262-798-8098 ▪ 800-798-4966 ▪ FAX: 262-798-8099 ▪. e-mail: info@metassoc.com
www.metassoc.com

The stress-strain curves for these samples are provided as separate Excel spreadsheets.

Respectfully submitted,

Thomas C. Tefelske

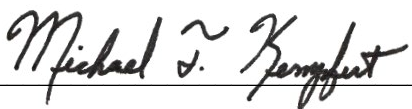Thomas C. Tefelske,
President

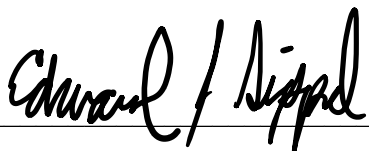**Architectural Engineering**

Capstone Report Approval Form

Master of Science in Architectural Engineering -- MSAE

Milwaukee School of Engineering

This capstone report, entitled "Experimental and Analytical Evaluation of the Flexural and Axial Capacity of Rectangular Steel Hollow Structural Section (HSS) End-Plate Connections," submitted by the student Edward J. Nelson has been approved by the following committee:

Faculty Advisor: _____ Date: _____05/08/2024_____

Dr. Christopher Raebel, Ph.D.

Faculty Member: _____ Date:_____05/08/2024_____

Dr. Michael Kempfert, Ph.D.

Faculty Member: _____ Date: _____05/08/2024_____

Dr. Edward Sippel, Ph.D.